# AN ABSTRACT OF THE THESIS OF

Bandar Alkhudhiri for the degree of Master of Science in Radiation Health Physics presented on December 04, 2013.

Title: Utilization for a Triple-Layer Phoswich Detector for Beta Spectral Stripping.

Abstract approved:

_____

David M. Hamby

To quantify the relative activity contributions of beta emitters in mixed emission source spectra, the triple-layer phoswich detector was modeled to generate beta energy absorption spectra from mixed beta sources. These mixed sources include four pure beta emitters (C-14, Tc-99, Sr-90, and Y-90). Monte Carlo N-Particle (MCNP) computer code was used to simulate electron energy absorption in the first and second layers (beta detector). A spectral stripping technique was developed to de-convolve the multi-response distribution (beta energy absorption spectrum) into its component parts for the identification and quantification of its constituent radionuclides. The method provided reliable results in identifying the studied radionuclides and determining their relative combination of source activity. The results revealed variations in percentages between the original emission and collected spectra that was found to be less than 2% in all studied spectra. Those variations were believed to be attributed to some degree of uncertainty in the spectral stripping method and some energy loss prior to detection.

# Utilization for a Triple-Layer Phoswich Detector for Beta Spectral Stripping

by
Bandar Alkhudhiri

A THESIS

submitted to

Oregon State University

in partial fulfillment of
the requirements for the
degree of

Master of Science

Presented December 04, 2013
Commencement June 2014

Master of Science thesis of Bandar Alkhudhiri presented on December 04, 2013

APPROVED:

Major Professor, representing Radiation Health Physics

Head of the Department of Nuclear Engineering and Radiation Health Physics

Dean of the Graduate School

I understand that my thesis will become part of the permanent collection of Oregon State University libraries. My signature below authorizes release of my thesis to any reader upon request.

Bandar Alkhudhiri, Author

# ACKNOWLEDGEMENTS

First and above all, I would like to praise and thank God, almighty for providing this opportunity and granting me the capability to proceed successfully, and whose blessings have made me who I am today.

This thesis appears in its current form due to help and guidance of several people. I would therefore like to offer my sincere thanks to all of them.

I would like to express my deepest thanks to my parents for all the prayers and emotional and financial support throughout this journey.

I would like to express my sincere thanks to my major advisor Dr. David Hamby for his guidance and patience throughout my educational path, and for teaching me how to question thoughts logically and put them into actions.

I would like to thank the ministry of high education of Saudi Arabia for the scholarship I was given and the financial support to finish my graduate work and earn my degree.

I would also like to thank all the laboratory members, colleagues, and friends who helped me making the objectives of this research possible.

# TABLE OF CONTENTS

TABLE OF CONTENTS (Continued)

TABLE OF CONTENTS (Continued)

Page

# LIST OF FIGURES

Figure Page

# LIST OF FIGURES (Continued)

Figure Page

# LIST OF FIGURES (Continued)

Figure Page

# LIST OF FIGURES (Continued)

Figure Page

# LIST OF TABLES

Table Page

# 1.0 Introduction

Fission products created as a result of nuclear power generation are generally contained from the environment by the use of numerous engineered systems. Very small quantities of these fission products, however, can find their way out of the reactor facility and into the environment. Identification and quantification of these releases to the atmosphere or environmental waters is of great importance in order to show that potential hazards are minimal. Systems are in place to monitor for fission products by detecting gamma or gross alpha/beta in facility emissions at various locations throughout a given facility. Several fission products emit only beta particles (electrons) and as such can be very difficult to identify. The recent development of a simultaneous beta/gamma spectrometer allows us to conduct beta spectroscopy on fission-product emissions to better characterize radionuclides released to the environment. Complete use of the beta spectrometer requires the development of a computer algorithm that will de-convolve the full beta energy spectrum into its component parts for the identification and quantification of its constituent radionuclides.

## 1.1 Problem Statement:

The need for information about the level of radioactivity in air at various nuclear facilities is very important for worker safety. Recently, the detection and analysis of beta particles has been carried out using a simple gross-beta screening, and using the alpha-to-beta ratio and/or alpha spectral analysis. Therefore, we set out to study beta spectroscopy in order to obtain a better understanding of beta detection in the presence of numerous beta and gamma emitters in the form of noble gases, halogens, and fission fragments following nuclear fission reactions. This work will provide important insights for better identification and analysis of pure beta emitters.

Further, such study is critically desirable to better evaluate the radiological hazards from nuclear reactions that include beta particle emissions from radionuclides. Thus, our long term goal is to optimize a phoswich detection system for beta particles detection that provides a detailed analysis of the beta energy deposition spectrum. Results from this study will be used to better identify and quantify the radioisotopes that are of interest in nuclear power plant emissions.

## 1.2 Objectives:

Our specific objectives are to:

1) Adapt and optimize a triple-layer phoswich detector to provide a more defined mixed beta/gamma field energy spectral measurement;
2) Conduct spectral stripping and analysis of the studied beta particle spectra; and
3) Identify and quantify pure beta emitters through sophisticated spectral analysis.

## 1.3 Expected Outcomes:

We have put forward a study to specifically define and characterize beta contamination in nuclear power plant effluents utilizing a new generation of high-speed detection technology. Special emphasis has been put on pure beta emitters due to their potentially high contribution to radiation hazards and their difficulty of detection. The results may be very useful in beta dosimetry shielding and hazards assessment.

# 2.0 Background

The detection and characterization of ionizing particles and photons depends heavily on their interaction with matter. Radiation interactions can be divided into two types: direct ionization and indirect ionizations. Direct ionization is a result of the flow of charged particles, such as alpha and beta particles, through materials. In direct ionization, a charged particle directly causes ionization or excitation of an atom through Columbic interactions with matter. Indirect ionization, however, takes place when an uncharged radiation, such neutrons and photons, interacts with matter. To transfers its energy to charged particles, nuclei and orbital electrons due to electromagnetic or nuclear interactions.

## 2.1 Beta Decay:

In nuclear physics, beta decay is a type of radioactive process in which a beta particle, either electron or positron, is emitted from a nucleus with too many neutrons or too many protons, respectively. Beta decay involves the transformation of a neutron into a proton; and so high-speed electron is emitted by a nucleus as result of the energy release in this radioactive process. The energy of the electron may possess any value up to the maximum energy available by the transformation. There are two types of beta decay mechanisms: beta minus decay, beta plus decay. In beta minus decay, a neutron simultaneously decays into a proton, an electron, and a massless and chargeless particle called an antineutrino. In beta plus decay, a proton is transformed into a neutron, a positron, and a neutrino. Table 2-1 summarizes the two beta decay mechanisms:

**Table 2-1: Beta decay mechanisms**

| Decay Type | Process | Occurs when Parent is…. |
|---|---|---|
| Beta Minus | ${}^{1}_{0}n \rightarrow {}^{1}_{1}p + {}^{0}_{-1}\beta^{-} + {}^{0}_{0}\nu$ | Neutron rich, Q>0 |
| Beta Plus | ${}^{1}_{1}p \rightarrow {}^{1}_{0}n + {}^{0}_{1}\beta^{+} + {}^{0}_{0}\nu$ | Proton rich, Q>1.022 |

Where n: The neutron

p: The proton

${}^{0}_{-1}\beta^{-}$ = Negative beta particle, electron, produced in the nucleus

${}^{0}_{1}\beta^{+}$ = Positive beta particle, positron, produced in the nucleus

${}^{0}_{0}\nu$= The antineutrino

The emitted beta particle has continuous energy spectrum, ranging from 0 to the maximum available energy (Q). The kinetic energy of the beta particle depends on the nuclear states of product and daughter involved in decay.

## 2.2 Beta-Particle Interaction:

Beta particles (i.e. energetic electrons) lose their energy to the absorbing medium when they interact with orbital electrons in four different ways: direct ionization, electric excitation, production of bremsstrahlung, and Cerenkov radiation. In terms of energy transfer, the most important mechanisms are direct ionization and bremsstrahlung production.

Electrons can interact with an atomic nucleus, as well as orbital electrons, as they travel through the absorbing medium. When beta particles pass through nuclei, they get deflected due the Coulomb force, which may result in loss of their kinetic energy to absorbing material. Coulomb

repulsion between beta particles and orbital electrons typically results in ionization. A beta particle loses a portion of its energy, transferring it to kinetic energy of an orbital electron, thus releasing it from the atom in the absorbing material. This process results in the creation of an ion pair (Martin, 2006). One beta particle can generate 50 to 150 ions pairs per centimeter in air. As a result of this interaction, characteristic X-rays are produced when the vacant internal electron orbitals are refilled with other electrons. The charge of a beta particle determines its final destiny. After losing its kinetic energy, a beta particle with negative charge either combines with a positive ion or becomes a free electron. However, a positively charged beta, a positron, gets attracted to the opposite charge electrons. The electron and the positron then annihilate to produce "annihilation radiation" in the form of two photons.

Further, when beta particles travel through a high-Z material near a nucleus, they get deflected and decelerated by another charged particle, which results in the producing of photons, known as Bremsstrahlung or "braking radiation". This photon emission is the important phenomenon in the generation of X-rays. Beta particles can also cause excitation of external orbital electrons which leads to the emission of photons, as well. The photon emission following beta interactions with materials may interfere in beta particle measurements and cause distortion to the beta energy spectrum.

Electron emission is a type of radioactive process in which a beta particle, either positron (positively charged particle) or electron (negatively charged particle) is emitted. The beta minus emission occurs in the form an electron, whereas the beta plus occurs in the form of a positron. In the case of electron emission, a massless uncharged particle, called an antineutrino, is also released; while positron emission is accompanied by a neutrino. The emitted beta particles have a continuous kinetic energy spectrum, ranging from 0 to the maximally available energy, which

depends on the parent and product nuclear states that participate in the decay process. The shape of the beta energy emission curve can be predicted as Figure 2-1. A typical energy value is around 1 MeV, however it could start from a few keV to a few tens of MeV.

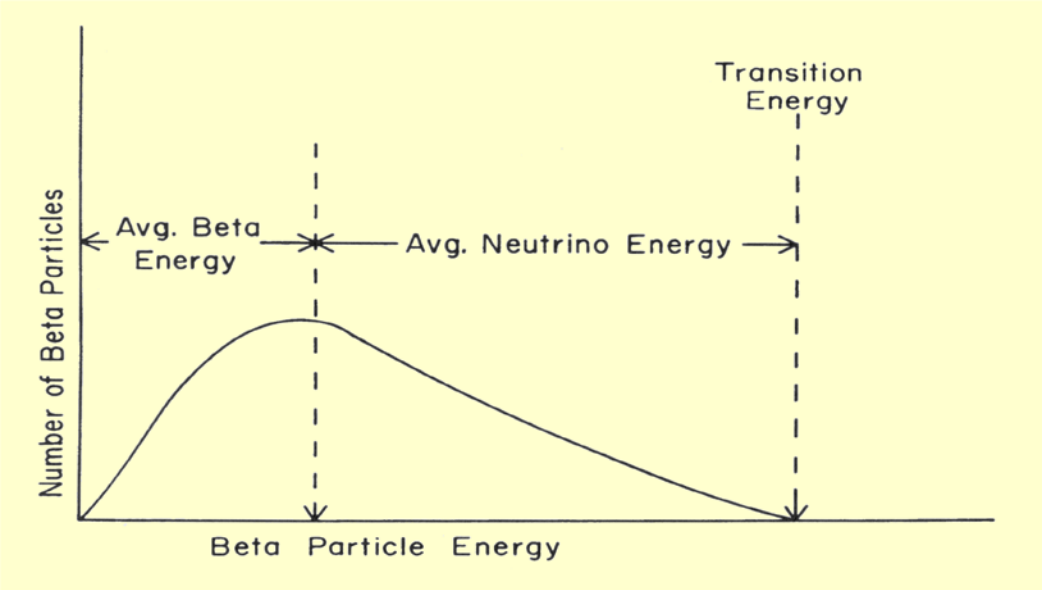


**Figure 2-1: Beta energy spectrum (Sprawls, n.d.).**

## 2.3 Stopping Power:

As beta particles interact with absorbing materials, they experience path deflections following a tortuous path through the medium. This incremental loss of energy of a beta particle when passing through an absorbing material is defined as the linear stopping power. The equation of the stopping power is given as the following:

$$S = -\frac{dE}{dx} \tag{2.1}$$

Where S: Specific energy loss.

dE: The incremental energy loss.

dx: The incremental thickness of the material related to the incremental energy loss

$$-\frac{dE}{dx}=\frac{4\pi e^4 z^2 NZ}{m_0 v^2}[\ln\frac{2m_0 v^2}{I}-\ln(1-\frac{v^2}{c^2})-\frac{v^2}{c^2}] \quad (2.2)$$

v and ze are velocity and charge of particle, c is speed of light, N and Z are the number density and atomic number of the absorber atoms, $m_0$ is rest mass of the electron, I is average excitation and ionization potential of the absorber(Knoll, 2000).

Typically, this mechanism occurs through collisional and radioactive processes depending on the interaction cross sections or probabilities.

## 2.4 Internal Conversion and Auger Electron:

Electrons can be emitted from their orbital shells with no photon release. This phenomenon is known as internal conversion. In internal conversion process, an excited nucleus interacts electromagnetically with one of the electrons in lower atomic orbitals, which results in emitting the electron from the atom. When an atom is excited, it has energy above its ground state. The atom can relax by giving off some its energy to one of its outer shell electrons, which then will be ejected leaving a vacancy. As a result, an electron from a higher energy level falls into the vacancy; and this process results in characteristic X-rays emission. The ejected electron with low energy is known as Auger electrons. The kinetic energy of the Auger electron is equal to the energy of the excited atom minus the binding energy of the ejected electron. The auger effect happens in light atoms with low Z. The conversion electron has a well-defined discrete energy and so its energy spectrum takes the shape of sharp peak. This sharp peak can be readily identified on the beta energy distribution curve.

## 2.5 Beta Energy Spectra:

A beta energy spectrum is determined by the amount of kinetic energy initially carried by each emitted electron. The shape of the beta spectrum varies for different nuclides, but the general shape (Figure 2-1) can be predicted from Fermi theory of beta decay. During the beta decay process, either an electron or positron is released associated with either an antineutrino or neutrino, respectively. Copper-64 decays by positron emission to Ni-64 which decays by electron emission to Zn-64. The energy spectra for electron's and positron emissions look very different as shown in Figure 2-2. The observed difference is due to fact that the electron is attracted by the nucleus once it is born, whereas the positron is repelled.

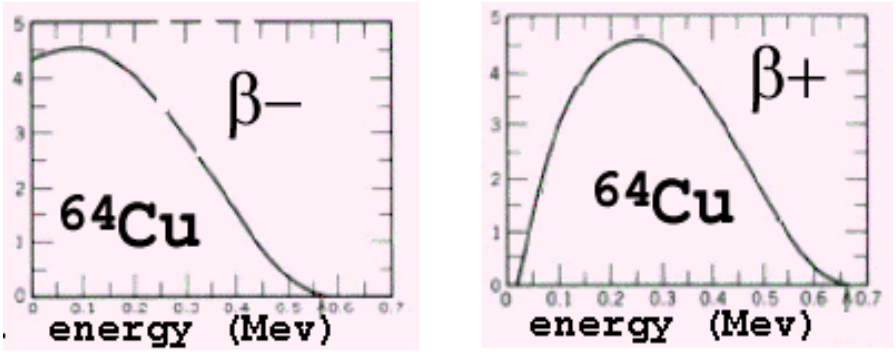


**Figure 2-2: Energy Spectra for electron versus positron**

## 2.6 Photon Emission:

The radioactive decay usually leaves the transforming nucleus in an excited state, and so protons and neutrons of that nucleus become loosely bound to their shells (Martin 2006). As a result, the excitation energy is released as electromagnetic radiation, or photons, as the protons and neutrons find their way to their lowest possible energy state. Therefore, the energy of photons emitted is defined as the difference between the energy states of those protons and neutrons.

Therefore, beta decay is usually followed by photon release. Photon emission takes place after a radioactive transformation such as alpha or beta particle decay. The classical example of gamma emission after beta decay is shown below in the Cs-137 decay scheme (Figure 2-3).

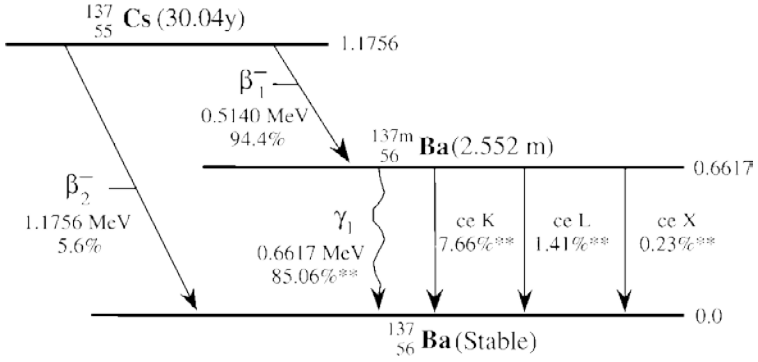


**Figure 2-3: Decay scheme of Cs-137**

## 2.7 Photon Interactions:

The probability of interaction of photons depends highly on the energy of the photon and the atomic number of the material. Photons interact with a given medium in four different ways, only three of which are important here: photoelectric effect, Compton scatter, and pair production. Figure 2-4 shows the three interaction processes as a function of photon energy and Z of the absorbing medium.

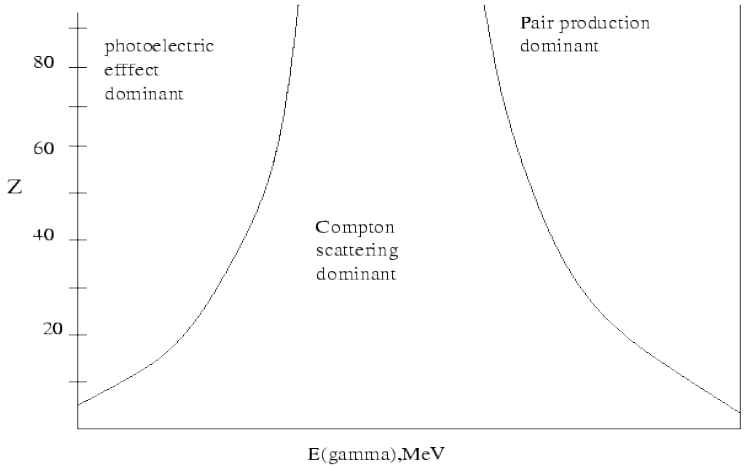


**Figure 2-4: Mechanisms of photon interaction with matter**

## 2.7.1 Photoelectric Effect:

This phenomenon happens when an electron is released from an atom following an incident photon interacting with the medium, in the ionization process. The energy of the emitted electron is equal to the energy of the incident photon, minus the orbital shell binding energy of the emitted electron. Equation (2.3) dictates this process:

$$KE = hv - BE \tag{2.3}$$

Where KE: Kinetic energy of the emitted electron

hv: Energy of incident photon

BE: Binding energy of the electron in its original shell

After being emitted, the electron loses its energy as it moves through matter. This is the predominant process of low energy photons, as Figure (2.4) indicates.

## 2.7.2 Compton Scattering:

When a photon of intermediate energy interacts with an electron causing an increase in the electron energy, this electron is ejected from its orbital shell. As a result of this process, new photon with smaller energy is emitted. This photon either escapes from matter or be absorbed through the photoelectric effect. The scattered photon energy is given by equation (2.4):

$$hv' = \frac{hv}{1+\frac{hv}{m_0c^2}(1-\cos\theta)} \tag{2.4}$$

Where $hv'$: The energy of the scattered electron.

$hv$: Incident photon energy.

$m_0$: The rest mass of electron.

$c$: The speed of light.

$\theta$: The angle of scattered photon.

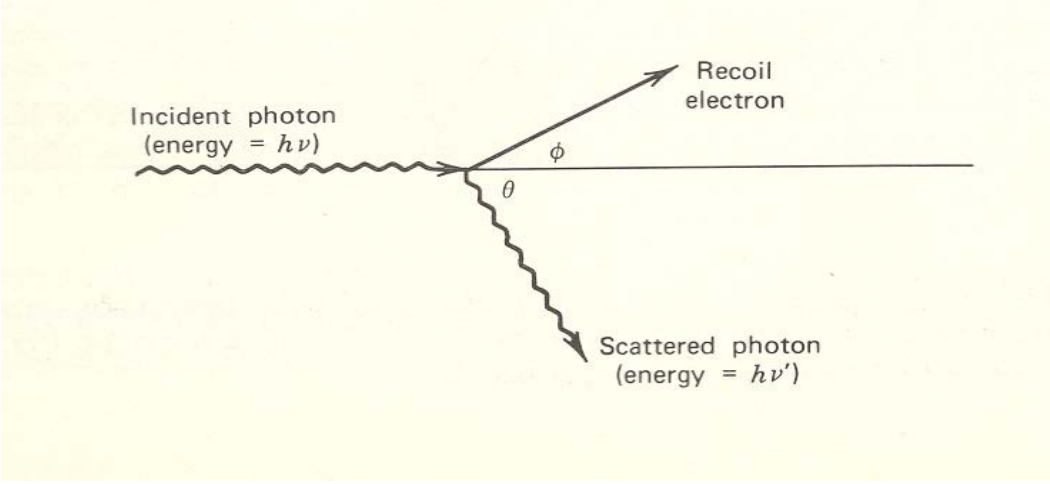


**Figure 2-5: An incident photon interaction with an electron in Compton scattering**

The change in the energy of the photon appears as the kinetic energy of the recoil electron, $KE_e$,

$$KE_e = hv - hv' \qquad (2.5)$$

Compton interactions are more likely to occur when a photon of medium energy interacts with low-Z materials, figure 2.4.

## 2.7.3 Pair Production:

When a high energy photon, higher than 1.022 Mev, interacts in a strong electrometric field, its energy is absorbed and a pair of electron masses is created as electron and positron. These two electron masses will share the remaining photon energy after they both are created. The positively charged nucleus repels the positron, which gives an extra push to its kinetic energy, while the electron slows down with a decrease in energy. The positron eventually will annihilate creating an energy equivalent to two electron masses, each with energy of 0.511 Mev. The reaction is depicted in Figure 2-6.

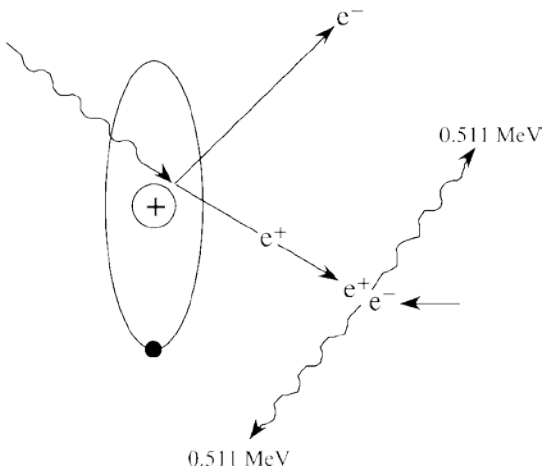


**Figure 2-6: An incident photon interaction in pair production**

## 2.8 The Theory of Scintillations Detection:

The basic principal of a scintillation detector is that the detector scintillates as the incident radiation particles interact. As a result of the scintillation process, the crystal produces visible photons, which are transmitted to a photomultiplier tube (PMT), where these photons will absorbed. As a result, multiple electrons are emitted, which produces an electrical signal. The signal is then transmitted into a plus, which signifies the incident photon. The ideal scintillation materials should have the following properties:

1) They should have high scintillation efficiency (converting energy to light);
2) The crystal should be transparent to its emission wavelength;
3) The materials should have short decay time;
4) The conversion process from energy to light should be linear; and
5) Index of refraction should be near that of glass for optimal coupling to PMT.

In scintillation detectors, fluorescence is defined as the prompt emission of light from the material as a result of nuclear excitation. And, phosphorescence is referred to as emission of light with longer wavelength than fluorescence, with much slower time. The delayed fluorescence is the process similar to fluorescence, but with much longer emission time after the excitation. Scintillators with good functionality should convert as much absorbed energy as possible to fluorescence, thus minimizing the effect of phosphorescence and delayed fluorescence (Knoll, 2000).

The fluorescence intensity is given by equation (2.6):

$$I = I_0 e^{-t/T} \tag{2.6}$$

Where $I_0$ : The intensity of prompt fluorescence,

$I$ : The intensity fluorescence following excitation time t;

t: Time following excitation; and

T : Fluorescence decay time.

### 2.8.1 Types of Scintillators:

Scintillators can be categorized into two types: organic and inorganic. Organic-based scintillators have low density, low Z-value, and low and non-linear light output. They have high hydrogen content and can be used for fast neutron detection. Organic scintillators generally have fast decay times and pulse-shapes vary between different types of particles. Due to their hydrogen content, organic scintillators are favored for beta particles and fast neutron detection.

Inorganic-scintillators have high density and Z-value materials. These detectors generally have higher and more linear light output and slower decay times. The inorganic scintillators are preferably used for gamma measurements because of their high Z-values and high density.

The advantages of inorganic scintillators:

- They have long luminesece decay time;
- They count at higher rates;
- They have higher light output; and
- They give better temporal resolution.

The disadvantages of inorganic scintillators; include:

- They are not effective for non-dispersive spectroscopy application;

- They are slower than the organic ones; and
- They have to be kept in an air-tight tube to be protected from moisture, which can be called hygroscope.

### 2.8.2 Plastic Scintillators:

Plastics scintillators are often used for detection of charged particles. However, because their density and atomic numbers are relatively low, plastics are not used for gamma ray detection. The scintillation emission wavelength of a typical plastic has a maximum of about 400 nm. Plastics scintillators are characterized by a large light output and a short decay time, which makes them very suitable for fast timing measurements.

## 2.9 Beta emitters Following Fission Reactions:

Nuclear fission is defined as a process in which a heavy nuclide splits into two or more unstable, smaller atoms with comparable masses. As the result of instability, the reaction releases a large amount of energy as heat and radiation. This process can be divided into types of reactions: spontaneous fission and induced fission. In a nuclear reactor, fission reactions are triggered by neutrons, and most of fission products are beta emitters, which then decay by emitting beta particles to get to the stable state. Some of the beta emitters do not emit photons, known as “pure beta emitters”. Four different pure beta emitters are considered here: C-14, Sr-90, Y-90, and Tc-99.

### 2.9.1 Carbon-14:

Carbon-14 is a beta emitter with a half-life of 5,730 years, decaying to nitrogen-14 through beta decay by the following mechanism,

$$^{14}_{6}C \rightarrow ^{14}_{7}N + e^{-} + \bar{\nu} \qquad (2.7)$$

The maximum energy of the emitted particle is about 157 keV, whereas the average energy is 49 keV. In a nuclear reactor, C-14 could be produced by different neutron absorption reactions, with stable oxygen. Table 2-2 shows the most important routes for C-14 production.

**Table 2-2: Possible routes for C-14 production**

| Parent Isotope | Neutron Type | Reaction |
|---|---|---|
| $^{14}N$ | Thermal Neutron | $^{17}O(n,\alpha)^{13}C$ |
| $^{13}C$ | Thermal Neutron | $^{13}C(n,\gamma)^{14}C$ |
| $^{17}O$ | Thermal Neutron | $^{17}O(n,\alpha)^{14}C$ |
| $^{16}O$ | Fast Neutron | $^{16}O(n,\,^{3}He)^{14}C$ |

### 2.9.2 Technetium-99:

Technetium-99(Tc-99) is a beta source nuclide with half-life of 211,000 years and maximum energy of 0.294 Mev. This nuclide is produced in nuclear reactors with highly enriched uranium. It also can be generated by medical cyclotrons for medical imaging purposes. Tc-99 is considered the most significant long-lived product of uranium fission, generating the largest fraction of the total long-lived nuclear waste (http://en.wikipedia.org/wiki/Technetium-99). Figure 2-7 demonstrates the decay scheme of Tc-99 with the associated energy values, yield

fractions, and half-lives. Tc-99m with half-life of approximately 6 hours decays by emitting gamma rays to Tc-99, which then transforms, by emitting beta particles, to stable ruthenium, Ru-99.

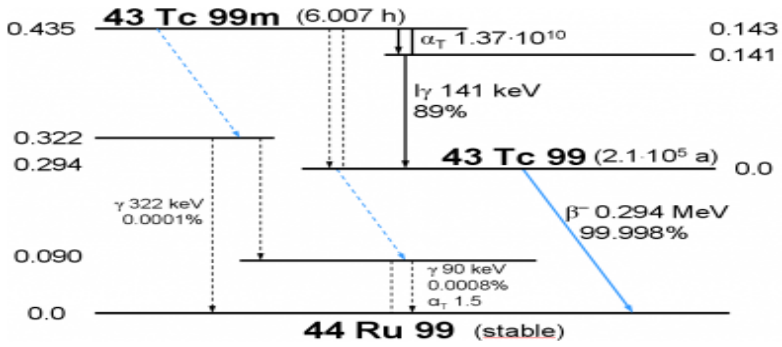


**Figure 2-7: Schematic of Tc-99 radioactive decay**

## 2.9.3 Strontium-90:

Strontium-90 is along-lived fission product. It has huge abundance in nuclear spent fuel, and so it is considered a waste product that could be found in the liquid waste of nuclear reactors. It undergoes pure beta decay with the half-life of 28.8 years and a maximum energy of 0.546 MeV as the schematic in Figure 2-8 displays. Strontium-90 is considered a pure beta emitter and it decays to Youtrium-90 (with a very weak gamma yield).

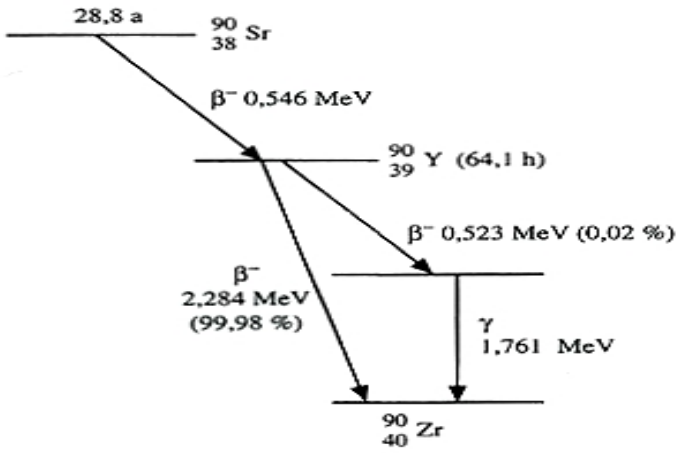


**Figure 2-8: Schematic of Sr-90 radioactive decay**

## 2.9.4 Yttrium-90:

Yttrium-90 is also a pure beta emitter essentially. It decays to zirconium-90 with a half-life 64 hours and maximum energy of 2.28 Mev, Figure 2.8. Yttrium-90 emits gamma rays with a yield of 0.02% (1.76 MeV), but this emission is insignificant and essentially ignored. When uranium is fissioned, Y-90 eventually makes up about 5% of the nuclear products. It also can be obtained by chemical high-purity separation from Sr-90.

# 3.0 Literature Survey

## 3.1 Early Studies for Beta Spectrometry:

Schier et al. (1997) developed a beta spectrometer to measure aggregate beta energy spectra of U-235, U-238, and Pu-239, as a function of decay time following neutron fission. In that study, only fission fragments with short decay times were considered. The resulting beta spectra from fission fragments with short decay times have continuous, but structureless shapes. His design consisted of a helium-jet system used to rapidly transfer the fission fragments from a fission chamber to a low background counting area. The fission fragments were deposited onto a moving tape, and then delivered to the spectrometer. Ideally, the helium-jet system should transfer all fission products with equal probability. It is important for this beta spectrometer to have a high degree of insensitivity to gamma rays, since gamma rays typically accompany beta decay of fission fragments. The design included the following properties:

1) compatibility with helium-jet system;
2) High degree of insensitivity to gamma rays;
3) Linearity to beta energy up to 10 Mev;
4) high energy resolution for beta particles;
5) minimum distortion due to edge effect; and
6) Simplicity of response function.

A plastic scintillator detector (3'x 3') with a thin window was used to meet the design features. A thin scintillator disk of a diameter 1.5" by thickness 0.020" was positioned at the face of the detector, which had been covered with a thin aluminum foil. When beta particles pass through

the scintillator disk, a signal is triggered in the main scintillator. Also, the distortion of the beta spectrum is due to some recoiling secondary electrons in beta particle stopping events escaping the main detector; this results in a scintillation pulse that does not represent the full beta energy. Therefore, by choosing a 1.5" diameter disk, most secondary electrons are kept away from the cylindrical wall of the detector and so they deposit their full energy in the main scintillator, which eliminates distortion in the beta spectrum due to edge effects.

O. Gurler et al. (2005) developed a study to investigate the energy distribution of beta particles interacting with a certain matter thickness experimentally and theoretically. This study measured the energy distributions of beta particles emitted from Ti-204 using a surface barrier solid state detector with depletion layer of 1 mm in thickness. The experimental and theoretical energy spectra were obtained using two different aluminum thicknesses for source cover, corresponding to 0.02g/cm^2 and 0.047g/cm^2. The energy spectra for each thickness were later compared. The source cover with a higher thickness resulted in a shift of the energy spectrum toward low energy region. The results obtained implied that the probability of measuring low energy beta particles is small because low energy particles do not have enough energy to penetrate the source cover. The results also indicated that high energy particles lose some of their energies as they penetrate though the medium.

Loidl et al. (2009) conducted a study to measure the pure beta energy spectrum of Pu-241 (maximum energy of 20.4 KeV) utilizing a metallic magnetic calorimeter (MMC). In this detector, the energy of a particle is counted in the form of a temperature rise, which is proportional to energy rise. The metallic magnetic calorimeter consists of a metallic absorber in tight thermal contact with paramagnetic thermometer. A magnetic field is applied to magnetize the thermometer. When a particle deposited its energy in the absorber, this energy is transferred

to the metals conduction electrons, causing a temperature rise in the absorber and the thermometer. Plutunium-241 source was placed between two thin gold foils (functioning as MMC absorber) to be measured. The obtained experimental spectrum was compared against the theoretical one. The results showed a good agreement between the two spectra at high energies; however, there has been a discrepancy observed at low energy region.

Farsoni and Hamby et al. (2005) introduced a triple-layer phoswich detector, which consists of BC-400, CaF2:Eu, BC-444 with decay time constants of 2.4, 940, and 264 ns, respectively. The detector was designed to model photon and beta particle interactions at each layer. The thickness of the first layer was designed to stop 0.1 MeV electrons, the second layer was designed to stop 1.0 MeV electron, and 2.5 MeV in the third layer. The energy deposition of mono-energetic beta particles in each layer was calculated using Monte Carlo N-Particle (MCNP) version 4B. For MCNP simulations, seven possible energy deposition tracks for electron energies less than 2.5 MeV in the triple-layer phoswich detector were modeled. Figure 3-1 displays the different scenarios of interactions along with the type of material and the thickness of each layer.

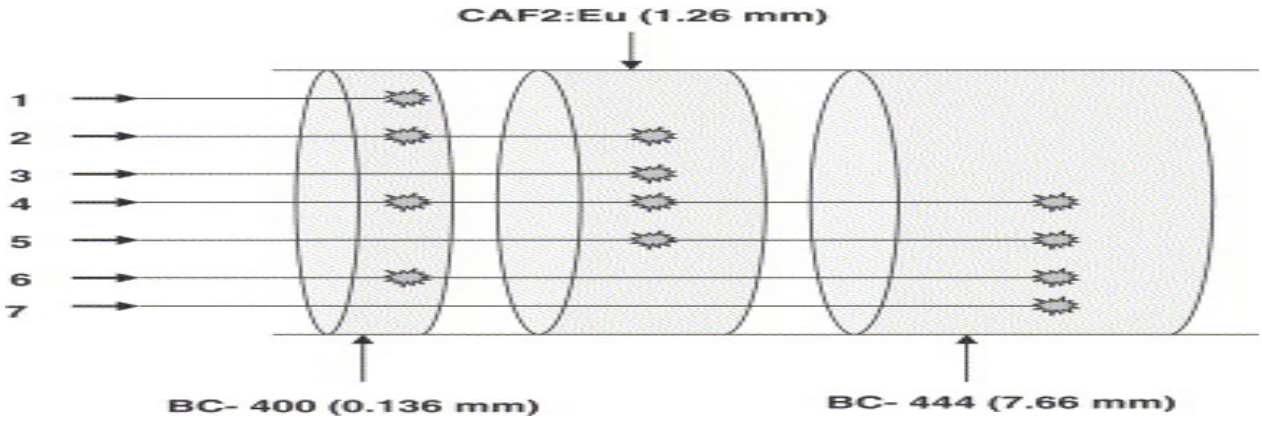


**Figure 3-1: Possible interaction scenarios occurring in different layers of the scintillator**

In the above figure, little stars represent beta particles energy released in each layer, which results in the production of a light pulse with amplitude above the detection threshold.

## 3.2 Phoswich Detectors:

A phoswich ("phosphor sandwich") is a combination of scintillators with dissimilar pulse shape characteristics optically coupled to each other and to a common PMT (or PMTs). Pulse shape analysis distinguishes the signals from the two scintillators, identifying in which scintillator the event occurred (Saint-Gobain crystals and doctors, n.d.).

Typically, a scintillation detector consists of scintillation material and a photomultiplier tube (PMT) or photodiode to convert scintillation light to an electrical signal pulse (Figure 3-1). The use of different scintillation materials, with different decay times, results in the generation of different output pulse timing characteristics from a pulse shape analyzer to discriminate between interaction scenarios (Farsoni, 2006). For example, the first layer, which usually a thin plastic scintillator, is used to detect beta and conversion electrons. The second layer is a CaF2 scintillator designed to detect low energy photons; and the third layer, NaI, is intended to measure high energy photons.

These types of detectors were originally designed to detect low-energy gamma and x-rays and also to detect high-energy alpha and beta particles in ambient background. Figure 3-2 displays a schematic of a triple-layer phoswich detector, shown the thickness of each layer and other dimensions of cylindrical detector.

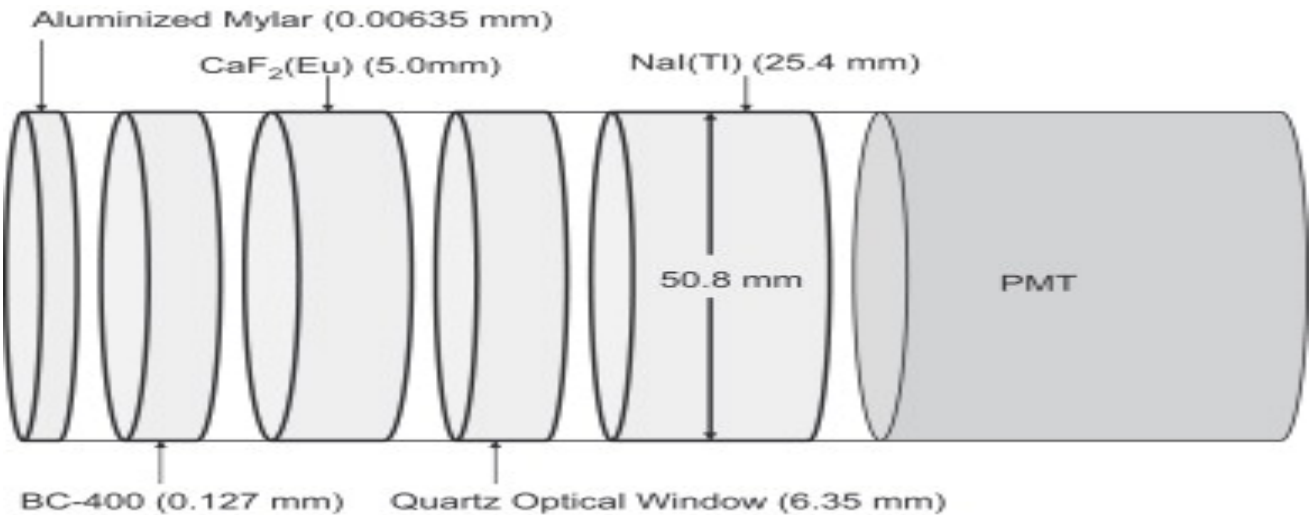


**Figure 3-2: Triple-layer phoswich detector for beta, X-rays, and gamma measurement**

## 3.3 Early Designs of Phoswich Detectors:

Bardelli et al. (2002) designed a triple-layer phoswich detector for measurement of fast charge particles. The design utilized three different scintillation materials, BC 404, BC 444 and CsI (T1). The decay time for each material were given as 1.8 ns, 180 ns, and ~100 ns, respectively. The sum of the three signals gives the anode signal of the detector. The energy loss of the impinging particle in each determines the relative amplitudes of the anode signal.

Usude et al. (1997) developed a triple-layer phoswich for alpha, beta, gamma, and fast neutrons measurements. The design is shown in the Figure 3-3. The analog pulse-shape discrimination technique was used to distinguish different pulses produced from different radiation types. The first layer, ZnS(Ag), is sensitive to alpha particles and it is almost transparent to the other radiation scenarios. Anthracene, which is the second layer, was meant to detect gamma, beta, and fast neutrons. This layer is also relatively transparent to thermal neutrons. Figure 3-4 shows the rise-time distribution measurements for various radiation interactions occurring at different

materials in this detector. Different interactions have differing rise time, and each radiation interaction type could be by distinguished by its corresponding rise time.

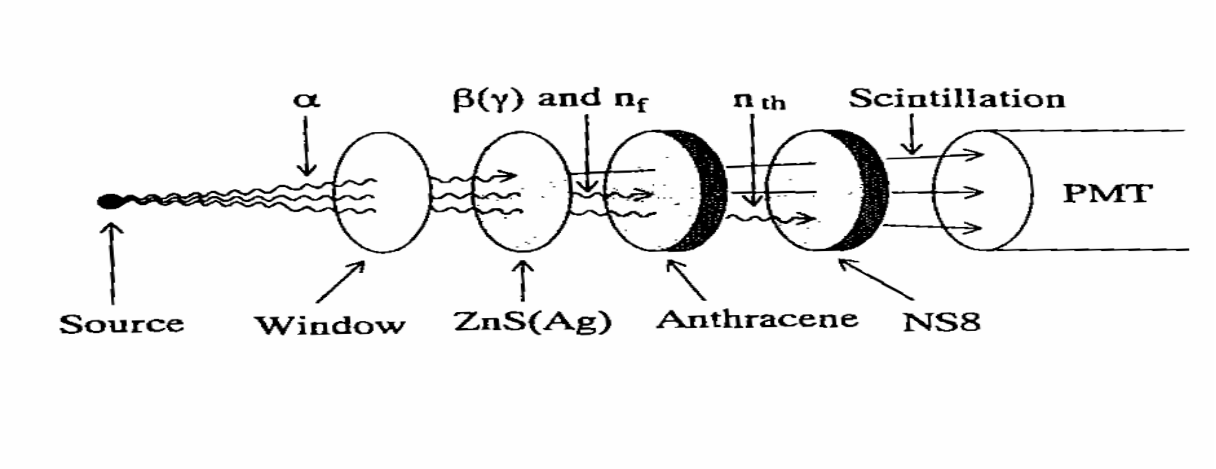


**Figure 3-3: Scintillator designed to measure alpha, beta, gamma, and fast neutrons**

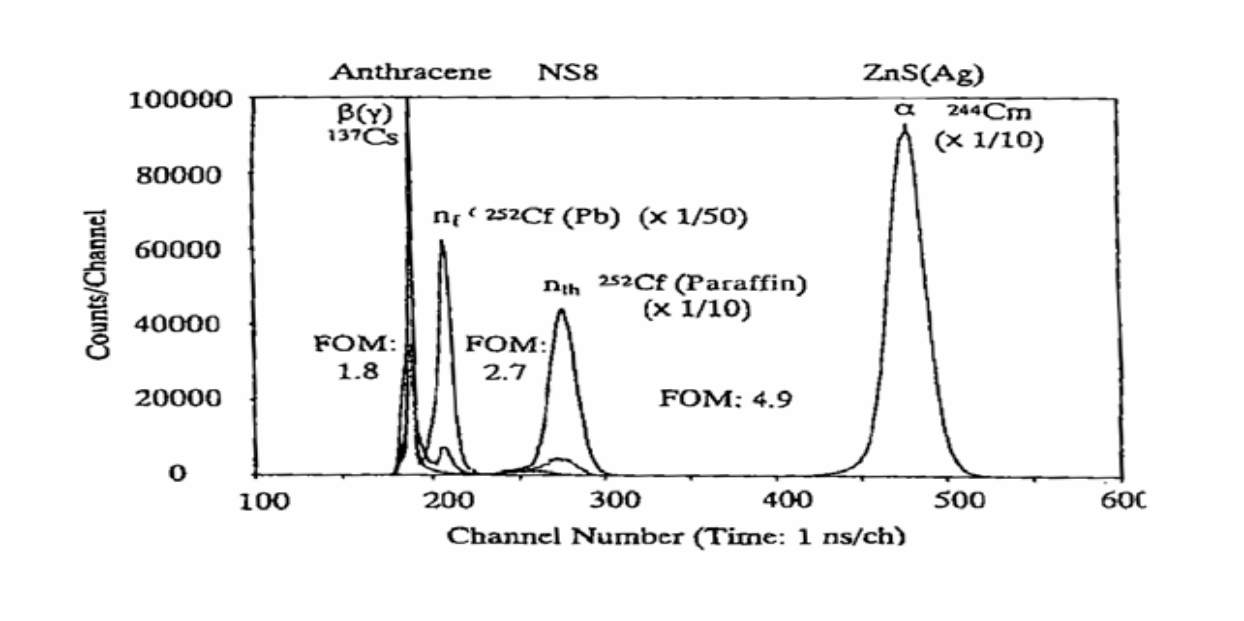


**Figure 3-4: Rise-time distribution for photons and particles interactions in various layers**

Childress et al. (2002) has developed a triple crystal phoswich detector for alpha, beta, and gamma radiation measurements. The design contained a ZnS:Ag, a CaF2:Eu, and a NaI:Tl layers for alpha, beta, and gamma radiations detection, respectively. This work utilized the usability of a triple crystal phoswich detector to determine energy thresholds and beta/gamma

crosstalk probabilities. In this study, low energy beta, < 0.250 MeV, and gamma radiation, < 0.05 MeV, were found to be undifferentiable.

Bubble Technology Industries (BTI) has designed a complete suite of probes for gamma, X-rays, neutrons and beta measurements. The BTI B-probe is a portable phoswich scintillator that was developed to detect beta particles with spectral range from 0.1 MeV up to 3 MeV. This portable detector has a gamma rejection ration of > 50:1, and it is capable of eliminating distortions in beta energy spectra due gamma interference. The beta energy spectra measured by B-PROBE was shown to highly agree with theoretical spectra.

Farsoni et al. (2006) designed a triple-layer phoswich detector based on the previous MCNP analysis of a prototypic phoswich detector (Farsoni and Hamby 2005) but with different materials. This detector was constructed to simultaneously measure beta and gamma energy spectra with minimal cross-talk. The materials used for this detector were: a thin plastic scintillator (BC-400) for first layer, an inorganic crystal (CaF2:EU) as the second layer, and third layer is an inorganic scintillator (NaI:T1). The first two layers were chosen to specifically detect beta particles with energies up 3.2 MeV, whereas the third one was chosen to measure gamma rays. This design was used in conjunction with a customized digital pulse processor (DPP).

Farsoni et al. (2012) used phowich technology to design a detector for measuring beta-gamma coincidence events from xenon radioisotopes. This approach was meant to measure ultra-low concentrations of radioxenon in the atmosphere with very low sensitivity to background radiation. This detector consists of three scintillation layers: BC-400, CSI (Tl), and BGO. The design was based on another design called the Actively-Shielded Phoswich Detector (ASPD) with Compton suppression capability. To improve the system in measuring beta and gamma

coincidence events and xenon radioisotopes, real time digital pulse processing firmware was developed using a Field-Programmable Gate Array (FPGA).

# 4.0 Materials and Methods

A triple-layer phoswich detector was designed and built to simultaneously measure the beta particle and gamma ray energy spectra with minimal cross-talk (Farsoni and Hamby, 2007). The detector can also be used to collect beta/gamma coincidence events employing a digital pule processing scheme. The first two layers, BC-400 and $CaF_2$ , are used for beta measurements; whereas the third layer, NaI, is used for gamma-ray spectroscopy (Figure 4-1).

The following sections will discuss the design of this detector and the materials used, and introduce the Monte Carlo N-Particle (MCNP) detector model that was developed in this research to simulate electron interactions in the first and second layers (i.e., the beta detector).

## 4.1 Triple-Layer Phoswich Detector Design:

The design consists of three layers of different scintillation materials. The first layer is chosen to be a thin plastic scintillator (BC-400), which has the fastest decay time. The second layer is an inorganic crystal ($CaF_2$(Eu)), which has a much slower decay time. The first two layers were designed to measure beta particles, and both layers together are capable of stopping beta particles with energies up to 3 MeV. The third layer is also an inorganic scintillator (NaI(Tl)), and is used to measure gamma rays. Table 4-1 shows the physical properties of each material in the detector:

**Table 4-1: The properties for each layer's material**

| Scintillator | Density (g/cm^3) | Wavelength (nm) | Light Output (% of NaI) | Decay Constant | Index of Refraction |
|---|---|---|---|---|---|
| BC-400 | 1.032 | 423 | 26 | 2.4 | 1.58 |
| CaF2(Eu) | 3.19 | 435 | 50 | 900 | 1.47 |
| NaI(Tl) | 3.67 | 415 | 100 | 230 | 1.85 |

Figure 4-1 exhibits each layer in this detector with the corresponding thickness values.

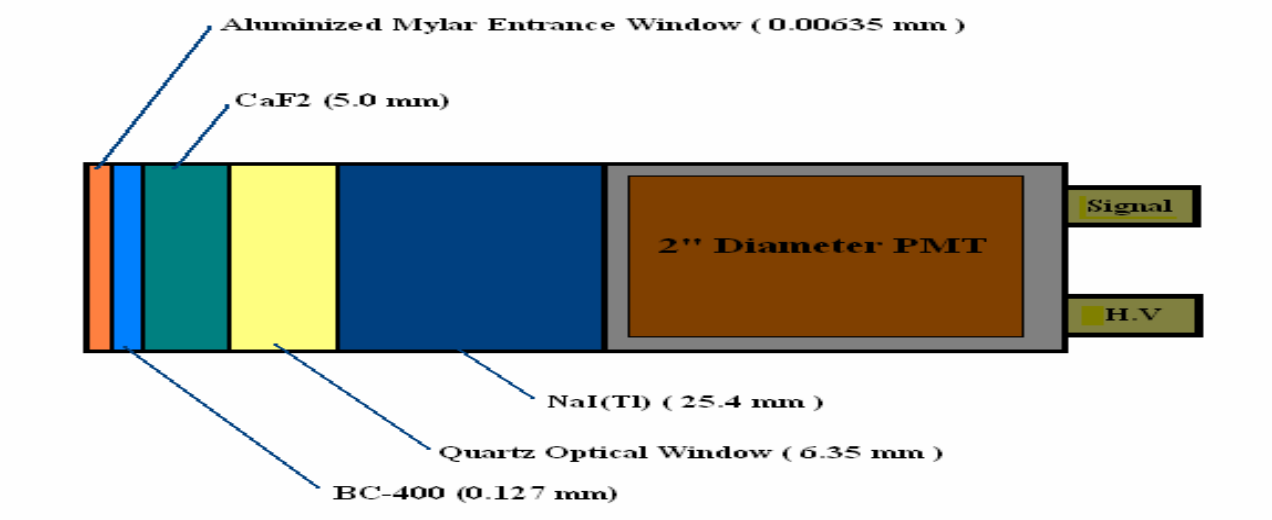


**Figure 4-1: Schematic of triple-layer phoswich detector**

The scintillator is capable of detecting different combinations of events of beta particles and gamma rays. The interaction pattern depends on how a given particle or photon releases its energy within each layer. Table 4-2 displays different combination of possible interactions in the layers.

**Table 4-2: Seven possible interaction scenarios for photons and beta particles**

| Event | Scintillation Layers | | | Type of Interaction |
|---|---|---|---|---|
| | BC-400 | CaF2 | NaI | |
| 1 | * | | | Beta Interaction |
| 2 | * | * | | Beta Interaction |
| 3 | | * | | Compton Scatter |
| 4 | | * | * | Compton Scatter |
| 5 | * | | * | Compton Scatter |
| 6 | * | * | * | Compton Scatter |
| 7 | | | * | Gamma-ray |

The stars in the table above indicate the layer in which interactions occur. Depending on the amount of energy, a particle/photon will deposit its energy in various ways. In the first and second event patterns, the most likely event is that a beta particle interacts in the first layer or in the first and second layers. The third, fourth, fifth, and sixth events, show interaction possibilities due to Compton scattering. The last event represents the interaction of a gamma ray in the third layer. For the purpose of this study, only interactions in the first and second layers (events 1 and 2) will be considered. Only beta measurement is of interest here. Even though the second layer is designed for the detection of beta particles, incident gamma photons have a considerable probability of interacting in this layer (Farsoni, Hamby, 2005).

## 4.2 Electron Range:

Four radionuclides, pure beta emitters, are considered in this research (C-14, Tc-99, Sr-90, Y-90). The energy values for each radionuclide range from 0 to the maximal available energy. The maximum depth of penetration into the medium depends on the maximum energy of each beta emitter and the density of the absorbing material. The maximum energy of each radionuclide and its penetration depth in each layer are presented in Table 4-3.

**Table 4-3: Maximum energies versus ranges of interaction in the beta detector for all four nuclides**

| Nuclides | Energy (MeV) | Range (g/cm^2) | Range in First layer (cm) | Range in Second layer (cm) |
|---|---|---|---|---|
| C-14 | 0.153 | 0.0271 | 0.0263 | 0.0085 |
| Tc-99 | 0.286 | 0.0724 | 0.0701 | 0.0227 |
| Sr-90 | 0.537 | 0.178 | 0.172 | 0.0558 |
| Y-90 | 2.28 | 1.073 | 1.040 | 0.336 |

The thickness of the first layer, BC-400, is 0.127 mm, and the thickness of 5.0 mm is used for the second layer, $CaF_2$. As shown in the Table 4-3, all electrons (except initial energies less than 0.1 MeV) are expected to interact in the first layer and penetrate through to the second layer where they will be completely stopped. The two layers together were designed to stop particles with energies up to 3.0 MeV.

## 4.3 Nuclide Data and Energy Spectra:

Table 4-4 provides the basic information for each one of the four radionuclides used in this study. As indicted, all radionuclides are pure beta emitters with yields of 100%. They all have long half-lives with the exception of Y-90 (in secular equilibrium with Sr-90).

**Table 4-4: Radionuclides data**

| Radionuclide | Half-Life (year) | Energy (Kev) | Emission Type | Yield (%) |
|---|---|---|---|---|
| C-14 | 5734 | 156.5 | Beta | 100 |
| Tc-99 | 2.1E+05 | 293.5 | Beta | 100 |
| Sr-90 | 28.8 | 546.2 | Beta | 100 |
| Y-90 | 0.007 | 2281.4 | Beta | 100 |

The beta energy emission spectrum for each of the radionuclides is provided in the Figures, 4-2 to 4-5. These energy emission distributions were utilized as input to the MCNP model.

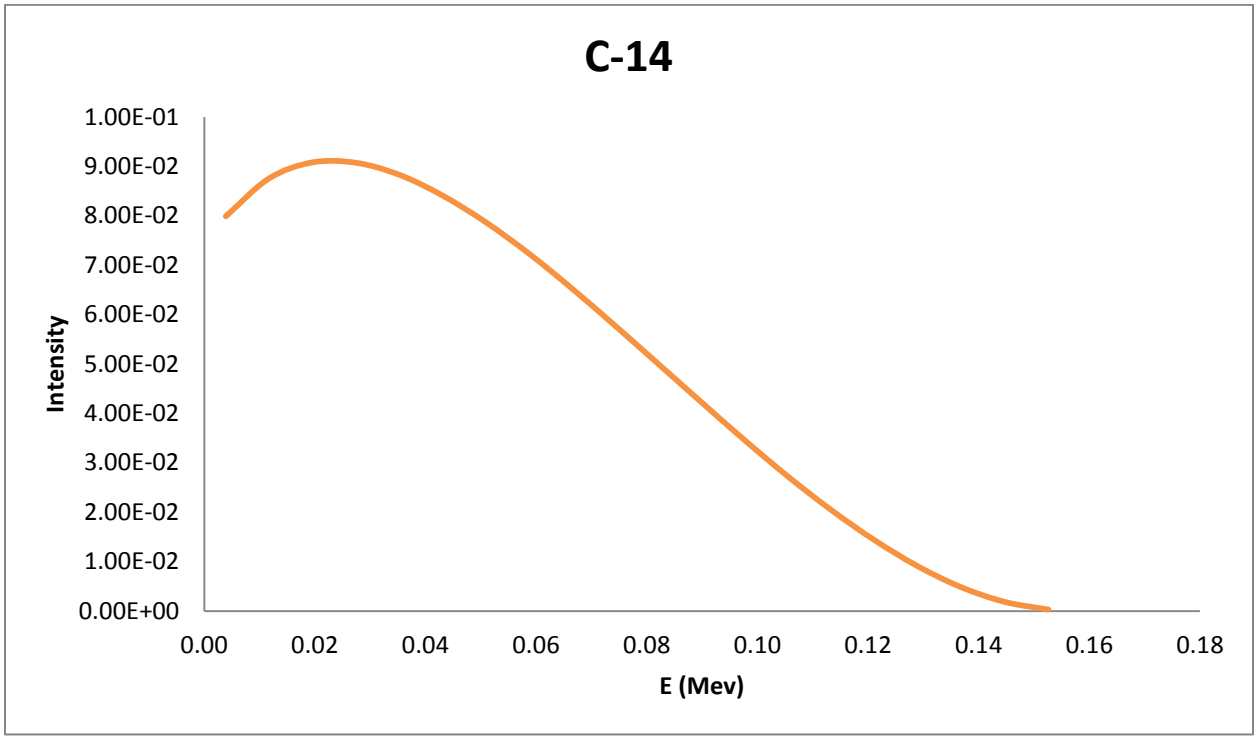


**Figure 4-2: C-14 beta energy emission spectrum**

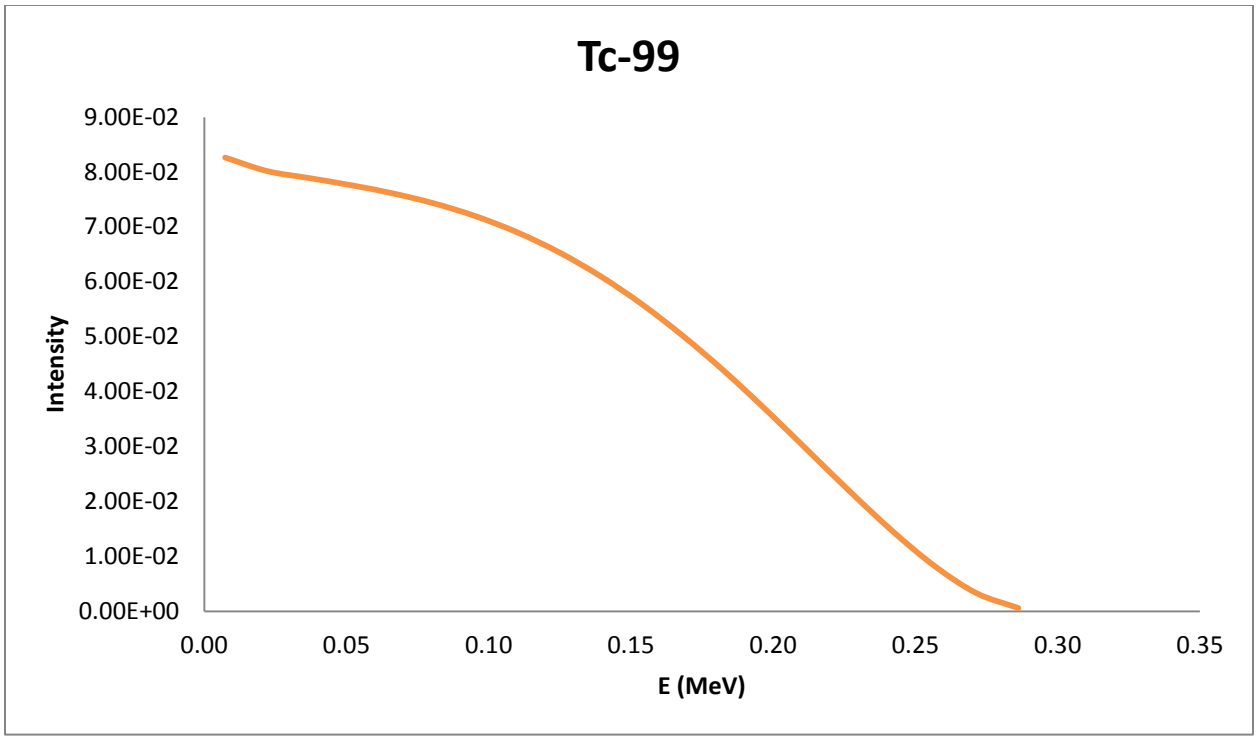


**Figure 4-3: Tc-99 beta energy emission spectrum**

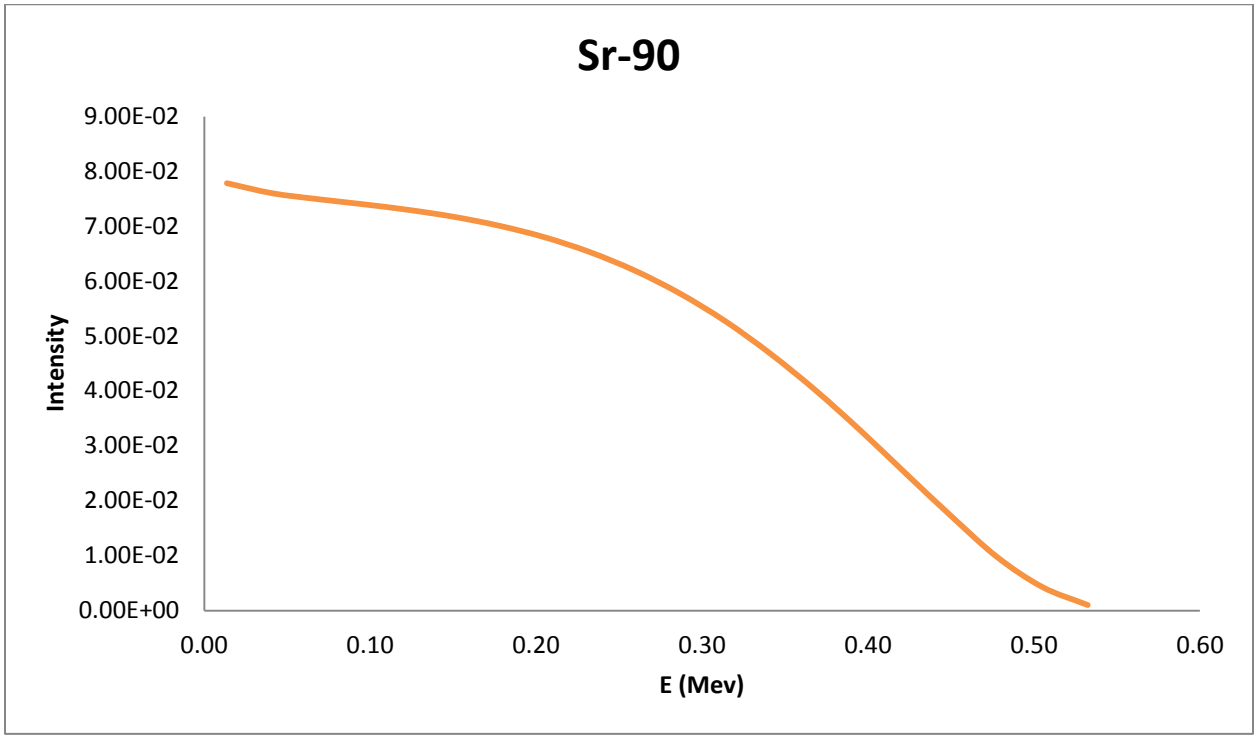


**Figure 4-4: Sr-90 eeta energy emission spectrum**

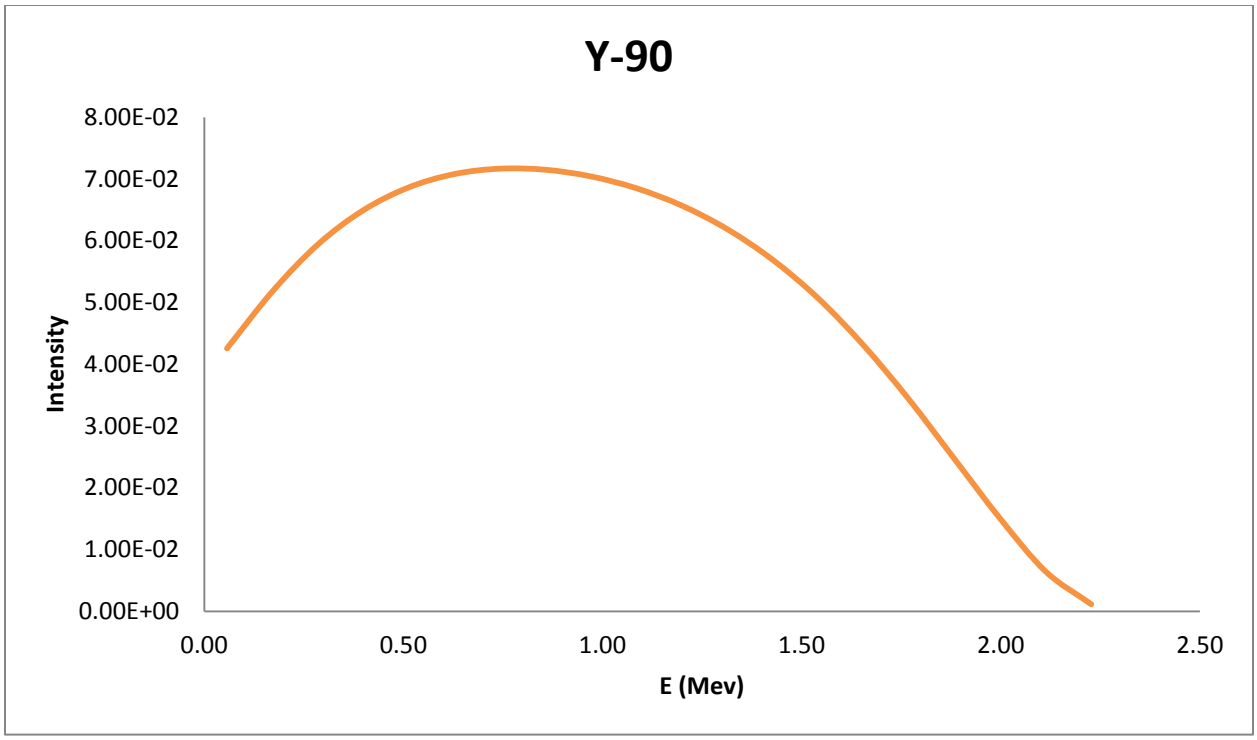


**Figure 4-5: Y-90 beta energy emission spectrum**

## 4.4 Monte Carlo N-Particle (MCNP) Code:

The Monte Carlo N-Particle code is a general software package that is typically used for calculating nuclear interactions during photon, electron, and neutron transport (LANL, 2009). The code can be applicable in, but not limited to, radiation protection, dosimetry, radiation shielding, detector design and analysis, medical physics, nuclear criticality safety, and fission and fusion reactor design. For the purposes of this study, the MCNP code was utilized to simulate the triple-layer phoswich detector and the electron interactions in the beta detector (first and second layers).

### 4.4.1 MCNP Model and Inputs:

MCNP input files were developed to simulate electron interactions in the beta detector. This simulation calls for the probabilities of particles interacting in each scintillation layer (the MCNP "F8" Tally) for a given set of energy intervals. The simulation tracks each particle interacting in a defined volume, and produces the probability of interaction per particle for a given set of energy intervals. Separate simulations were defined for the layers of interest to model the detector response (energy absorption distributions of beta interactions for a given set of energy intervals). For all MCNP runs, intervals of 1.25E-02 MeV were applied. The range of the energy intervals was defined to include the largest possible energy value for a given nuclide. The simulations performed full transport computations for electrons in the beta detector; Bremsstrahlung photons were assumed not to be significant for energy deposition.

In the simulation, a disk source parallel to the face of detector was modeled. The radius of the source was set equal to the radius of the detector (2.54 cm) and the thickness of the disk was assumed to be 6.5E-4 cm, same as the thickness of the mylar, to reduce possible absorption in mylar. The source was set to simulate combination of the beta energy emission distributions of the four beta emitters. The MCNP input file for each scenario is provided in the appendix.

### 4.4.2 Simulation of Phoswich Detector with a 2D disk source:

In this simulation, the activity of a two-dimensional disk source includes emission from all four radionuclides at varying activity contributions. This isotropic emission of beta particles from the source was modeled to generate mixed emission source spectra for the studied nuclides. The source was placed 1 cm from the face of the detector perpendicular to the detector longitudinal axis. The gap between the detector and the source was chosen to include only air. In order to

obtain the total beta energy deposition probability in the beta detector for a given energy interval, the first and second layers (beta detector) were defined as one cell. Other layers, in the cylindrical detector, were defined as separate cells. Beta particles were tracked in all designated layers and in the spherical space within 50 cm of the detector.

### 4.4.3 Simulation of Phoswich Detector with a 3D cylindrical source:

In this simulation, the radioactive source was uniformly distributed in a three-dimensional cylindrical filter paper with thickness of 0.3 cm. The diameter of the paper was equal to the diameter of the detector face (5.04 cm). The gap between the face of the detector and the source was designed to have cylindrical shape with the same diameter, but with a thickness of 1 cm. This gap was made to include only air. The model was designed to study the effect of self-absorption on the beta energy absorption distribution.

### 4.4.4 MCNP Inputs:

The probability histogram of the beta energy emission distribution over a set of intervals for each nuclide was integrated and normalized to unity (1). This process allowed setting all energy emission probabilities for all four beta emitters to a constant rate. The polynomial function for each normalized emission spectrum was generated, assuming each energy emission spectrum followed a continuous distribution. The values of each energy interval, within an increment of 1.25E-2 MeV, were entered into the functions ranging from 0 to the maximum available energy, which set all spectra to the same energy scale. The outputs of the functions (normalized beta energy emission probability) for each spectrum were multiplied by a multiplication factor (MF), representing the percentage of a radionuclide presence in a source mixture. The product of this multiplication yielded the relative abundance contribution of each radionuclide into the mixed

energy emission source spectrum. The relative abundance contributions for all four radionuclides were summed together, for each energy interval, to obtain the mixed energy emission source spectrum, total abundance of all nuclides, (Table 4-5). The obtained mixed energy emission source values were used later in the MCNP inputs to determine the detector response and regenerate the mixed beta energy absorption spectrum (multi-response distribution) as measured by the detector. The functions describing emission probability per energy interval are provided for each radionuclide, Figure 4-6 to Figure 4-9.

**Table 4-5: Curves functions and abundance equations developed in spreadsheet**

| Nuclide | Energy Emission Curve Function | MF | Abundance (Ab) |
|---|---|---|---|
| C-14 | $Y_{C-14} = 11489x^3 - 3006.7x^2 + 123.61x + 10.519$ | $MF_1$ | $Ab_{C-14} = (Y_{C-14})(MF_1)$ |
| Tc-99 | $Y_{Tc-99} = 3451x^4 - 1795x^3 + 214.7x^2 - 16.17x + 5.986$ | $MF_2$ | $Ab_{Tc-99} = (Y_{Tc-99})(MF_2)$ |
| Sr-90 | $Y_{Sr-90} = 163.3x^4 - 170.5x^3 + 43.88x^2 - 5.378x + 3.051$ | $MF_3$ | $Ab_{Sr-90} = (Y_{Sr-90})(MF_3)$ |
| Y-90 | $Y_{Y-90} = 0.0315x^4 + 0.0686x^3 - 0.4013x^2 + 0.7247x + 0.3499$ | $MF_4$ | $Ab_{Y-90} = (Y_{Y-90})(MF_4)$ |
| SUM | | | $Ab_{sum} = Ab_{C-14} + Ab_{Tc-99} + Ab_{Sr-90} + Ab_{Y-90}$ |

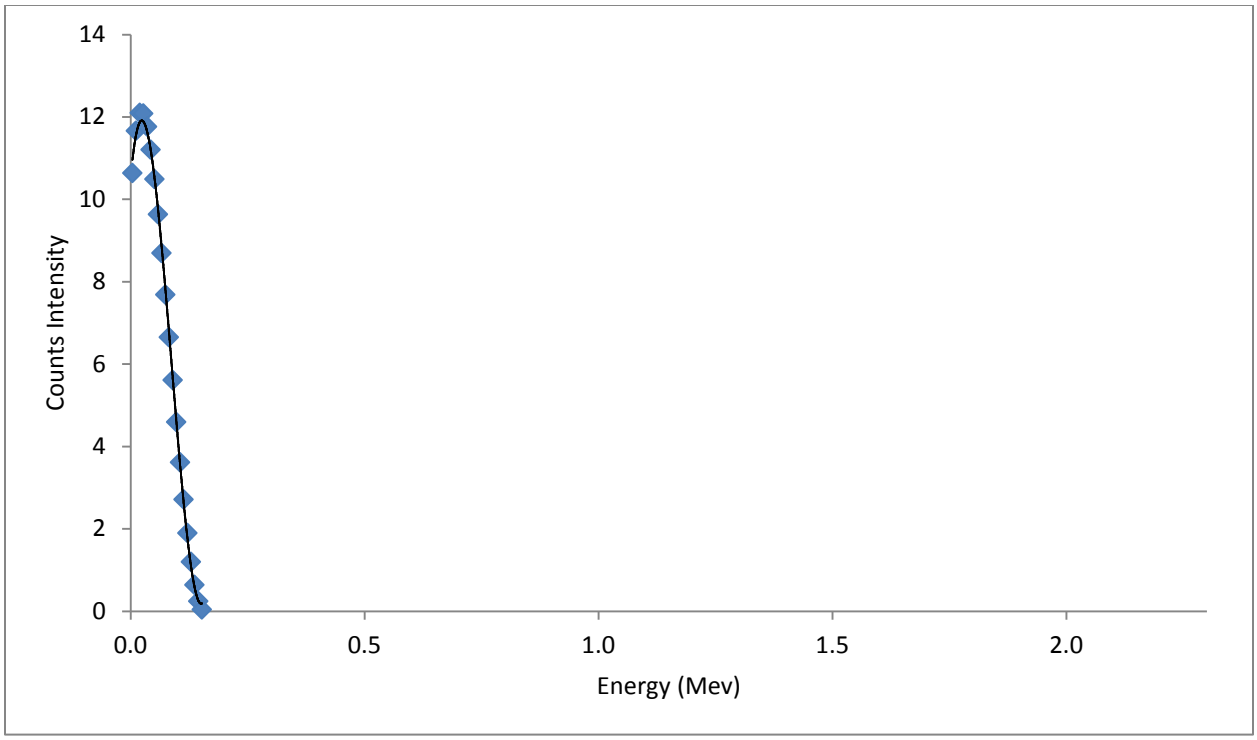


**Figure 4-6: C-14 normalized beta energy emission spectrum**

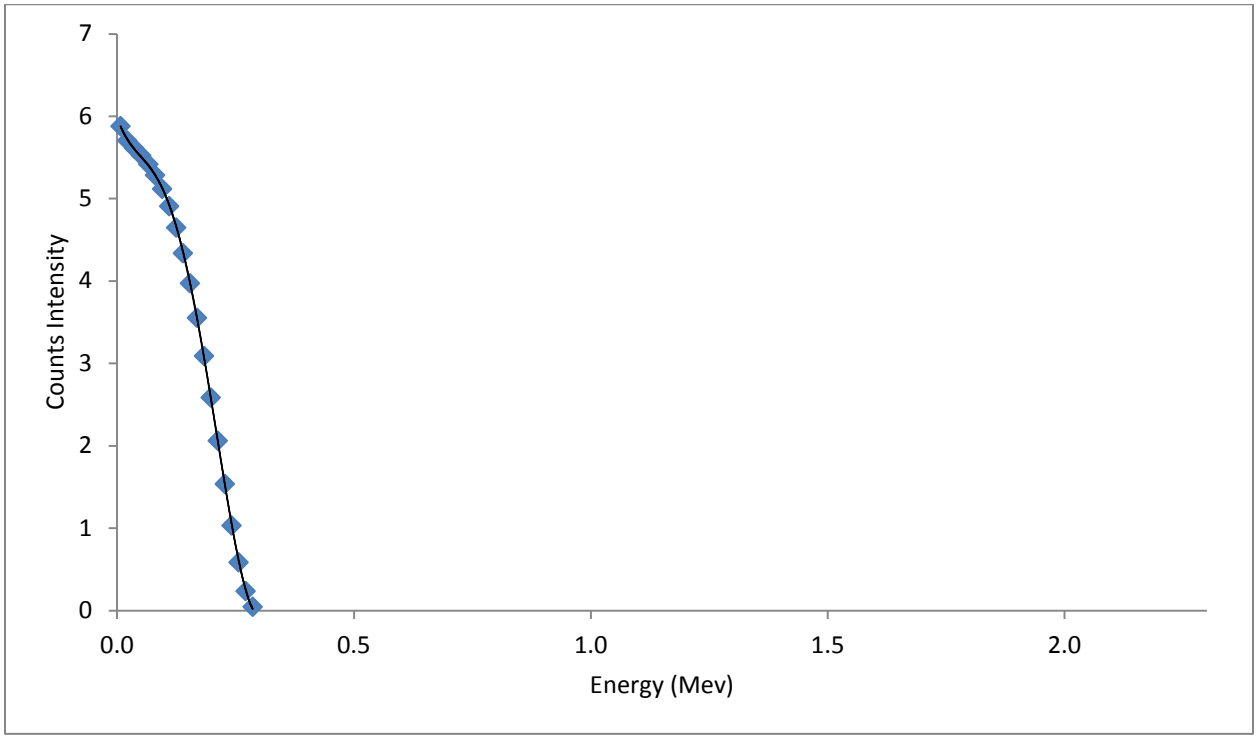


**Figure 4-7: Tc-99 normalized beta energy emission spectrum**

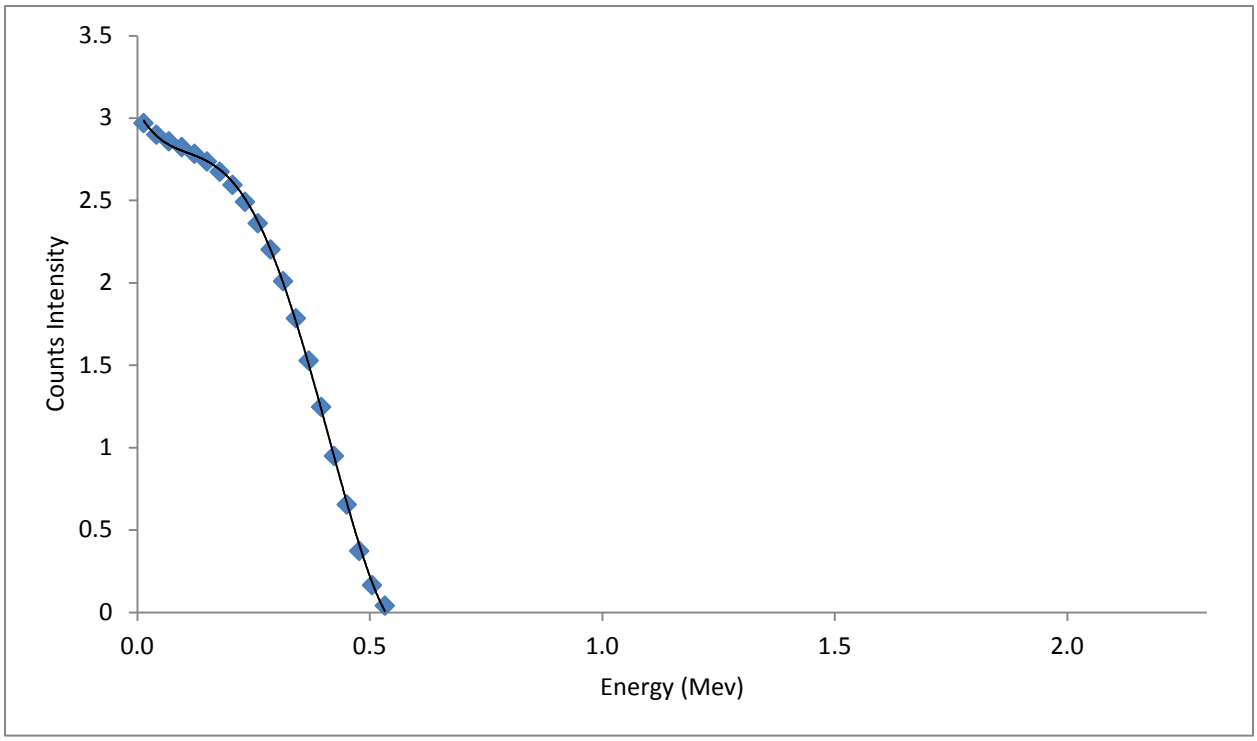


**Figure 4-8: Sr-90 normalized beta energy emission spectrum**

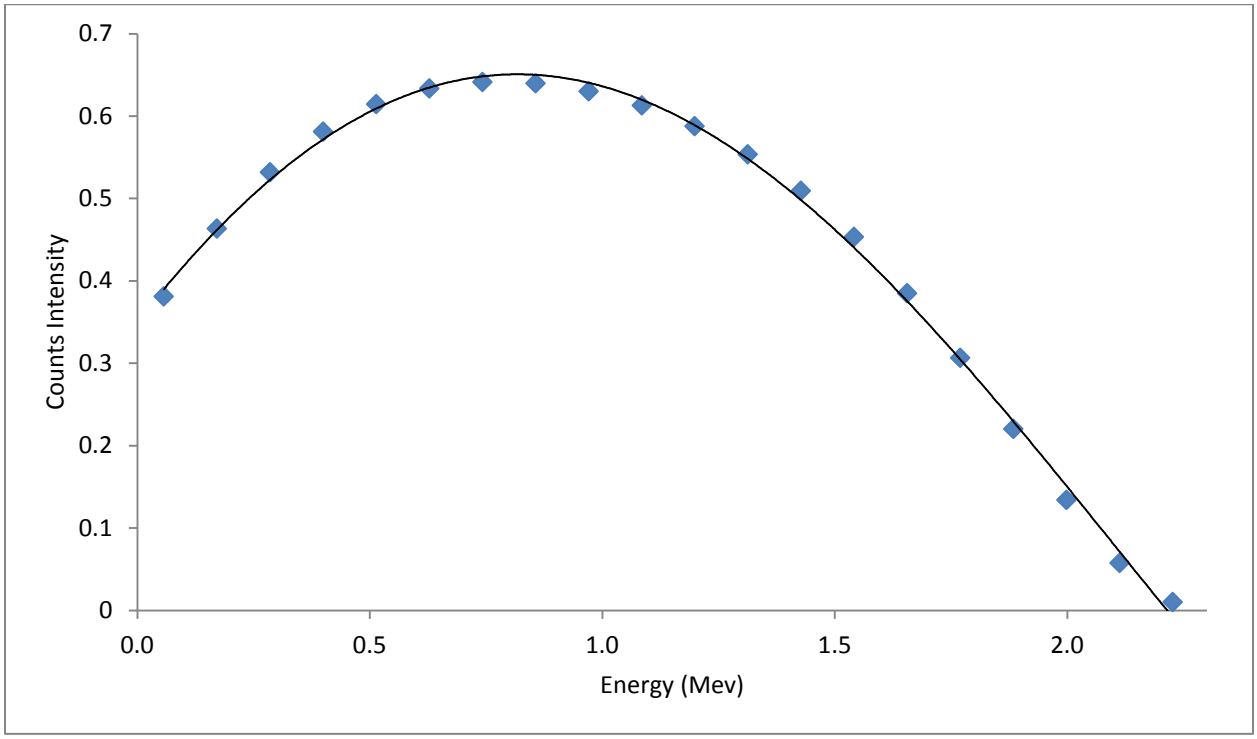


**Figure 4-9: Y-90 normalized beta energy emission spectrum**

The materials simulated in the MCNP model are shown in Table 4-6. The casing material is aluminum, as shown, along with its Z-value of the material and weight fractions.

**Table 4-6: The materials used in MCNP model**

| Material | Z-value | Weight Fraction | Atom Fraction |
|---|---|---|---|
| Aluminum | 13 | 1 | |
| Air | 8<br>6<br>7<br>18 | 0.00012<br>0.75527<br>0.23178<br>0.01283 | |
| Mylar | 6<br>1<br>8 | 0.625017<br>0.041959<br>0.333025 | |
| BC-4000 & CaF2 | | | 0.01577<br>0.01740<br>0.64455<br>0.32228 |
| Quartz | 14<br>8 | 0.4674<br>0.5326 | |
| NaI | 11<br>53 | 0.15337<br>0.84663 | |
| Glass | 5<br>8<br>11<br>13<br>14<br>19 | 0.04006<br>0.53956<br>0.02819<br>0.01164<br>0.37722<br>0.00332 | |

## 4.4.5 MCNP Scenarios:

The MCNP model was utilized to generate a beta energy absorption probability spectrum for a single radionuclide (individual response distribution). The beta energy emission distribution values for a single nuclide provide the input for MCNP and run separately to produce individual detector response distributions. Then, the beta energy emission distribution values for all four radionuclides were summed together and input into MCNP to produce mixed energy absorption

probability spectra (multi-response distributions), containing the four radionuclides with varying contributions, based on an individual response. The individual response distribution of each radionuclide was meant to be compared against the multi-response one for spectral stripping purposes. This process allows identifying radionuclides from their maximum energy values (endpoint energy), measuring the percentage of each radionuclide presented in the sample, and determining their contribution to the total abundance. All energy absorption spectra were measured as beta particles being directly emitted from a 2D disk source. For electrons with energy higher than 0.5 MeV, 9,000,000 source electrons, or more, were modeled. But, for electrons less than 0.5 MeV, 3,000,000 source electrons were enough to yield relative errors of 5% or less in higher energy bins.

This study included nine different scenarios of two or more source radionuclides. Every scenario includes variations in radionuclide contributions to the mixed emission source distributions. These nine scenarios were chosen to be representative of possible irradiated samples containing mixtures of fission products following fission reactions in real world nuclear reactors.

### 4.4.6 MCNP Runs:

The first scenario in this model included a combination of all four radionuclides. Figure 4-10 shows the relative contribution of each radionuclide available in the sample, such that there is 90% more C-14 than the other three nuclides, which were set to have the same abundance contribution in the source.

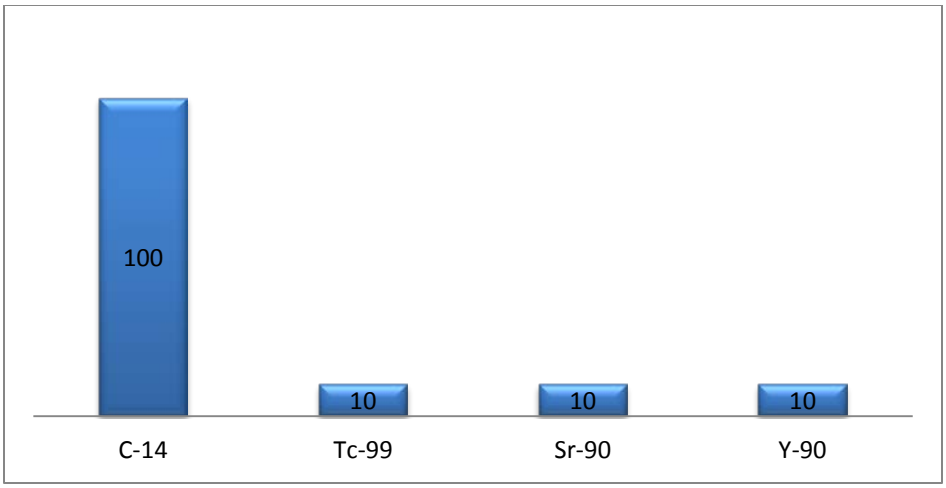


**Figure 4-10: Nuclides relative contributions present in scenario #1**

The relative contribution of each radionuclide for all scenarios is provided in Table 4-7. Each scenario was studied and analyzed individually. For visual representation, the bar graph of each case is provided in the appendix.

**Table 4-7: Nuclides relative contributions in each scenario**

| Scenarios | Multiplication Factors | | | |
|---|---|---|---|---|
| | C-14 | Tc-99 | Sr-90 | Y-90 |
| 1 | 100 | 10 | 10 | 10 |
| 2 | 10 | 100 | 10 | 10 |
| 3 | 10 | 10 | 100 | 10 |
| 4 | 10 | 10 | 10 | 100 |
| 5 | 10 | 10 | 10 | 10 |
| 6 | 0 | 100 | 50 | 50 |
| 7 | 100 | 0 | 0 | 50 |
| 8 | 100 | 50 | 0 | 0 |
| 9 | 0 | 100 | 50 | 0 |

## 4.4.7 MCNP Outputs:

The outputs obtained from MCNP provide the probability histograms of energy absorption versus energy intervals. The energy absorption probabilities (detector response distribution) were

plotted for a set of energy intervals ranging from 1.25E-2 MeV to maximum available energy. The plot is assumed to be continuous, representing the beta energy absorption probability per particle emitted for every energy interval, comprising the relative contributions of the four radionuclides. The probability values only in the beta detector (the first and second layer) were plotted here.

The absolute efficiencies were computed as a function of electron energy. The absolute efficiency for the beta detector was defined as the total probability that an electron releases any energy in the detector, the area under the probability curve (equation 4-1). The sum of all probability values for all energy bins yields the absolute efficiency for each scenario.

$$Absolute\ effciency = \Sigma Probablites\ of\ Interactions \tag{4-1}$$

For every scenario, the total emitted activity from the point source was defined to be equal to the number of source electrons in that scenario. The energy absorption probabilities were scaled up through multiplying each absorption probability value per beta particle, at a given energy interval, by the total "activity". The product of the multiplication gives the absorption rate, given in absorption per second. Equation (4-2) shows the relationship used to generate the interactions rates.

$$\dot{ABS}[\sec^{-1}] = (\sum A[\frac{\beta}{\sec}]) \times (\mathrm{P}[\beta^{-1}]) \tag{4-2}$$

Where $\dot{ABS}$ : Absorption rate in mixed energy absorption-rate spectrum

$\Sigma A$ : Total activity in the spectrum

P: Probability of absorption

## 4.5 Spectral Stripping Process:

The multi-response distribution was stripped and analyzed based on individual response. The absorption rates for each radionuclide were plotted against the mixed energy absorption- rate spectrum and then each portion in the graph pertaining to its corresponding radionuclide was numerically subtracted. The radionuclide with the highest energy bin value was subtracted first to be removed from the spectrum. The same process was completed for each radionuclide, one after another until no radioactivity is present in the mixed energy absorption-rate distribution. This method leads to identifying possible radionuclides available in the sample and also quantifying the activity for each.

The probability of absorption for individual nuclides (individual response distribution) is plotted against the energy intervals on the mixed energy absorption- rate spectrum. The probability of absorption plot (individual response distribution) for each nuclide was then scaled up to match and be comparable to the mixed energy absorption rate distribution. This scaling method was done by multiplying each absorption probability value by a multiplier (equation 4-3). The absorption rate is given as the number of beta particles absorbed in the detector per second.

$$\dot{abs}[\sec^{-1}] = (M[\frac{\beta}{\sec}]) \times (P[\beta^{-1}]) \tag{4-3}$$

Where $\dot{abs}$ : Individual absorption rate

M: The multiplier signifying the of relative activity of a nuclide in the mixed source

P: Probability of absorption

By choosing different multiplier values, we can find a value that gives rise to the best fit of tails on the two curves, an individual absorption-rate curve and the mixed energy absorption-rate curve. When matching occurs between the tails of the two curves, the multiplier value indicates the relative activity contribution for that radionuclide presents in the mixed source. The percentage of activity contribution for all radionuclides is equivalent in magnitude to the percent of relative abundance contribution for each radionuclide in the mixed energy emission source spectrum.

The radionuclide with greatest energy will be subtracted first and fit exactly to match the tail of the mixed absorption spectrum. When both tails are on a good match, or nearly matching, on one another, the values of the single radionuclide will be subtracted from the mixed energy absorption spectrum, which leaves the spectrum with a shorter tail and lower energy value. This process opens the door for another radionuclide of lower energy to come in and fit the tail and be subtracted from the residual spectrum of the mixed energy absorption graph, again. After that, our next candidate radionuclide with maximum energy will be plotted and brought to lie exactly on the tail of the spectrum to be removed. This elimination continues until no radioactivity is presented at the studied spectrum. The subtraction and stripping process will be on Excel using the following function, (equation 4-4).

$$RS = IF\,[CR\,(General) - CR\,(Individual\ Nuclide) < 0,\ 0,\ CR\,(General) - CR\,(Individual\ Nuclide)] \quad (4\text{-}4)$$

Where RS: Residual of the Original energy spectrum for all radionuclides

CR: (General) is counts rate for general spectrum

CR: (Individual Nuclide) is counts rate for an individual nuclide

The IF function will ensure elimination of any negative values that may appear in the resulting energy spectrum. Since the energy spectrum cannot have negative values, any negative difference between the general and single nuclide graph will be ignored and assumed to be zero.

# 5.0 Results and discussion

The results obtained from computer simulation provide the beta energy absorption probability per particle, occurring in the beta detector, from the source for a given energy (detector response distribution). The obtained multi-response distributions were analyzed and stripped based on the individual response for all studied scenarios as explained in the materials and methods section. The results for scenario #1 and #2 are provided and discussed individually in the following subsections. The results for remaining scenarios (tables and figures) appear in the appendix.

## 5.1 Scenario #1:

The beta energy absorption probability spectrum (multi-response distribution) was plotted for a set of energy bins ranging from 0 to 2.3 MeV (the maximum available energy) (Figure 5-1). This distribution indicates the probability of an emitted beta particle releasing its energy in the beta detector. The probability distribution of energy absorption indicates that for this scenario the most probable absorbed energy in the detector is 0.04 MeV (the peak of the probability curve). The most significant component of the probability plot shifts toward the lower energy region, as C-14 has the highest contribution to the spectrum in the first scenario. The energy absorption probability distribution has a similar shape to the energy emission probability distribution, which is expected. The small difference between the two distributions is attributed to energy loss and absorption in the air gap and mylar layer at the face of the detector.

The absolute efficiency for the beta detector was defined as the total probability that an electron deposits its energy in the detector, which is the area under the probability curve. The sum of all probability values for all energy intervals yielded the absolute efficiency for each scenario.

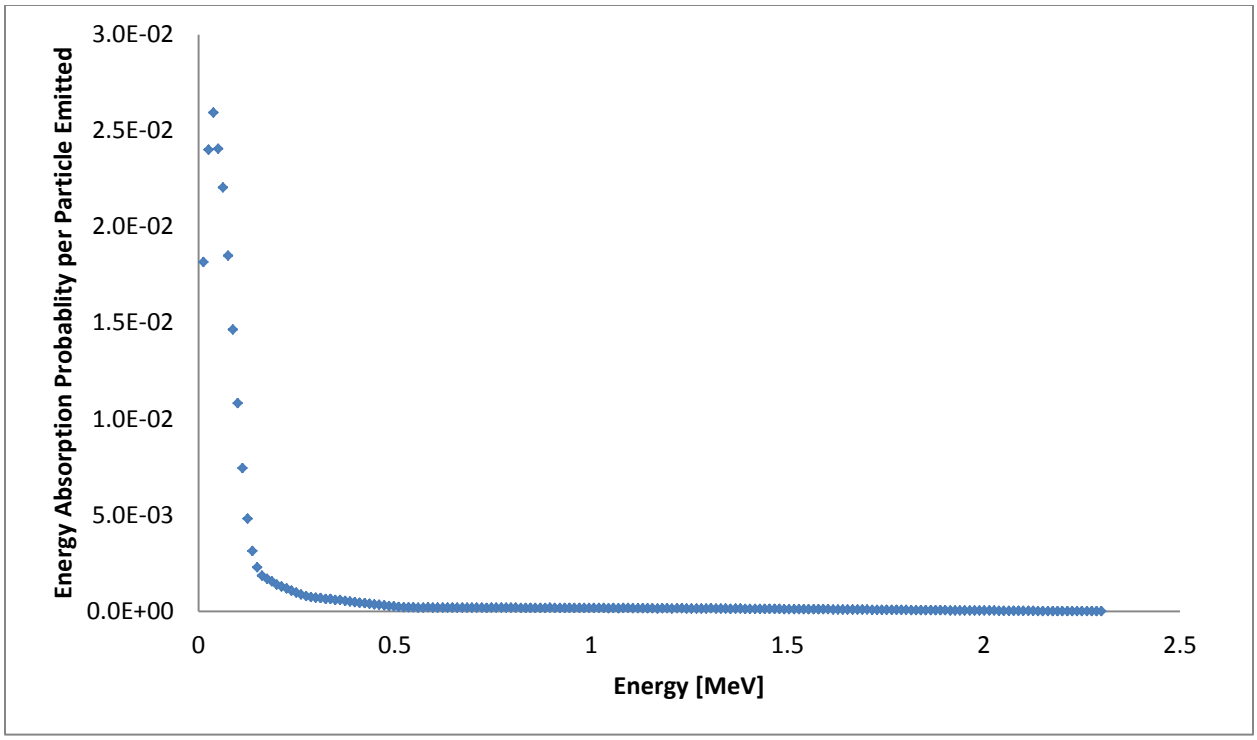


**Figure5-1: Probability of interaction for all 4 radionuclides in scenario #1**

The absorption rate was calculated by multiplying the absorption probability at each energy bin by the total activity (equation 4-1). The total activity is assumed to be the number of source electrons modeled in this simulation (e.g. 10,000,000 electrons). This multiplication process provides the number of electrons absorbed in the beta detector for each energy interval. The absorption rate here is presented as a function of energy. The absorption rate curve has a shape that similar to the probability curve since all probability values were multiplied by a constant (the total activity). The mixed energy absorption rate spectrum shows a distribution for all electrons absorbed in the beta detector over a set of energy values ranging from 0 to the maximum available energy (2.3 MeV). The mixed energy absorption-rate spectrum corresponds to electrons which were initially emitted from a source comprising all four radionuclides and counted by the detector; whereas, an individual energy absorption rate spectrum corresponds to

beta particles counted as being from a source emitting particles from only an individual radionuclide.

Figure 5-2 shows the mixed absorption-rate distribution containing all four radionuclides. The significant portion of the spectrum shifts toward the lower energy region. This indicates the abundance of low-energy beta emitters, resulting in the highest contribution to the spectrum. The graph clearly displays the presence of Y-90 as the high-energy tail lies at 2.3 MeV, Y-90's maximum energy value. Employing the spectral stripping process described previously, the mixed absorption-rate spectrum was stripped of each nuclide's contribution, which allowed us to determine the available activity for all nuclides. In scenario #1, Y-90 was first to be plotted on the general spectrum. The tail of the Y-90 graph was found to be in good alignment with the tail of the mixed spectrum with a multiplier of 770,000. This indicates that the activity contribution of Y-90 is 770,000 betas per second. The percentage of Y-90 activity was found to be nearly equivalent to the original percentage of Y-90 assumed for the source. This result was expected because the multiplier value corresponds to the portion of Y-90 available in spectrum. The portion of Y-90 on the mixed energy absorption-rate spectrum was subtracted from the spectrum. The removal of Y-90 left the spectrum with some residuals pertaining to Y-90 (due to uncertainties in stripping process) and a shorter tail lying on 0.54 MeV. Therefore, our next candidate radionuclide is Sr-90. Using the same procedure, the Sr-90 energy spectrum was graphed against the residual plot. The Sr-90 tail fell onto the 1$^{st}$ residual again showing an activity of 770,000 betas per second. Sr-90 was then removed from the spectrum leaving some residuals. The 2$^{nd}$ residual plot (Figure 5-3) ends at 0.3 MeV. Tc-99 (with maximum energy of 0.3 MeV) was next to be removed from the second residual. A good fit between the 2$^{nd}$ residual and Tc-99 plot suggested an activity of Tc-99 being 770,000 betas per sec. Eliminating Tc-99

from the 2nd residual leaves only C-14 present on the spectrum along with some residuals from previous removal processes, the 3rd residual. The energy endpoint of the 3rd residual lies at 0.15 MeV. Due to possible energy loss of low-energy electrons in the detector face (degradation due to the mylar), Figure 5-4 shows a slight lack of fit between the two graphs. This lack of fit resulted in a small portion of activity remaining in the spectrum (plotted as the 4th residual). The activity remaining in the 4th residual is assumed to be corresponding to the presence of C-14 and the other three radionuclides leftover in the spectrum. The noticeable difference between the 3rd residual and C-14 made it difficult to determine the activity of C-14 present. Radionuclides with maximum energies lower than 0.15 MeV are assumed to be readily shielded. The remainder in the fourth residual was assumed to be low-energy electrons, 0.15 MeV or less, or due to uncertainties in the stripping process.

The multiplication factor in Table 5-1 refers to the initial abundance of each radionuclide, relevant to the overall mixture, as being directly emitted from the source. Table (5-1) shows the results obtained for activities, and the corresponding percentages of each radionuclide.

**Table 5-1: Results for scenario #1**

| Radionuclide | C-14 | Tc-99 | Sr-90 | Y-90 | Total |
|---|---|---|---|---|---|
| MF | 100 | 10 | 10 | 10 | 130 |
| Percentage of MF (%) | 77 | 7.7 | 7.7 | 7.7 | 100 |
| Activity (beta/sec) | 7,690,000 | 770,000 | 770,000 | 770,000 | 10,000,000 |
| Percentage of Activity (%) | 77 | 7.7 | 7.7 | 7.7 | 100 |

From values in the table above, it can be clearly seen that radionuclides with the same multiplication factor (MF) have the same activity contribution. This activity percentage is equivalent to the value of the multiplication factor of a radionuclide over the total for all four

radionuclides. The results for all nine scenarios were found to be consistent with small degrees of variations in percentages in activity values versus multiplication factors.

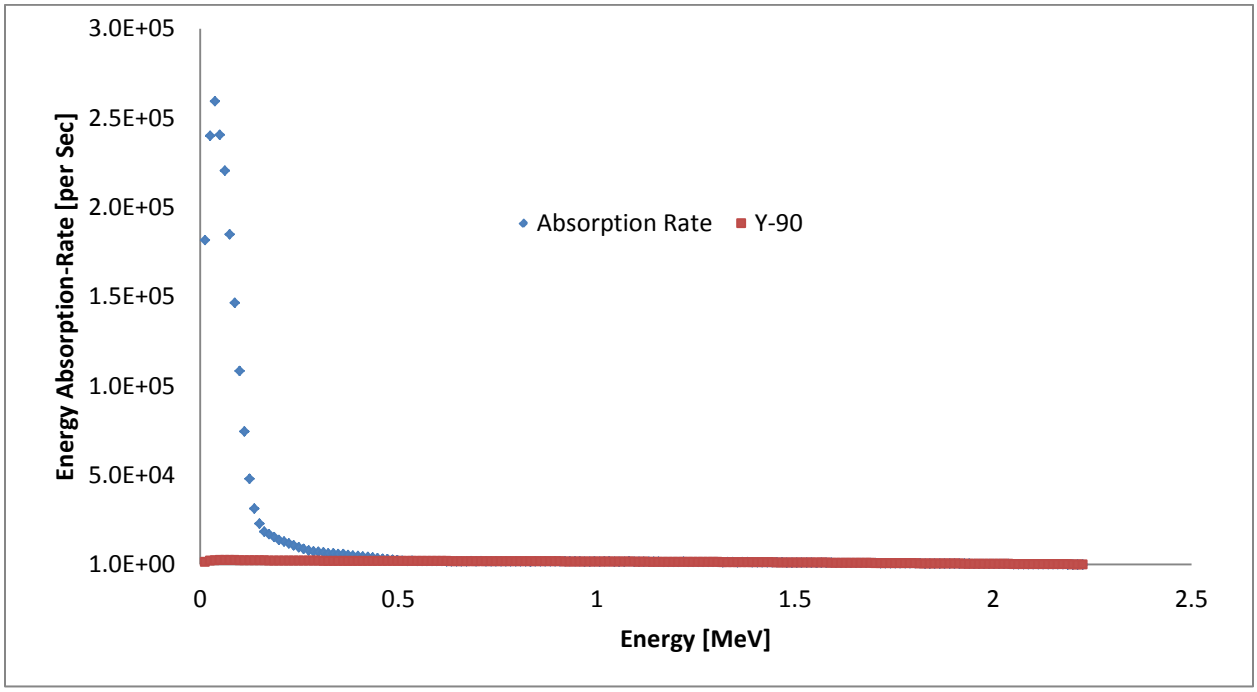


**Figure 5-2: Mixed absorption-rate spectrum vs. individual absorption-rate spectrum(Y-90) in scenario #1**

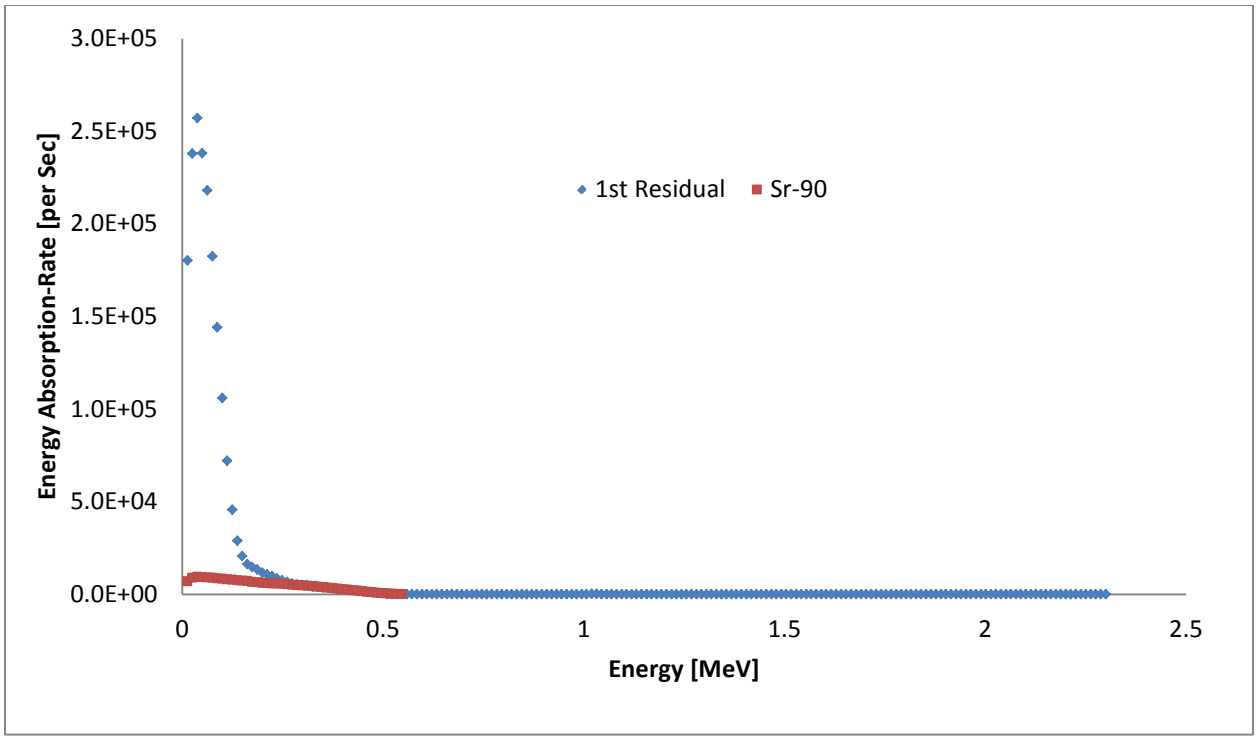


**Figure 5-3: 1st residual vs. individual absorption-rate spectrum (Sr-90) in scenario #1**

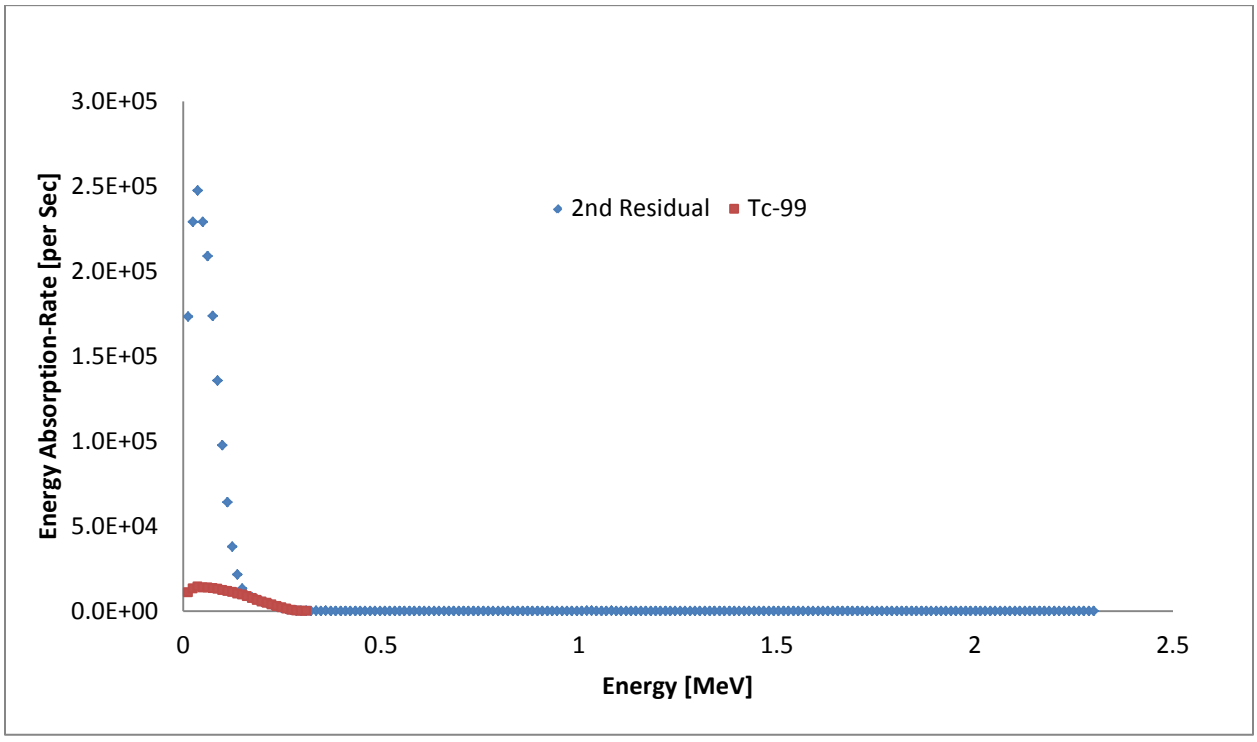


**Figure 5-4: 2nd residual versus individual absorption-rate spectrum (Tc-99) in scenario #1**

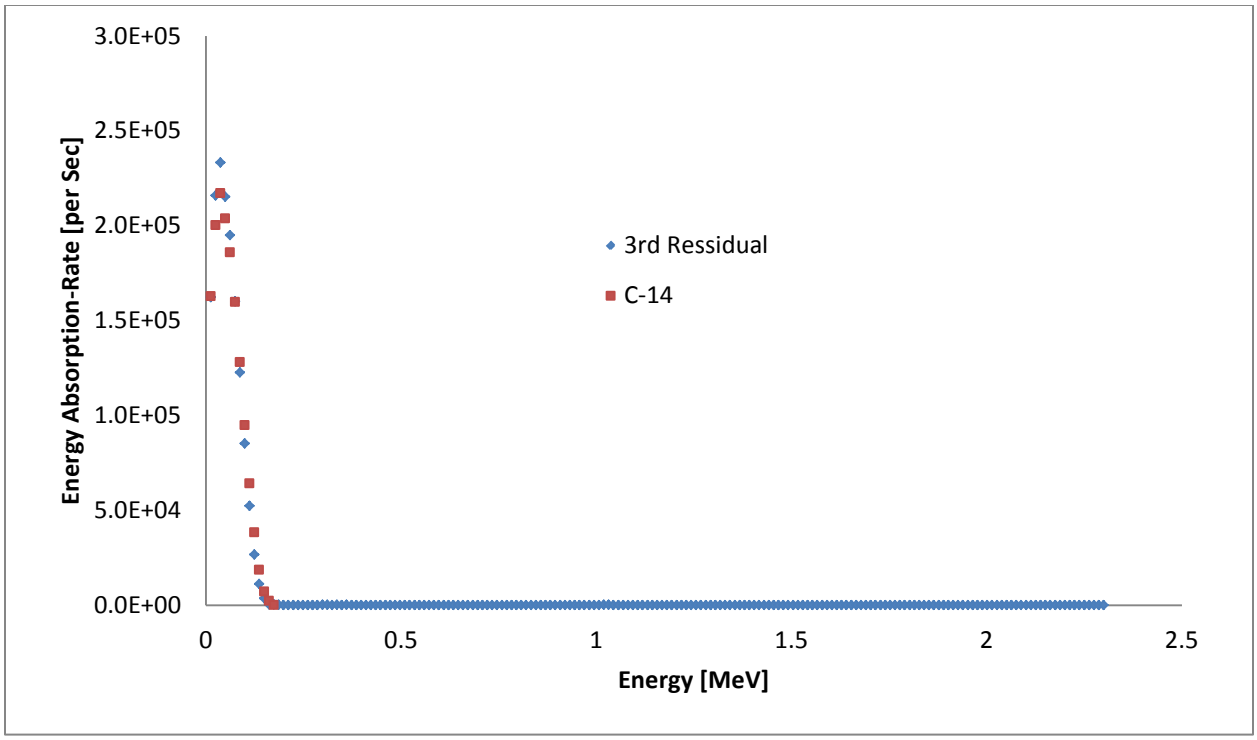


**Figure 5-5: 3rd residual versus individual absorption-rate spectrum (C-14) in scenario #1**

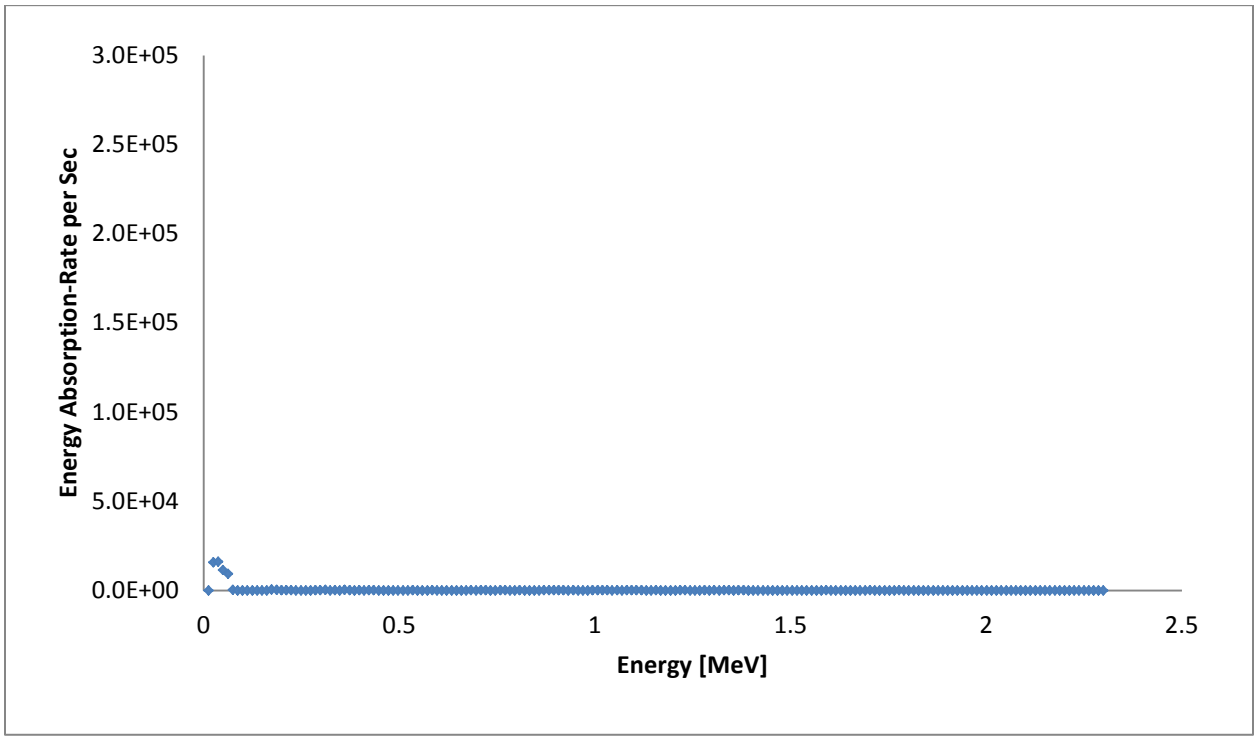


**Figure 5-6: 4th residual scenario#1**

## 5.2 Scenario #2:

The Figures 5-7 to 5-11 show the mixed energy absorption-rate distribution and all residuals in this scenario. In this case, a significant portion of the mixed energy absorption-rate spectrum moves toward the higher energy bins. This shift indicates the considerable relative contribution of high energy beta emitters, higher than 0.5 MeV. As shown in Table 5-2, Y-90 has the dominant presence in this scenario. The removal of the Y-90 portion from the mixed absorption-rate spectrum resulted in a considerable reduction in the overall distribution. The results from the stripping analysis are provided in Table 5-2. The percentages of activity were found to be nearly identical to the multiplication factors for all nuclides. The difference between activity percentage and multiplication factor for Tc-99 was found to be less than 0.5%. Other variations in percentages were obtained to be less than 2% in difference. The loss of percentages in the lower energy beta emitters (C-14 and Tc-99) is attributed to some possible low-energy electron absorption in the mylar, and also a conservative estimation of higher energy radionuclides (Y-90 and Sc-90) in the mixed absorption-rate spectrum.

**Table 5-2: Results for scenario #2**

| Radionuclide | C-14 | Tc-99 | Sr-90 | Y-90 | Total |
|---|---|---|---|---|---|
| MF | 10 | 10 | 10 | 100 | 130 |
| Percentage of MF (%) | 7.7 | 7.7 | 7.7 | 77 | 100 |
| Activity (beta/sec) | 770,000 | 740,000 | 771,000 | 7,719,000 | 10,000,000 |
| Percentage of Activity (%) | 7.7 | 7.4 | 7.7 | 77.2 | 100 |

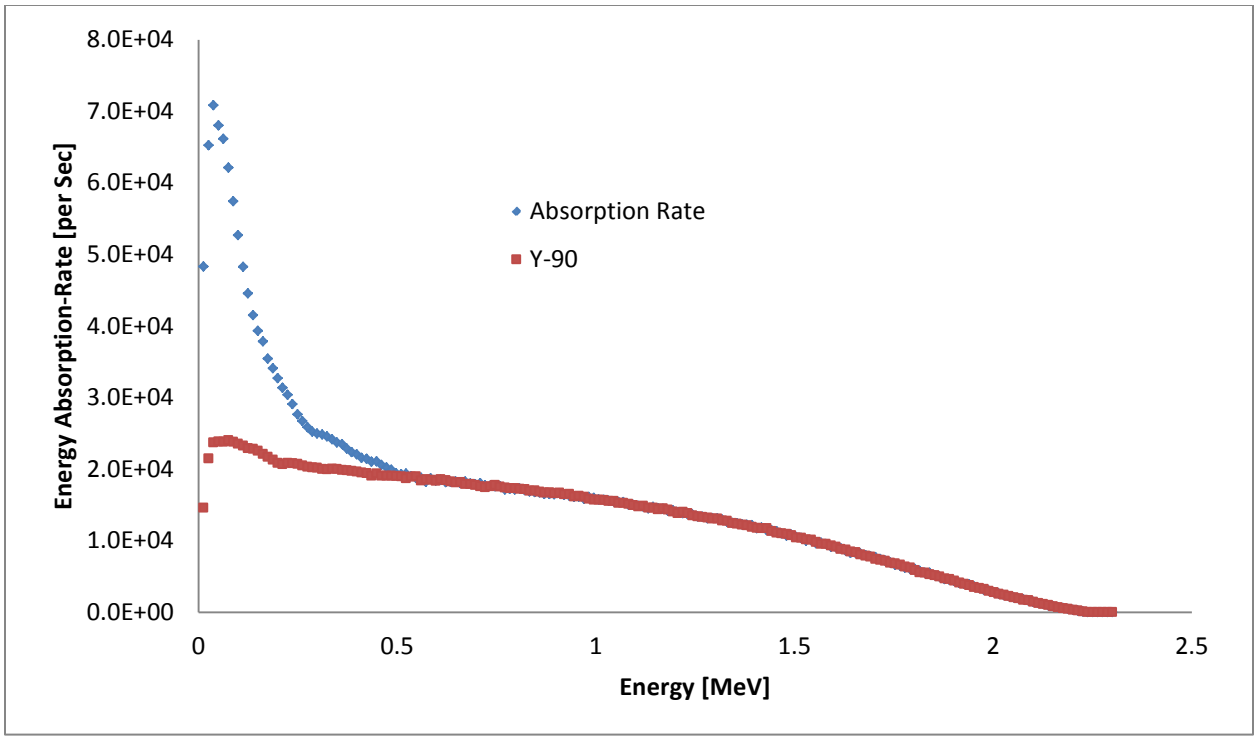


**Figure 5-7: Mixed absorption-rate Spectrum vs. individual absorption-rate spectrum(Y-90) in scenario #2**

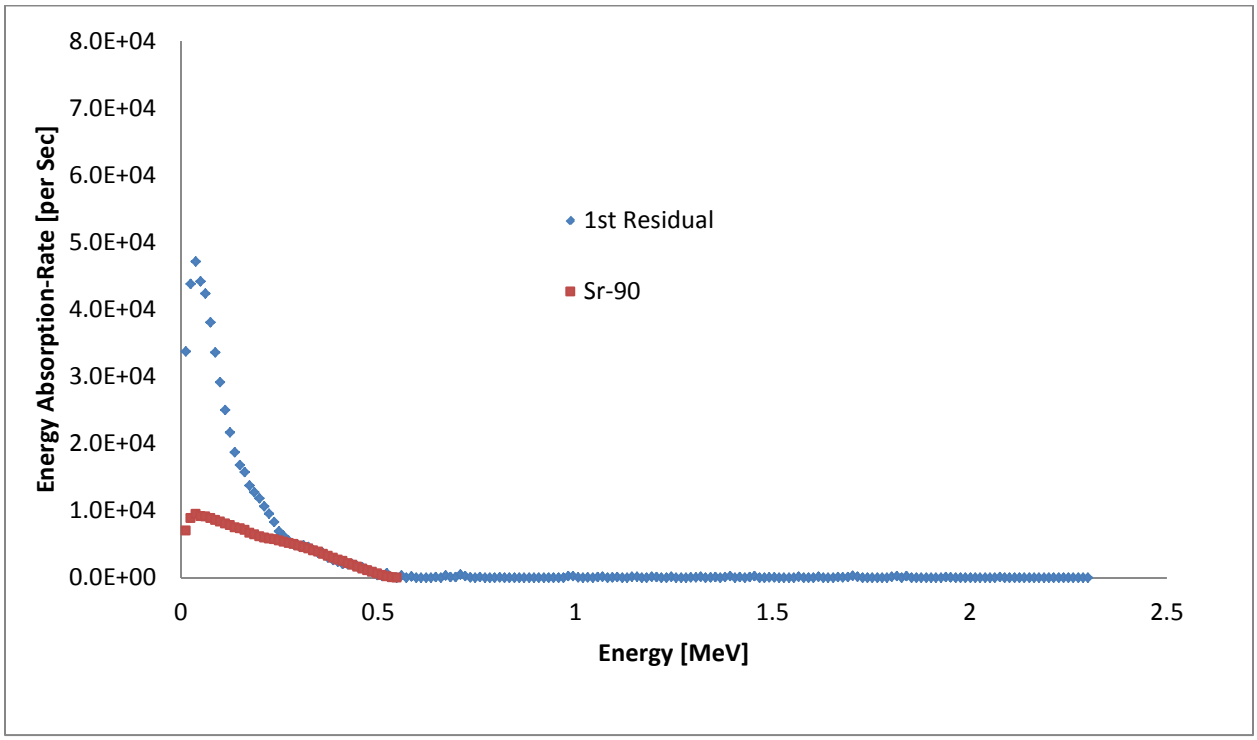


**Figure 5-8: 1st residual vs. individual absorption-rate spectrum (Sr-90) in scenario #2**

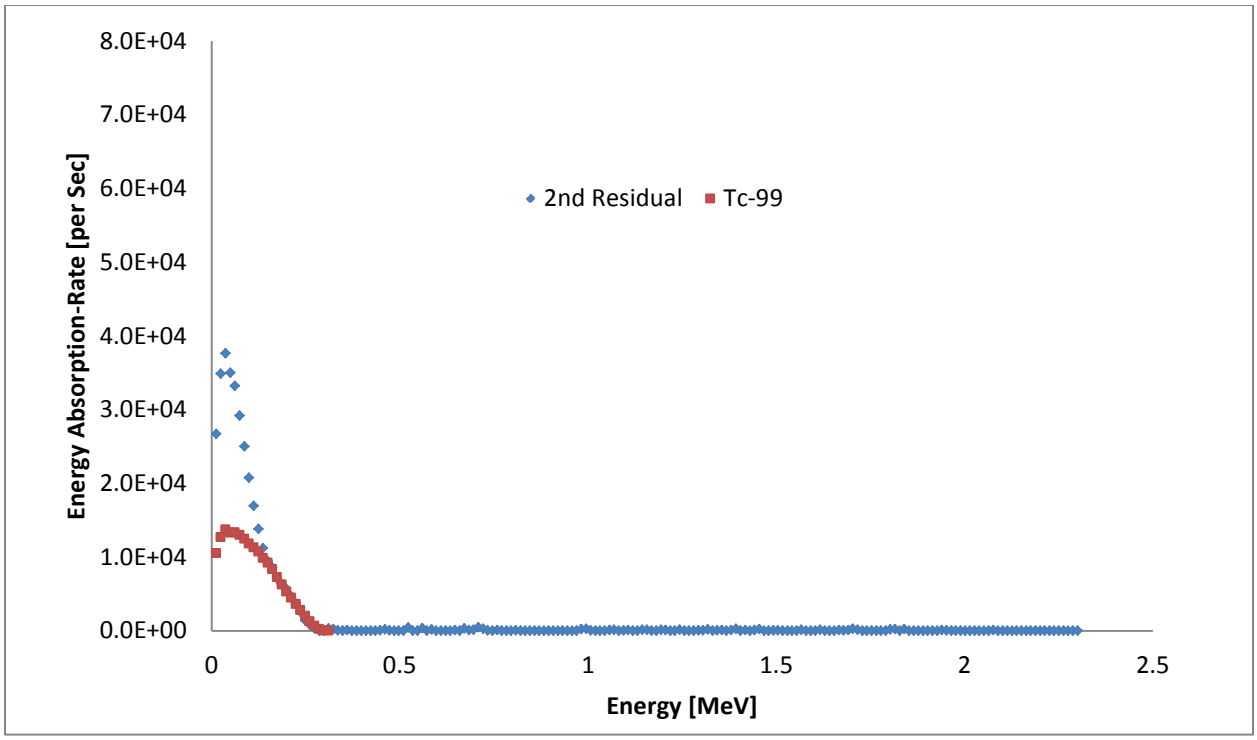


**Figure 5-9: 2nd residual vs. individual absorption-rate spectrum (Tc-99) in scenario #2**

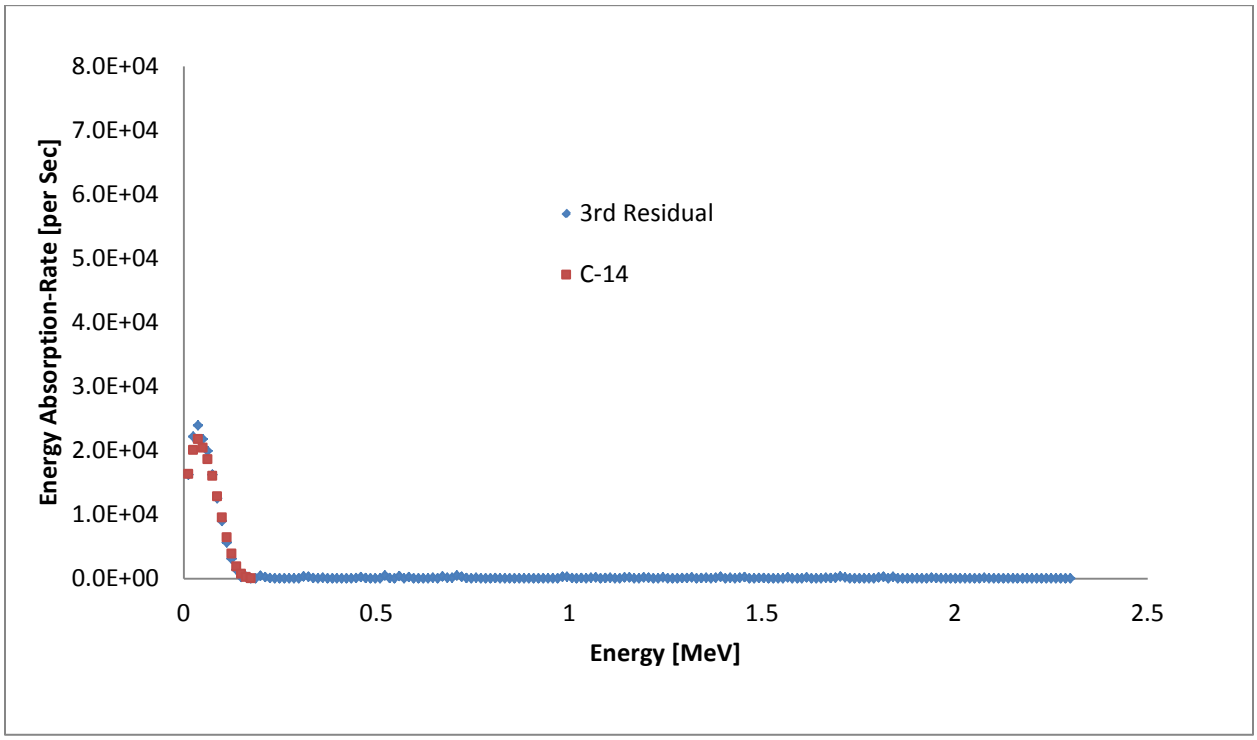


**Figure 5-10: 3rd residual vs. individual absorption-rate spectrum (C-14) in scenario #2**

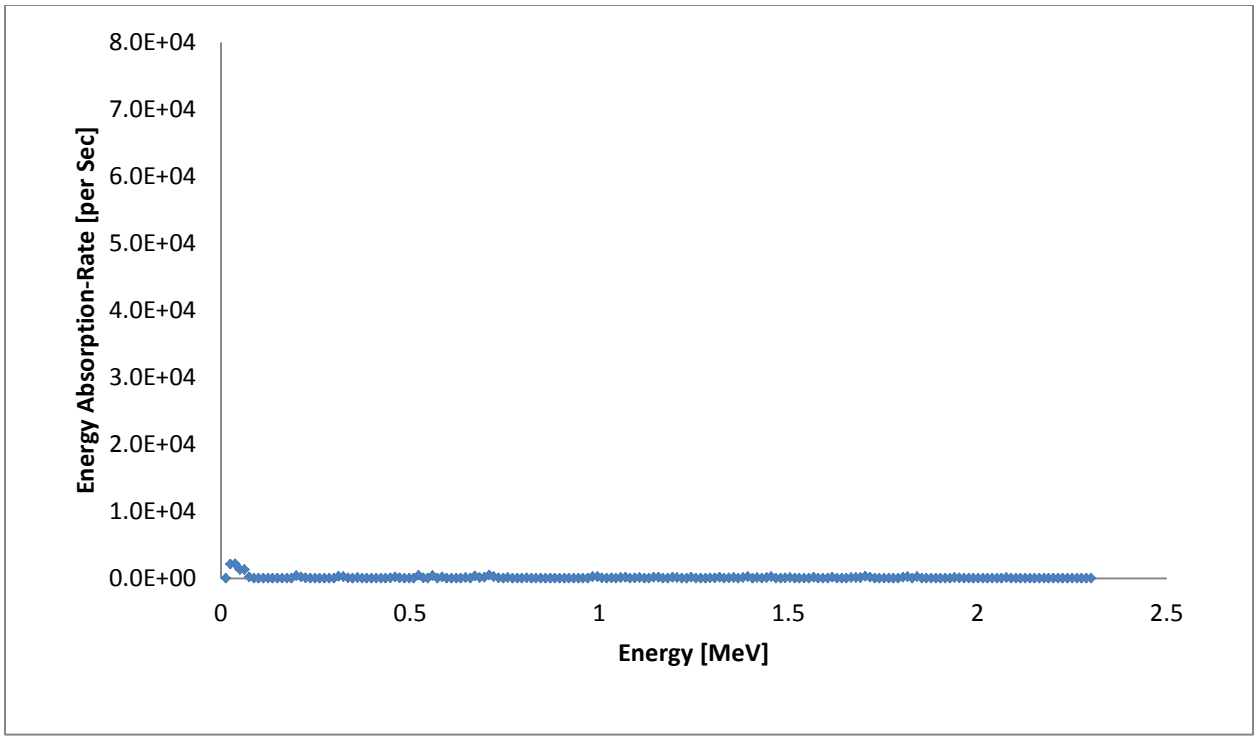


**Figure 5-11: 4th residual in scenario #2**

# 6.0 Conclusion

The objectives of this study were to develop a method for identifying the radionuclides present in a mixed beta source, and to develop a method for spectral stripping to quantify the activity of each radionuclide contributing to the detector.

The application of MCNP was useful in generating various beta energy deposition spectra for C-14, Tc-99, Sr-90, and Y-90. Simulations were designed to measure the emission of radioactivity from a 2D disk source emitting only beta particles. Additional simulations determined the emission of beta particles from a three-dimensional cylindrical source. The purpose of this simulation was to investigate the effect of degradation on the beta energy spectra due to some self-absorption in source.

The spectral stripping method was shown to provide reliable results identifying the studied radionuclides and determining their activity in various simulations of source spectra. Despite the lack of fit between low energy beta sources curves (Tc-99 and C-14) and the general spectra, this technique was found to be successful in quantifying the radioactivity of the higher- energy radionuclides (Sr-90 and Y-90).

Nine different scenarios were included in this research. Each scenario comprised two or more radionuclides emitting beta particles at varying intensity. The strength of the emission from a source was controlled through the multiplication factor (i.e., relative activity), which dictates the percentage of each radionuclide presented in the source. The results for all nine scenarios displayed a consistency in the activity and the corresponding percentages. The beta spectra generated for all four radionuclides from a disk source model were nearly similar in shape to the original beta energy distribution emitted by the source. The small difference in shapes was

believed to be attributed to energy loss in the thin myler layer on the face of detector; all emitted electrons must penetrate that layer to be counted. The variations in percentages between the original emission and collected spectra were found to be less than 2% in all studied scenarios. A drawback to this method was experienced with low-energy beta emitters, as a considerable portion of their energy was found to be reduced due to absorption in the absorbing medium. This absorption makes it uneasy to quantify the original activity emitted from the source, especially for C-14. The reduction in low-energy emission spectra can be modified through decreasing the thickness of the initial absorbing medium (mylar layer). Future investigations would have to be conducted to further study the applicability of this method on lower energy beta sources.

Similarly, the results from a 3D cylindrical source showed considerable energy loss due to self-absorption for low-energy beta emitters, such as C-14. The collected beta energy absorption spectrum from a cylindrical source emitting all beta sources showed a shift of considerable loss in low-energy region. These results will open the door for future development of utilizing and optimizing the phoswich detector to better quantify radioactivity of low-energy beta sources.

# 7.0 Future Work:

The intensity of source emission in the first scenario (Table 5-1) was simulated using the self-absorption model. The purpose was to determine the significance of the source absorbing its own beta energy. The MCNP results displayed a significant energy loss in the low energy region. The figure displays the energy mixed energy absorption probability distributions obtained from a 2D source the self-absorption source for the studied scenario. The distributions were plotted on logarithmic scale to more clearly demonstrate a considerable loss in energy absorption probability especially at low energies (up to 0.5 Mev). Absorption within the source was responsible for a reduction by almost two orders of magnitude.

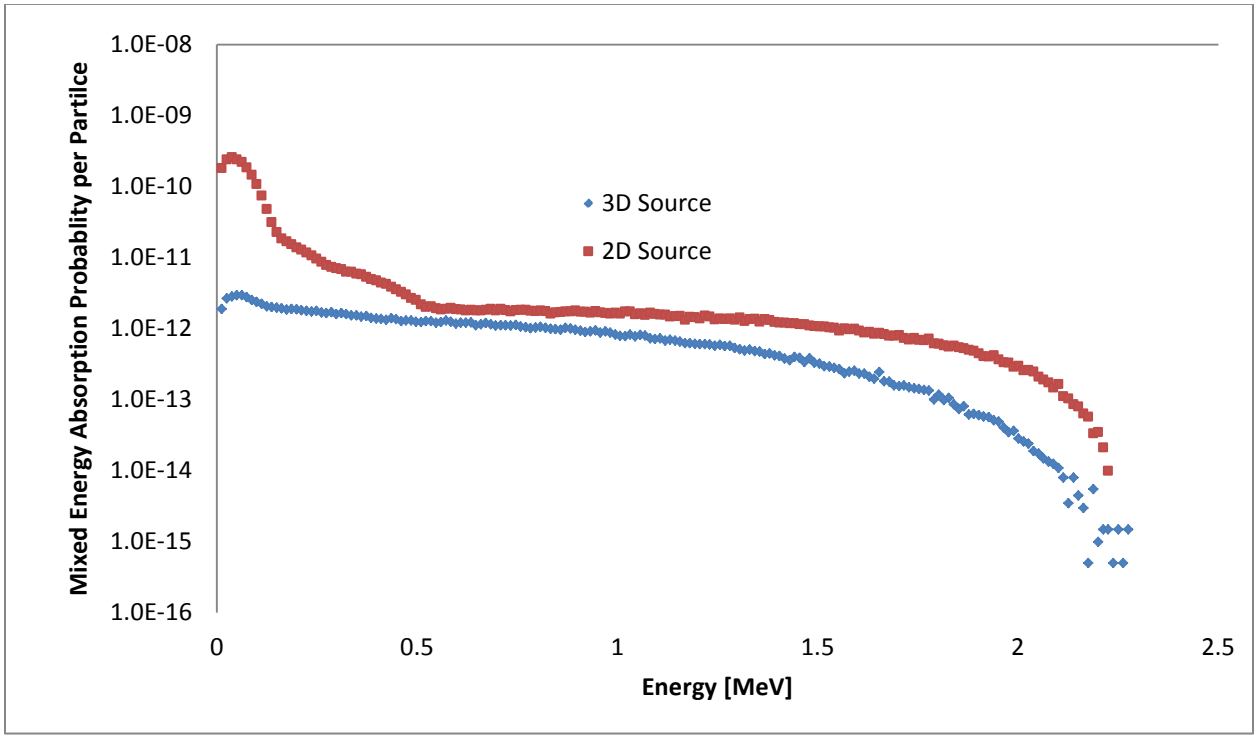


**Figure 7-1: The probability of energy released in beta detector per particle emitted from 2D source vs. 3D source**

This work will guide future development into conducting more research to better understand the effect of self-absorption on low energy beta emitters. Further work would require studying the percentage of energy loss in beta sources with energies lower 0.15 MeV with various degrees of self-absorption. This study may provide useful data for beta particle shielding.

The applicability of the spectral stripping method should be investigated again on low energy beta sources (lower than 0.15 MeV). Further development of spectral stripping will consider the effect of mono-energetic electrons (conversion electrons) on beta energy emission spectra. The conversion electron has a well-defined discrete energy and so its energy spectrum takes the shape of sharp peak. This spectral feature can be readily identified in the beta energy absorption distribution.

The long term goal is to expand the usability of the spectral stripping method further by carrying out sophisticated automated computer algorithms using software with an adequate user interface. The graphical interface will allow the users to specify and characterize the properties of each beta emitter and also sort the data for each radionuclide into separate files for easy access and modification, and link/run all files together. The software will make this technique more applicable in the realm of radiation detection.

# Bibliography

Guide to the Nuclear Wallchart. (2000). Beta decay. Retrieved from: http://www.lbl.gov/abc/wallchart/chapters/03/2.html

About.Com Chemistry. (2013). Electron Capture Definition. Retrieved from: http://chemistry.about.com/od/chemistryglossary/g/Electron-Capture-Definition.htm

San José State University. (n.d.). Electron and Positron Beta-Decay. Retrieved from: http://applet-magic.com/betadecay.htm

Matter. (2000). X-ray and Auger Electron Emission. Retrieved from: http://www.matter.org.uk/tem/electron_atom_interaction/x-ray_and_auger.htm

Wikipedia. (2013) Auger effect. Retrieved from: http://en.wikipedia.org/wiki/Auger_effect

Wikipedia. (2013). Internal Conversion. Retrieved from: http://en.wikipedia.org/wiki/Internal_conversion

University of Toronto. (n.d.). Module 3: Interaction of Radiation with Matter. Retrieved from: http://www.ehs.utoronto.ca/services/radiation/radtraining/module3.htm

Douglas J. Wagenaar. (1995). Stopping Power. Retrieved from: http://www.med.harvard.edu/jpnm/physics/nmltd/radprin/sect7/7.1/7_1.2.html

Nuclear Engineering & Radiological Sciences. (2007). Gamma Ray Spectroscopy. Retrieved from: http://www-personal.umich.edu/~ianrit/gammaspec.pdf

University of Waterloo. (n.d.). Fission Energy. Retrieved from: http://www.science.uwaterloo.ca/~cchieh/cact/nuctek/fissionenergy.html

University of Wisconsin Nuclear Reactor Tour. (n.d.). Nuclear Energy. Retrieved from: http://reactor.engr.wisc.edu/tour/fission.htm

EFDA. (2013). How Do Fission and Fusion Reactions Compare? Retrieved from: http://www.efda.org/faq/how-do-fission-and-fusion-reactions-compare/

Wikipedia. (2013). Strontium-90. Retrieved from: http://en.wikipedia.org/wiki/Strontium-90

Wikipedia. (2013). Yttrium-90. Retrieved from http://en.wikipedia.org/wiki/Yttrium-90

Wikipedia. (2013). Technetium-99. Retrieved from: http://en.wikipedia.org/wiki/Technetium-99

Sumer's Radiology Site. (2004). Tc-99 Decay Scheme. Retrieved from: http://sumerdoc.blogspot.com/2004/11/tc-99-decay-scheme.html

About.com chemistry. (2013) What Is Radioactivity? What Is Radiation? Retrieved from: http://chemistry.about.com/od/chemistryfaqs/f/radioactivity.htm

NDT Resource Center. (2012). What Is Bremsstrahlung? Retrieved from: http://www.ndt-ed.org/EducationResources/HighSchool/Radiography/bremsstrahlung_popup.htm

Wikipedia. (2013). Copper-64. Retrieved from: http://en.wikipedia.org/wiki/Copper-64

Bubble Technology Industries. (2004). Beta Probe. Retrieved from: http://www.bubbletech.ca/radiation_spectrometers_files/beta_probe.html

Farsoni, A.T. and Hamby D.M. (2006).Study of a Triple-Layer Phoswich Detector for Beta and Gamma Spectroscopy with Minimal Crosstalk, in Proceedings of the 28th Seismic Research Review. Ground-Based Nuclear Explosion Monitoring Technologies, LA-UR-06-5471, Vol. 2, pp. 794-792; 2006.

Farsoni, Abi T. Simulation Beta/Gamma Digital Spectroscopy. Copy Right (2006). Retrieved from Valley Library electronic Browsing Dissertations by Abi Farsoni.

Farsoni, A.T.; Hamby, D.M. (2005). MCNP Analysis of a Multilayer Phoswich Detector for Beta-Paticle Dosimetry and Spectroscopy. Nuclear Instuments & Methods in Physics Research, Section A: Accelerator, Spectrometers, Detectors and Associated Equipment. A555: 225-230; 2005.

Farsoni, A. T.; Alemayehu, B.; Alhawsawi, A.; Becker, E. (2012). Real-Time Pulse Shape Discrimantion and Radiooxenon Meassurement in Field-Programmable Gate Array. 2012 Monitoring Reaseach Review: Ground-Based Nuclear Explosion Monitoring Technologies, DE-AC52-09NA29324, pp. 594-606. 2012.

Childress, N.L.; Miller, W.H. (2002). MCNP Analysis and Optimization of a Triple Phoswich Detector. Nuclear Instruments & Methods in Physics Research, Section A: Accelerators, Spectrometers, Detectors and Associated Equipment. A490: 263-270; 2002.

Usuda, S.; Sakurai, S.; Yasuda, K. (1997). Phoswich Detector for Simultaneous Counting of Alpha-, Beta (Gamma) –Rays and Neutrons. Nuclear Instruments and Methods in Physics Reseach, Section A: Accelerator, Spectrometers, Detectors and Associated Equipment. A388 (1-2):193-198; 1997.

Bardelli, L.; Bini, M.; Poggi, G.; Taccetti, N. (2002). Application of Digital Sampling Techniques to Particle Identification in Scintillation Detectors. Nuclear Instruments & Methods in Physics Research, Section A: Accelerator, Spectrometers, Detectors and Associated Equipment. A491: 244-257; 2002.

Schier, W. A.; Campbell, J. M.; Couchell, G. P.; Li, S.; Nguyen, H. V.; Pullen, D. J.; Seabury, E. H.; Tipnis, S. V. (1997). Beta Particle Spectrometer for Measuring Aggregate Beta Spectra Following Fission. Nuclear Instruments and Methods in Physics Research, Section A: Accelerator, Spectrometers, Detectors and Associated Equipment. A 404: 173-180; 1997.

Yalcin, S.; Gurler, O.; Gundogdu, O.; Akar, O. (2011). Analytical Investigation of Energy Spectrums of Beta Rays Emitted from 90Sr and 204Tl Radioisotopes. Radioanalytical and Nuclear Chemistry, Volume 289, Issue 3, pp 923-926; 2011.

Loidl, M.; Rodrigues , M.; Censier , B.; Kowalski, S.; Mougeot, X.; Cassette, P.; Branger , T.; Lacour, D. (2010). First Measurement of the Beta Spectrum of 241Pu with a Wryogenic Detector. Applied Radiation and Isotopes, Volume 68, Issues 7–8, pp 1454–1458. 2010.

Shultis, J. K.; Faw, R. E. (2011). An MCNP Primer. Retrieved from: http://www.mne.ksu.edu/~jks/MCNPprmr.pdf

Los Alamos National Laboratory. (2010). A General Mote Carlo N-Particle (MCNP) Transport Code. Retrieved from: https://mcnp.lanl.gov/

Paulenova, A. (2011). “Radioactive Decay Mechanisms, Alpha and Beta Decay”. Lecture Notes. October 2011.

Knoll, G.F. (2000). Radiation Detection and Measurement (3rd Ed.). Hoboken, NJ: John Wiley & Sons, Inc.

Martin, J.E. (2006). Physics for Radiation Protection (2nd Ed.). New York: John Wiley and Sons, Inc.

Saint-Gobain Crystals and Detector (n.d.). Scintillation Products. Retrieved from: http://www.detectors.saint---gobain.com/Phoswich.aspx

# APPENDICES

## APPENDIX A: BAR GRAPHS FOR THE STUDIED SCENATIOS

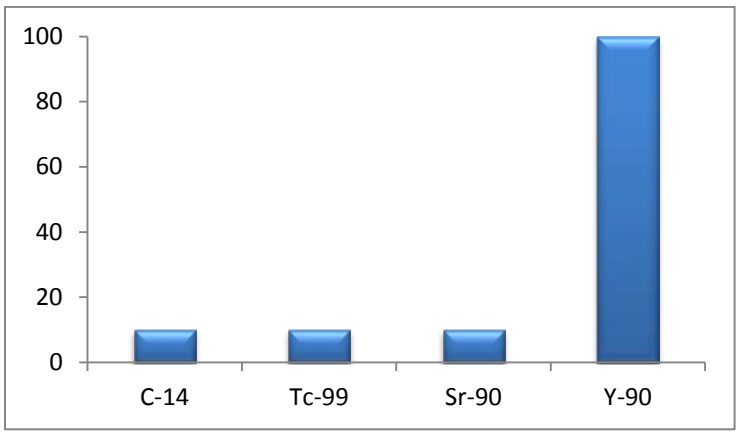


**Figure A-1: Nuclides relative contributions present in scenario #2**

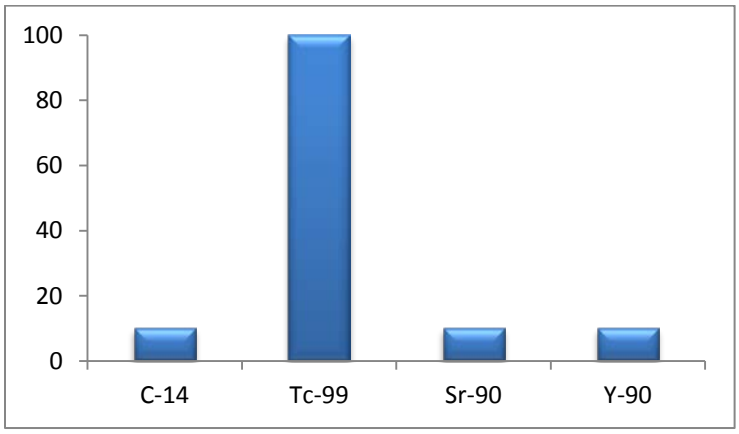


**Figure A-2: Nuclides relative contributions present in scenario #3**

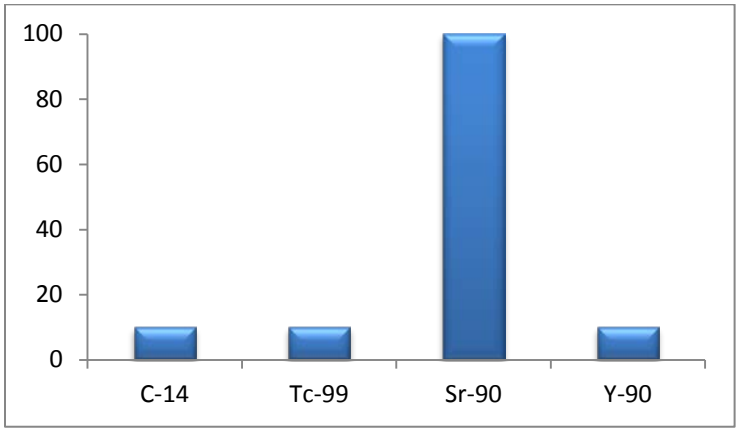


**Figure A-3: Nuclides relative contributions present in scenario #4**

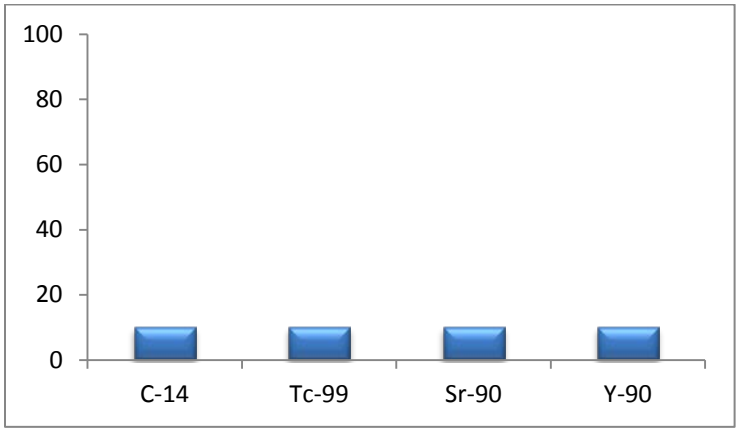


**Figure A-4: Nuclides relative contributions present in scenario #5**

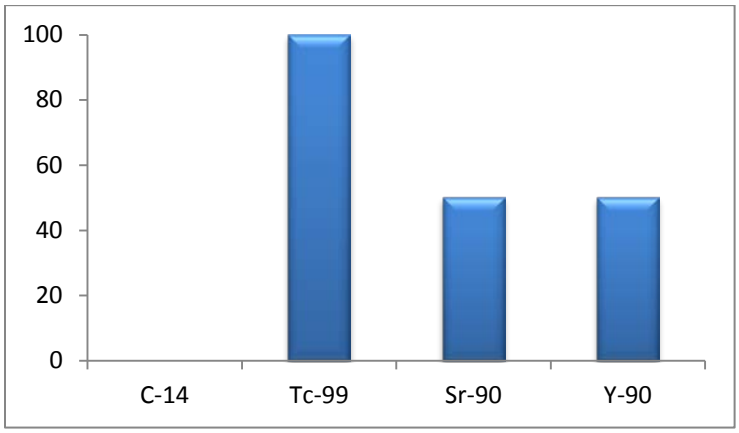


**Figure A-5: Nuclides relative contributions present in scenario #6**

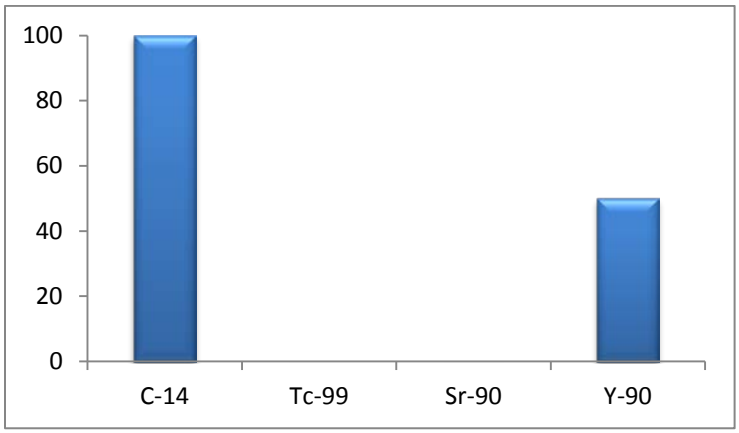


**Figure A-6: Nuclides relative contributions present in scenario #7**

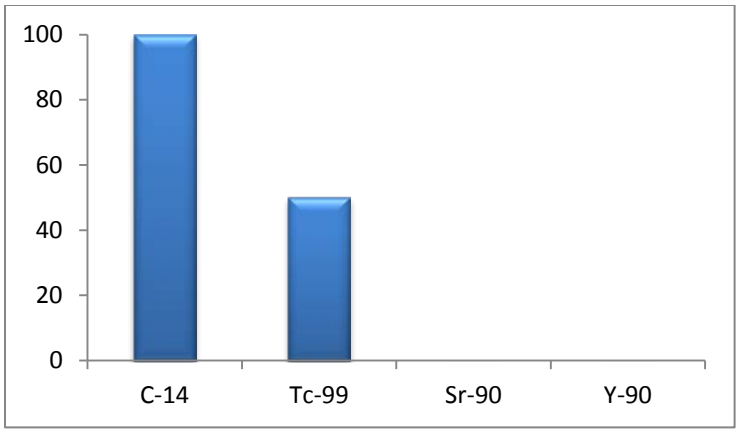


**Figure A-7: Nuclides relative contributions present in scenario #8**

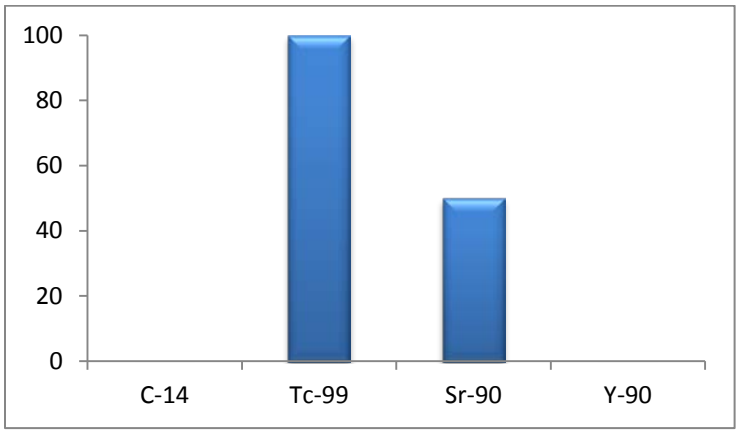


**Figure A-8: Nuclides relative contributions present in scenario #9**

## APPENDIX B: TABLES AND FIGURES FOR STUDIED SCENARIOS

**Scenario #3:**

**Table B-1: Results for scenario #3**

| Radionuclide | C-14 | Tc-99 | Sr-90 | Y-90 | Total |
|---|---|---|---|---|---|
| MF | 10 | 100 | 10 | 10 | 130 |
| Percentage of MF (%) | 7.7 | 77 | 7.7 | 7.7 | 100 |
| Activity (beta/sec) | 737000 | 7580000 | 840000 | 843000 | 10000000 |
| Percentage of Activity (%) | 7.3 | 75.8 | 8.4 | 8.4 | 100 |

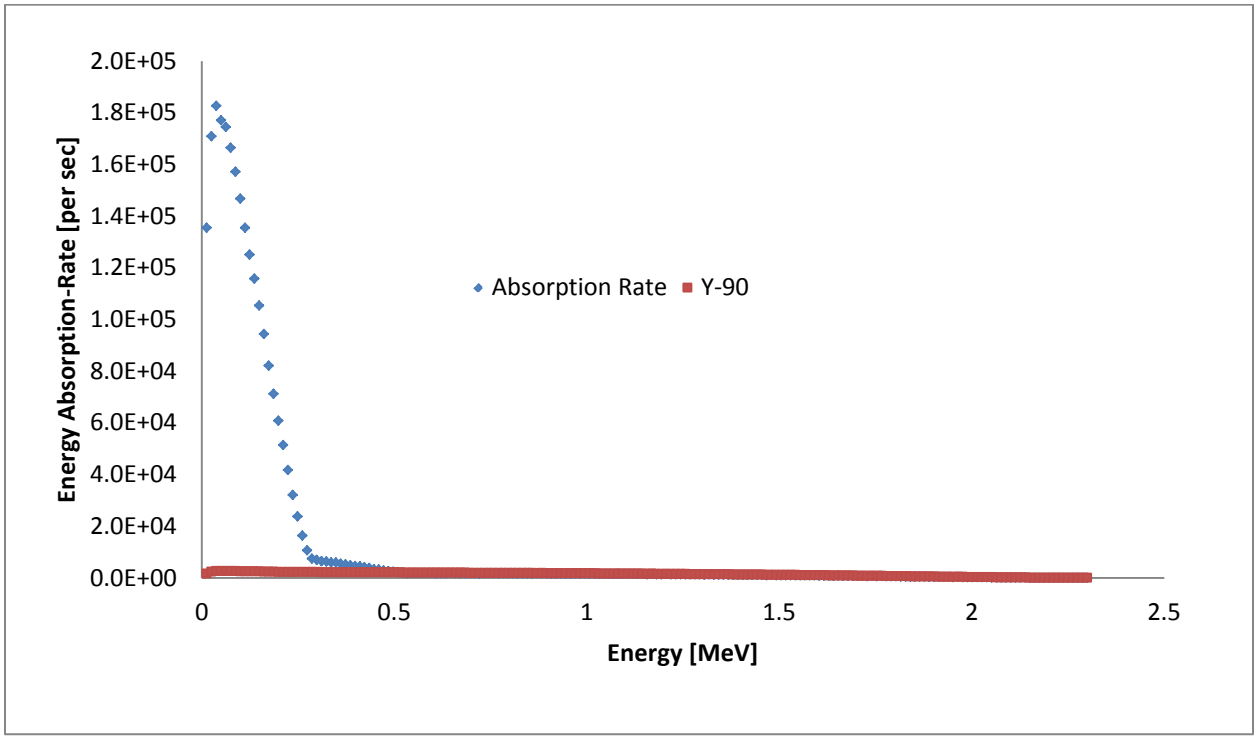


**Figure B-1: Mixed absorption-rate spectrum vs. individual absorption-rate spectrum(Y-90) in scenario #3**

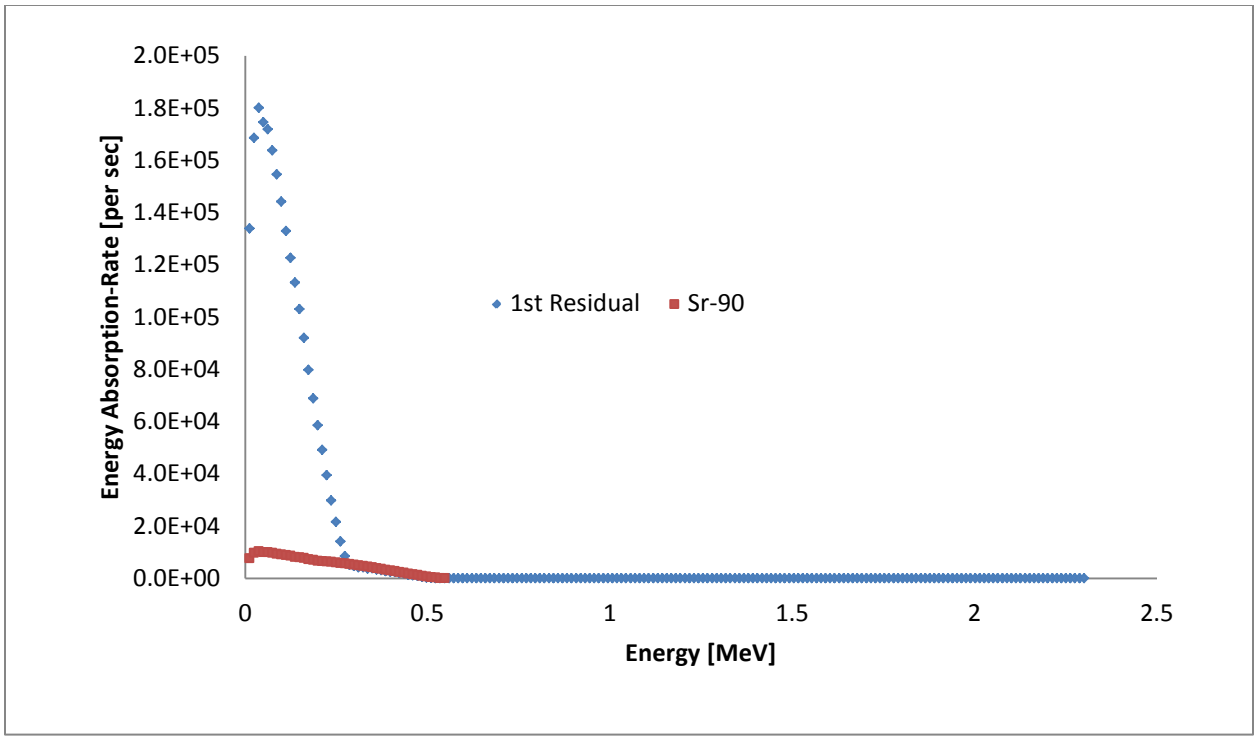


**Figure B-2: 1st residual vs. individual absorption-rate spectrum (Sr-90) in scenario #3**

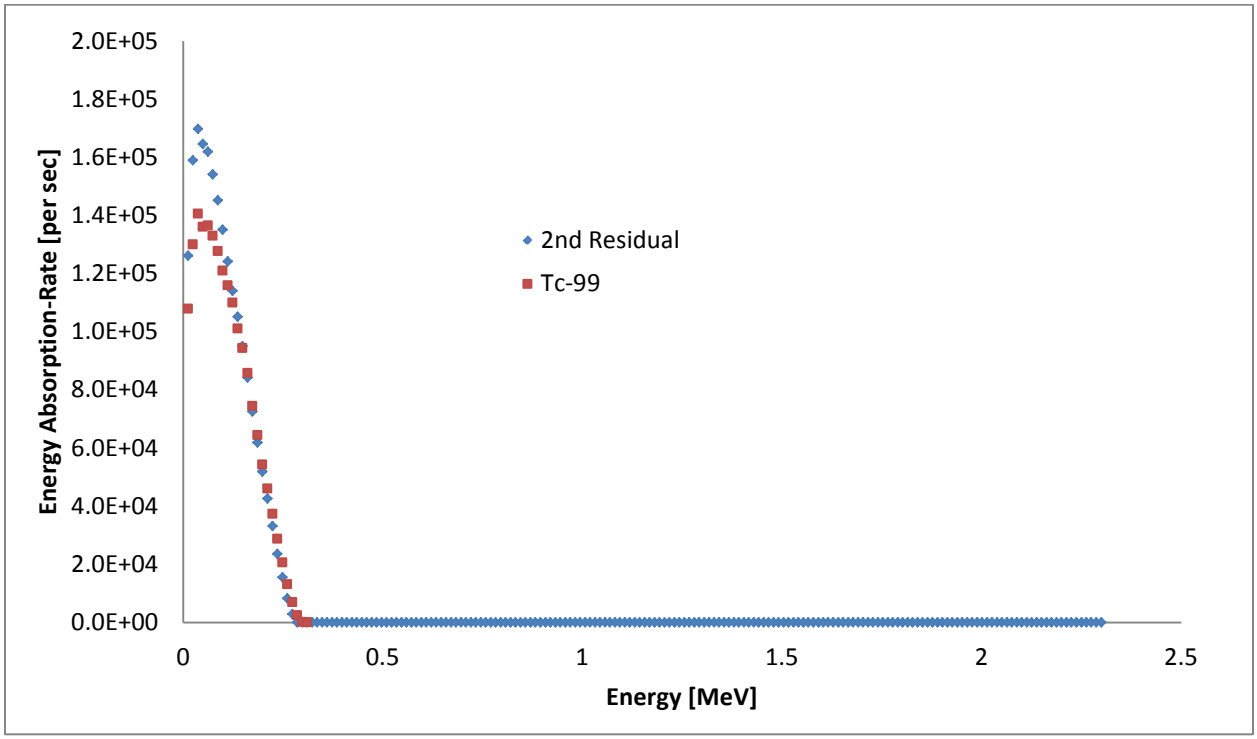


**Figure B-3: 2nd residual vs. individual absorption-rate spectrum (Tc-99) in scenario #3**

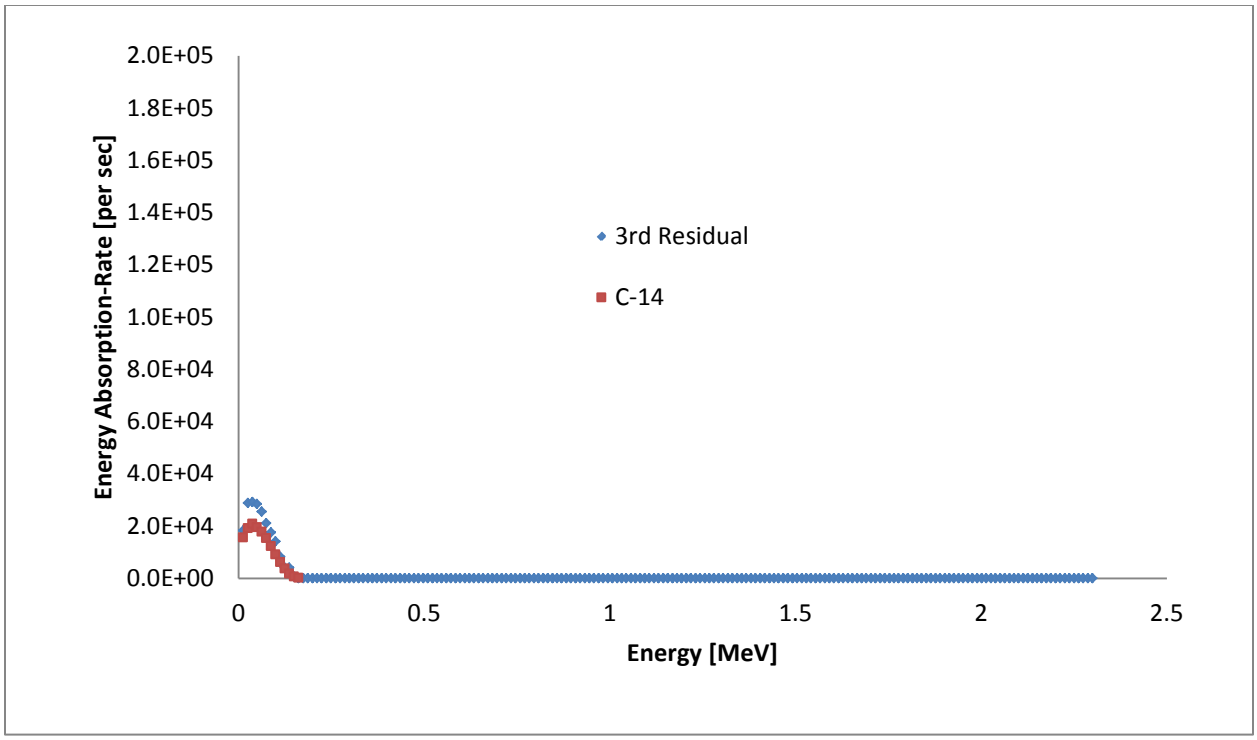


**Figure B-4: 3rd residual vs. individual absorption-rate spectrum (C-14) in scenario #3**

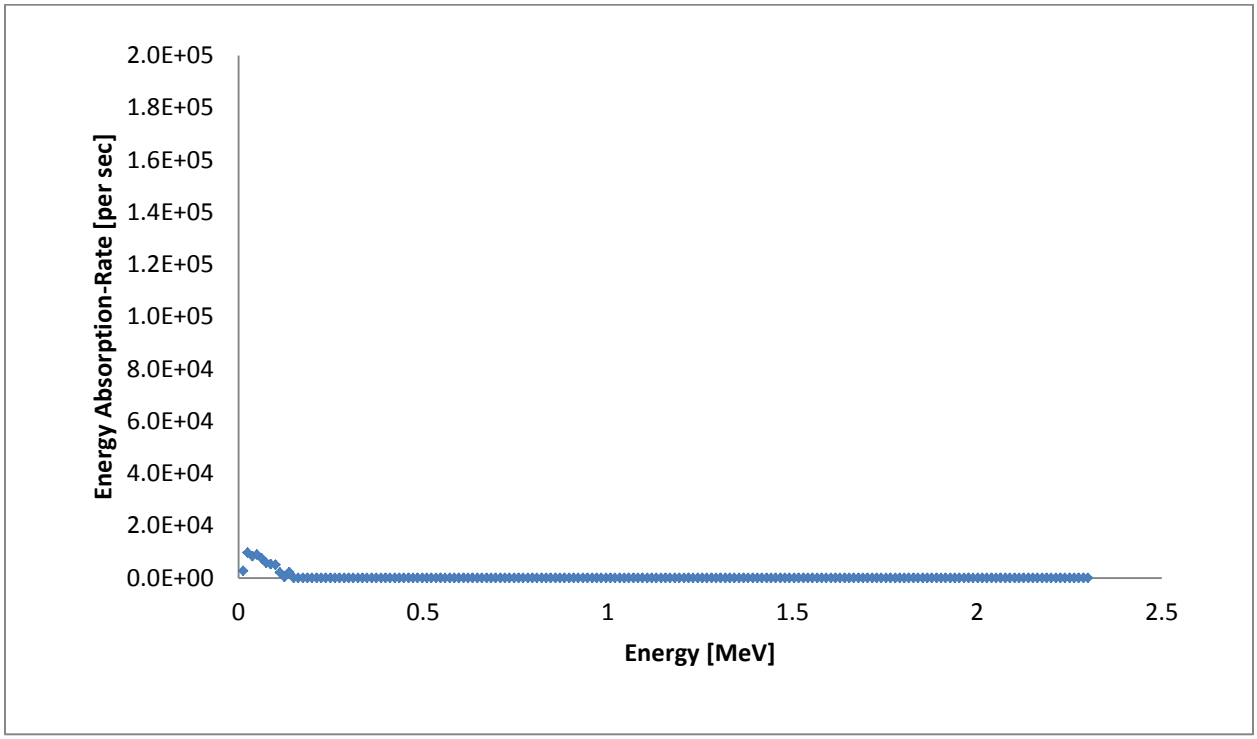


**Figure B-5: 4th residual in scenario #3**

**Scenario #4:**

**Table B-2: Results for scenario #4**

| Radionuclide | C-14 | Tc-99 | Sr-90 | Y-90 | Total |
|---|---|---|---|---|---|
| MF | 10 | 10 | 100 | 10 | 130 |
| Percentage of MF (%) | 7.7 | 7.7 | 77 | 7.7 | 100 |
| Activity (beta/sec) | 720000 | 780000 | 7740000 | 760000 | 10000000 |
| Percentage of Activity (%) | 7.2 | 7.8 | 77.4 | 7.6 | 100 |

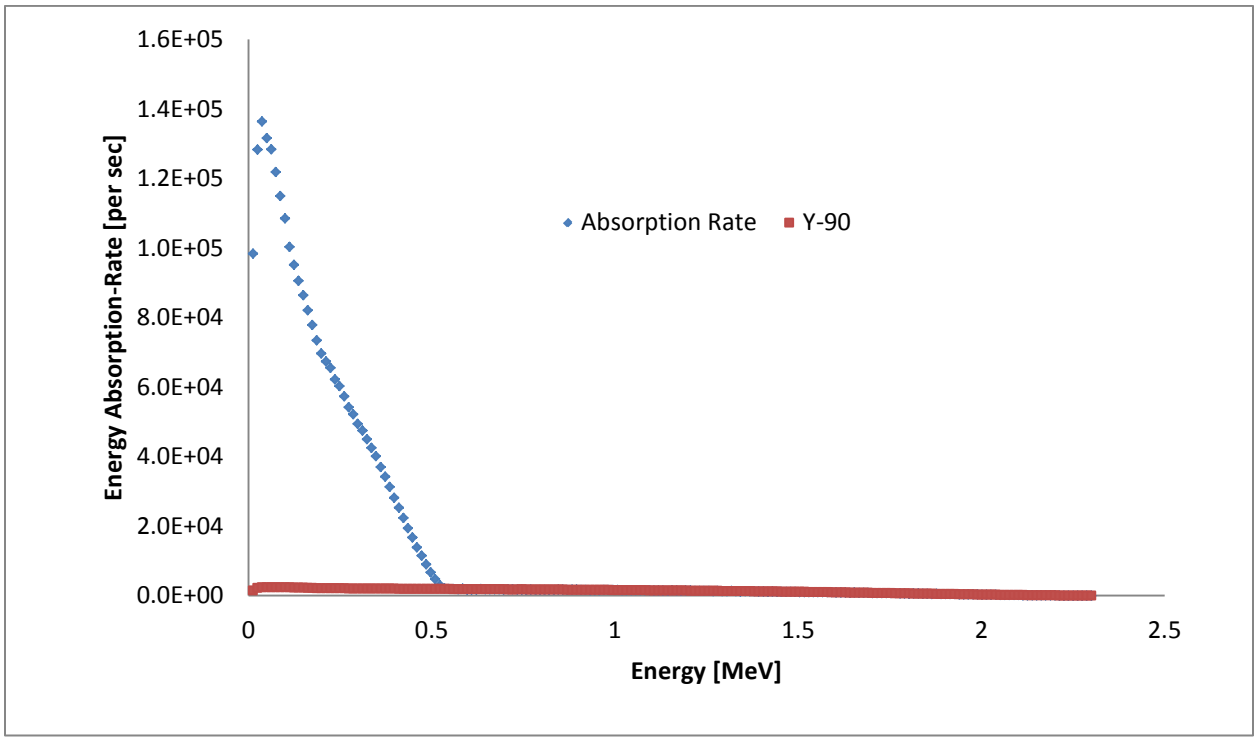


**Figure B-6: Mixed absorption-rate spectrum vs. individual absorption-rate spectrum(Y-90) in scenario #4**

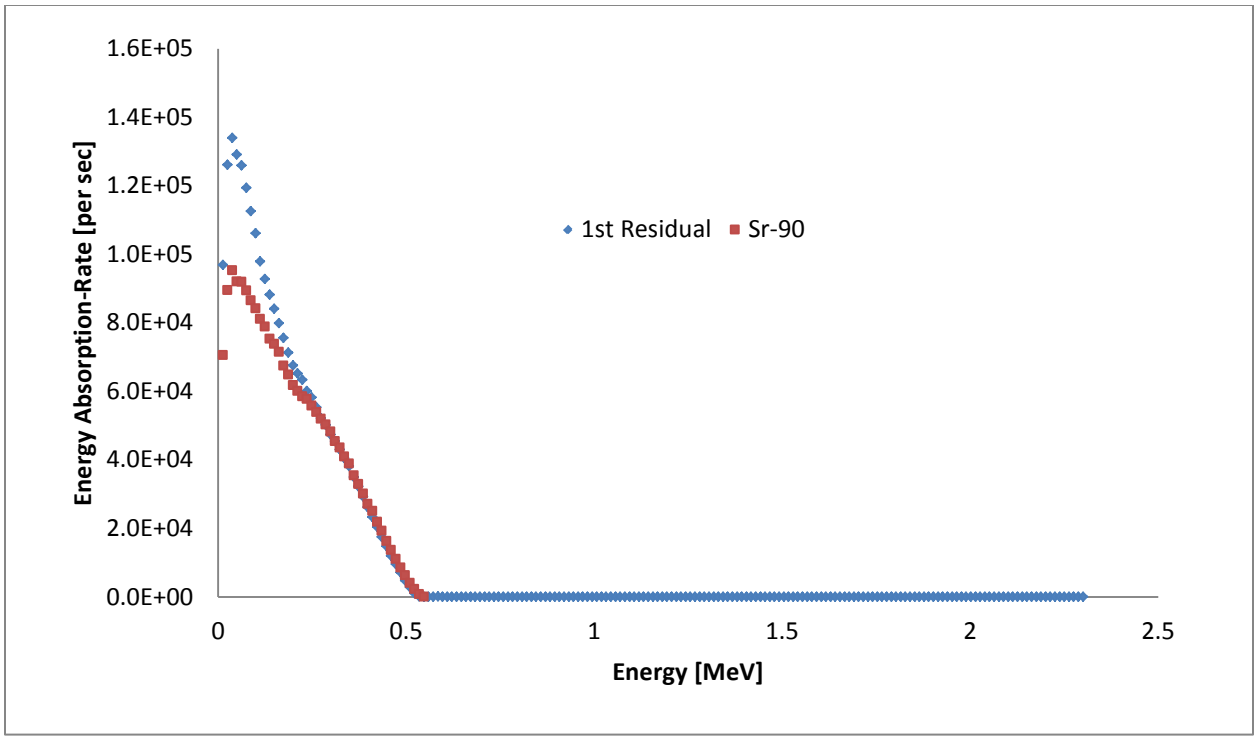


**Figure B-7: 1st residual vs. individual absorption-rate spectrum (Sr-90) in scenario #4**

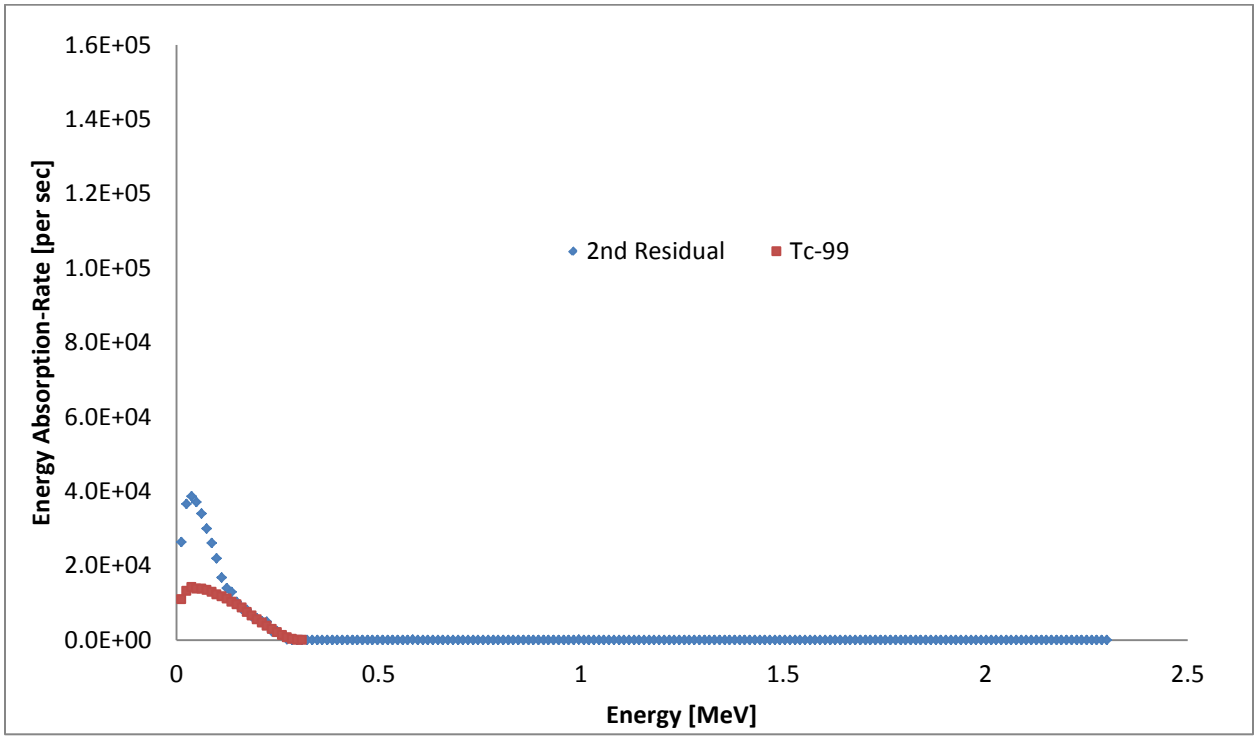


**Figure B-8: 2nd residual vs. individual absorption-rate spectrum (Tc-99) in scenario #4**

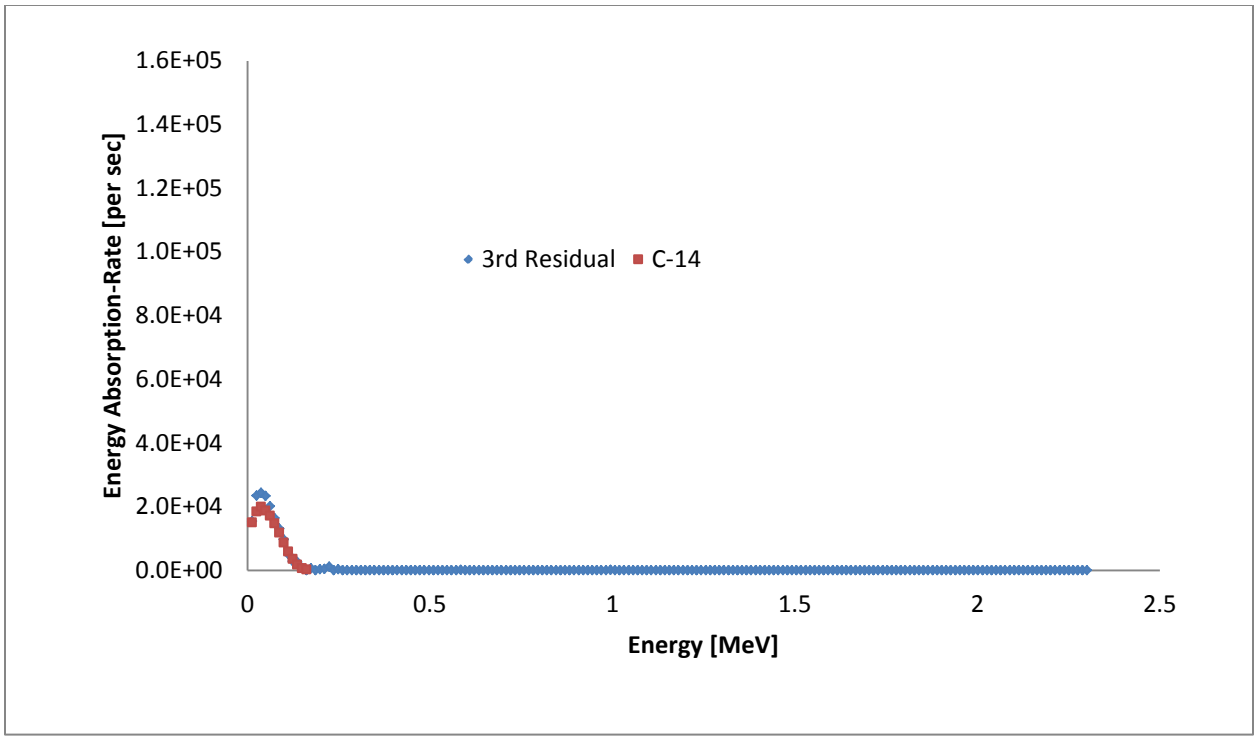


**Figure B-9: 3rd residual vs. individual absorption-rate spectrum (C-14) in scenario #4**

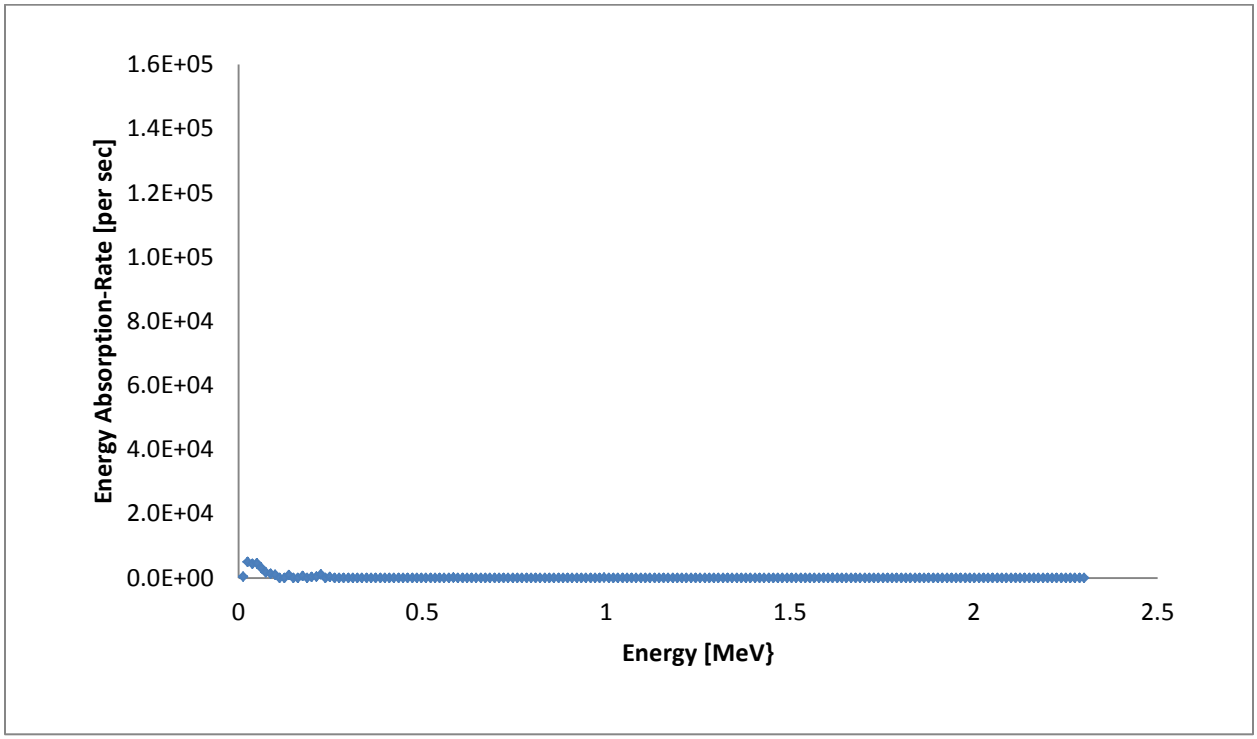


**Figure B-10: 4th residual in scenario #4**

**Scenario #5:**

**Table B-3: Results for Scenario #5**

| Radionuclide | C-14 | Tc-99 | Sr-90 | Y-90 | Total |
|---|---|---|---|---|---|
| MF | 10 | 10 | 10 | 10 | 40 |
| Percentage of MF (%) | 25 | 25 | 25 | 25 | 100 |
| Activity (beta/sec) | 2500000 | 2500000 | 2500000 | 2500000 | 10000000 |
| Percentage of Activity (%) | 25 | 25 | 25 | 25 | 100 |

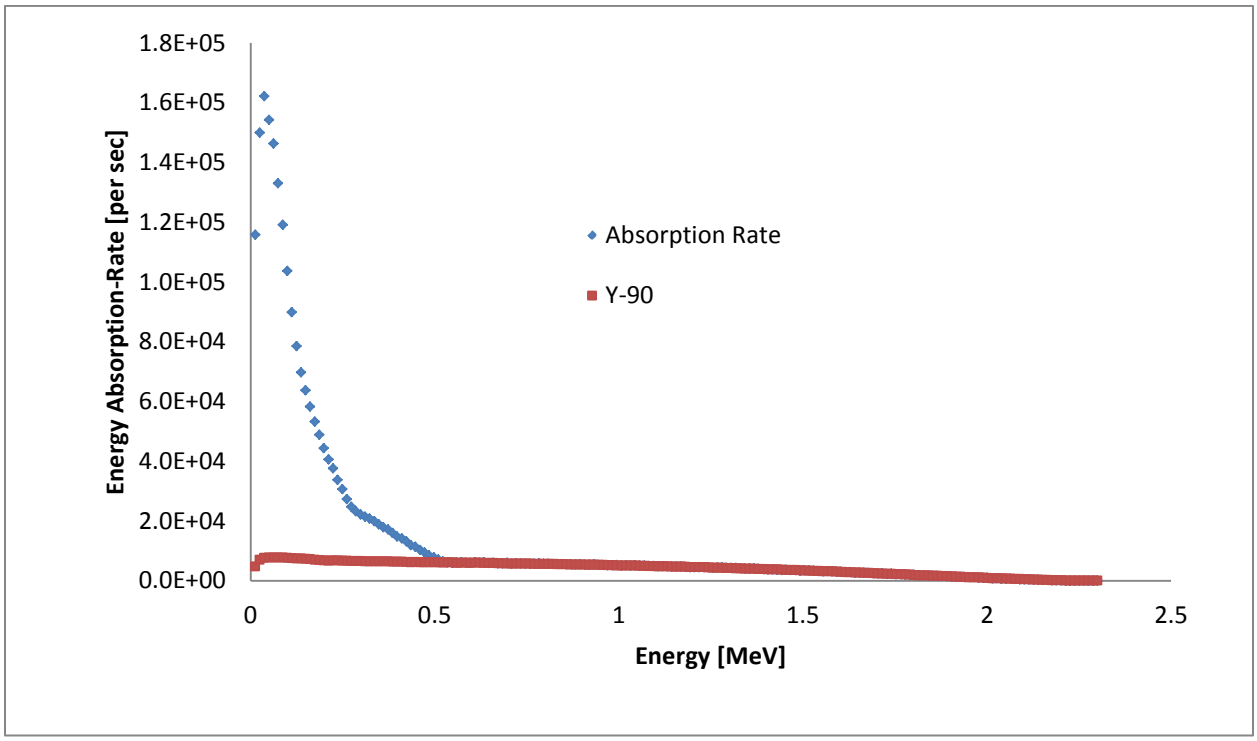


**Figure B-11: Mixed absorption-rate spectrum vs. individual absorption-rate spectrum(Y-90) in scenario #5**

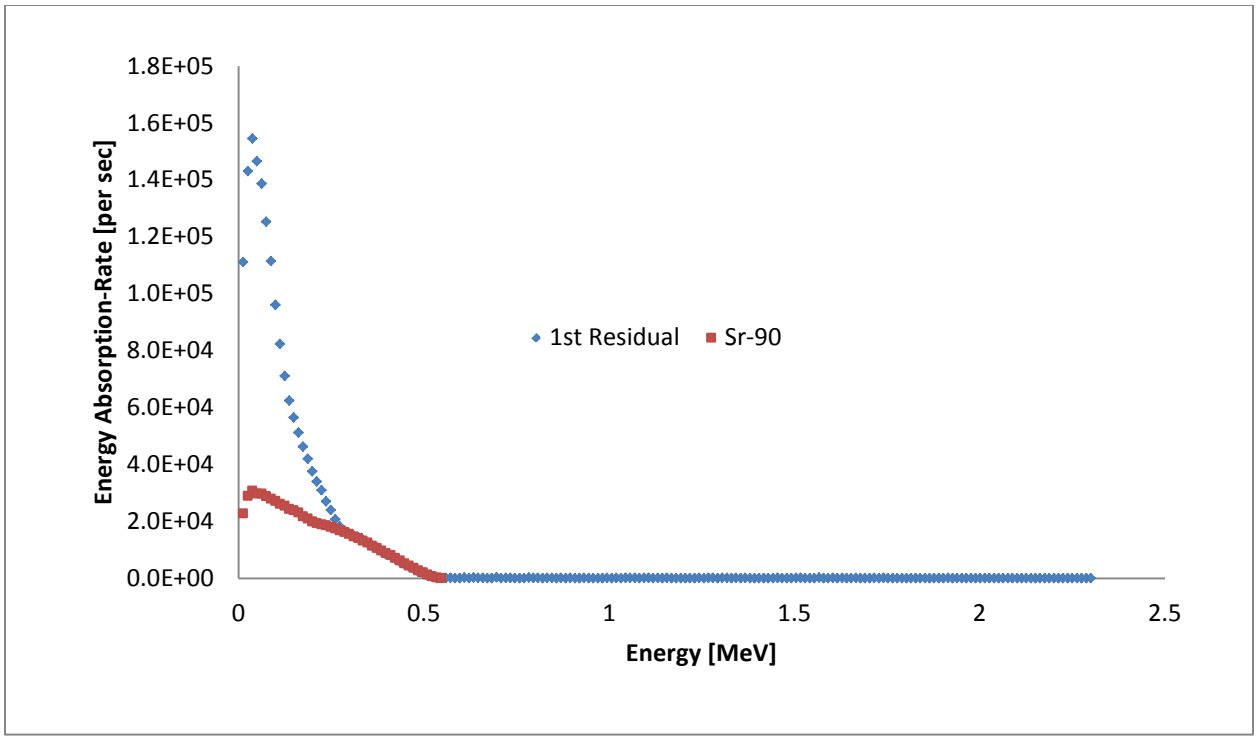


**Figure B-12: 1st residual vs. individual absorption-rate spectrum (Sr-90) in scenario #5**

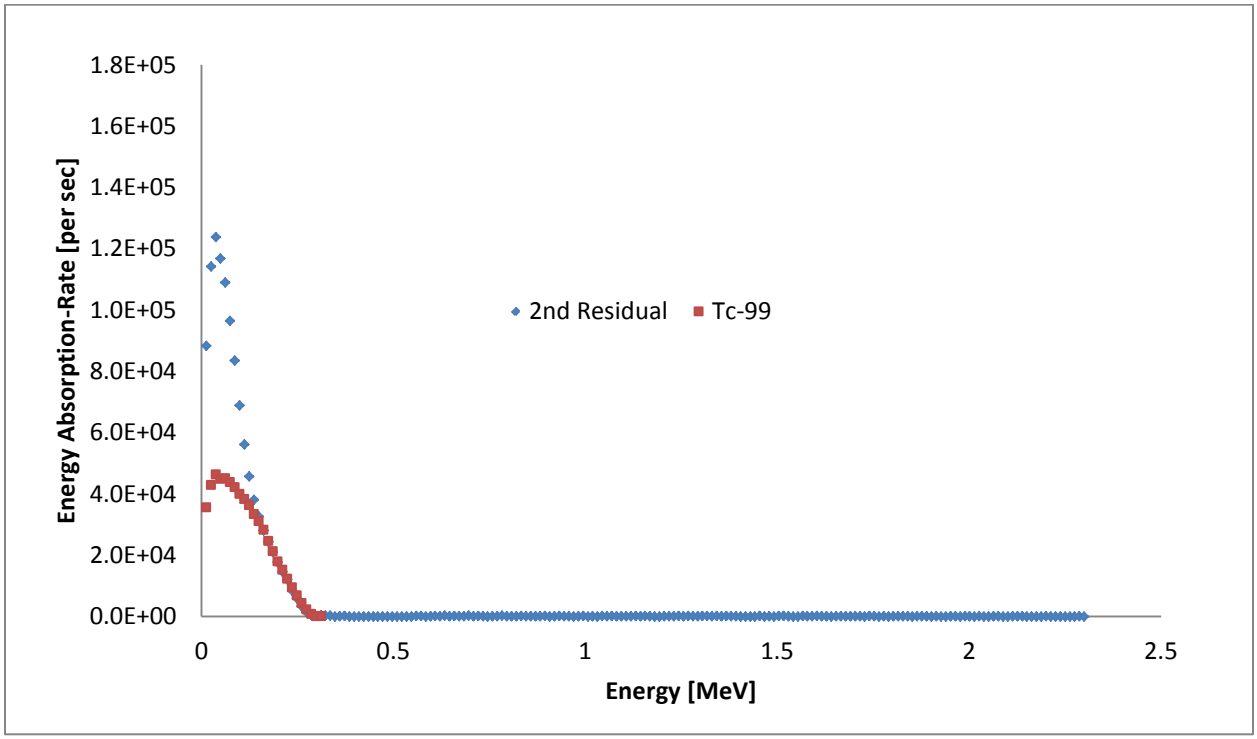


**Figure B-13: 2nd residual vs. individual absorption-rate spectrum (Tc-99) in scenario #5**

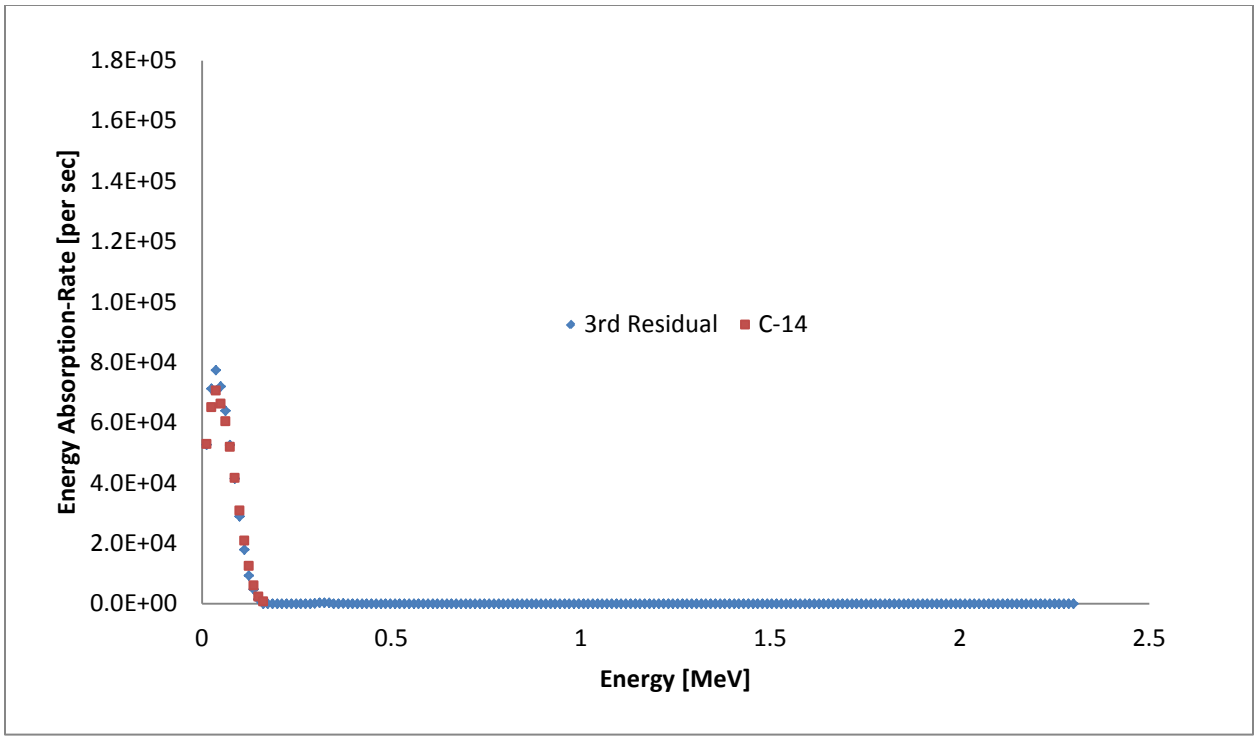


**Figure B-14: 3rd residual vs. individual absorption-rate spectrum (C-14) in scenario #5**

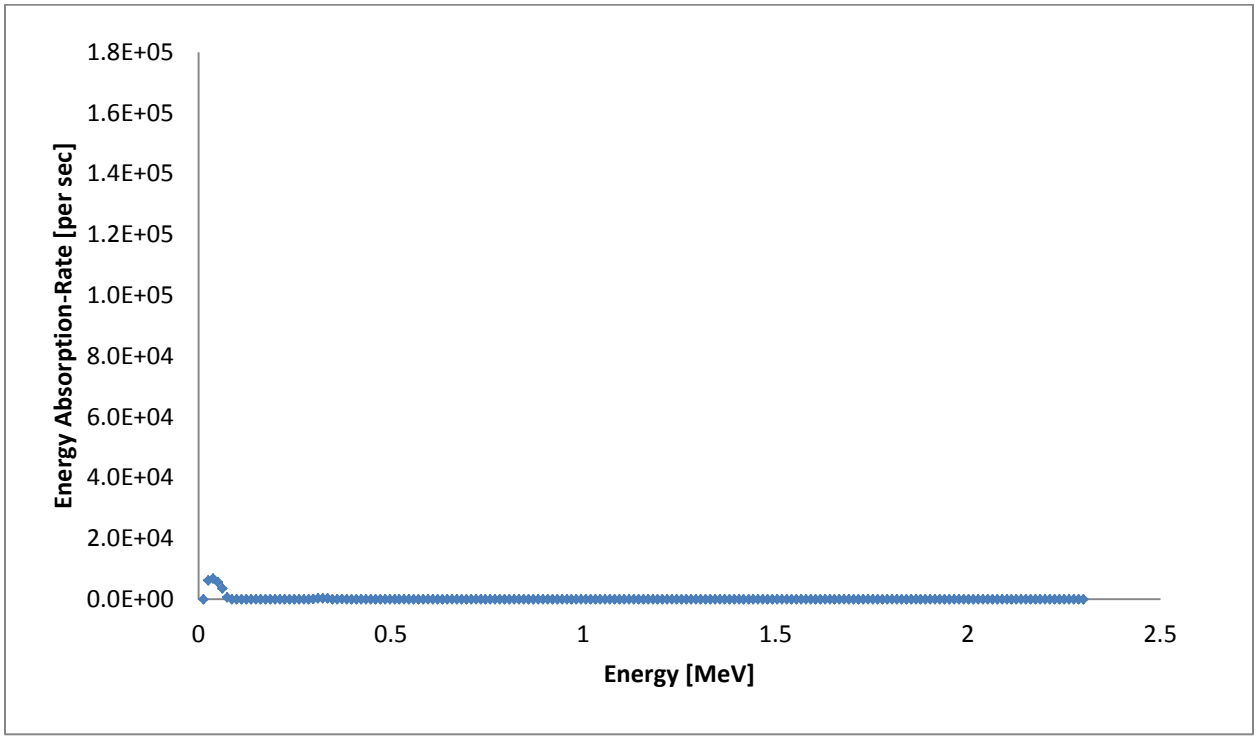


**Figure B-15: 4th residual in scenario #5**

**Scenario #6:**

**Table B-4: Results for scenario #6**

| Radionuclide | C-14 | Tc-99 | Sr-90 | Y-90 | Total |
|---|---|---|---|---|---|
| MF | 0 | 100 | 50 | 50 | 200 |
| Percentage of MF (%) | 0 | 50 | 25 | 25 | 100 |
| Activity (beta/sec) | 0 | 2250000 | 2220000 | 4530000 | 9000000 |
| Percentage of Activity (%) | 0 | 25 | 24.7 | 50.3 | 100 |

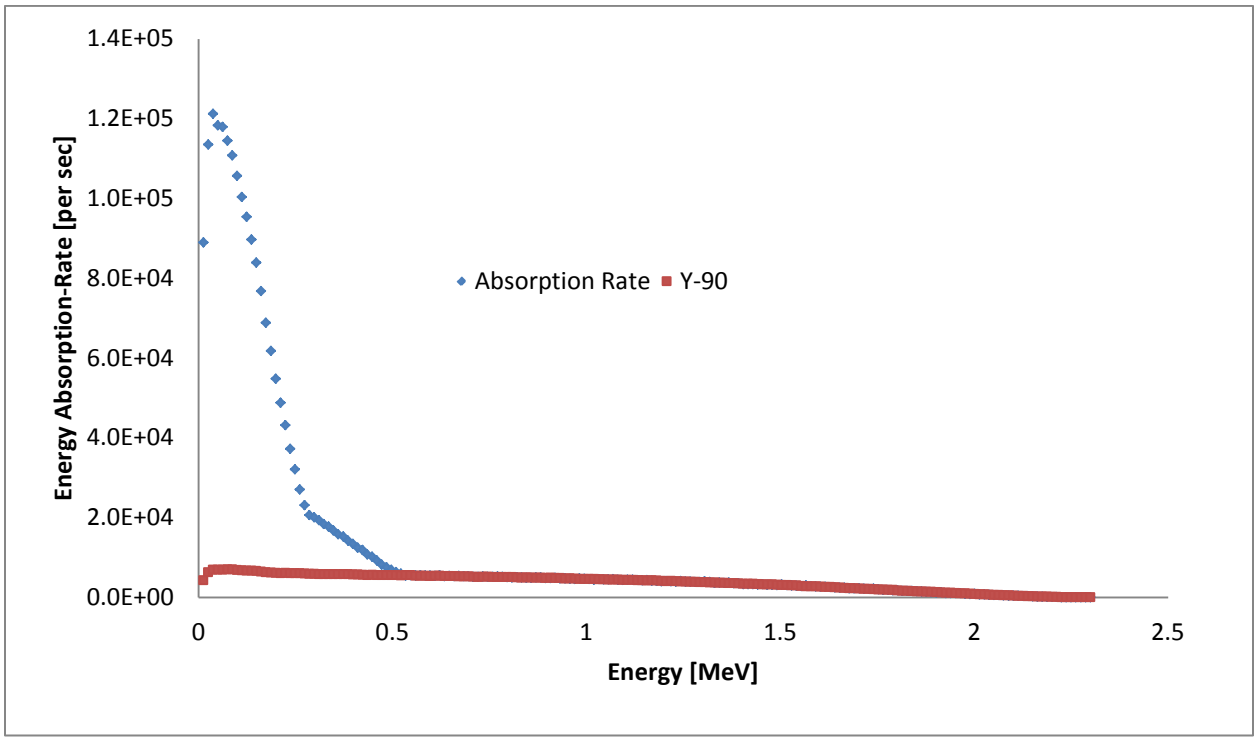


**Figure B-16: Mixed absorption-rate spectrum vs. individual absorption-rate spectrum(Y-90) in scenario #6**

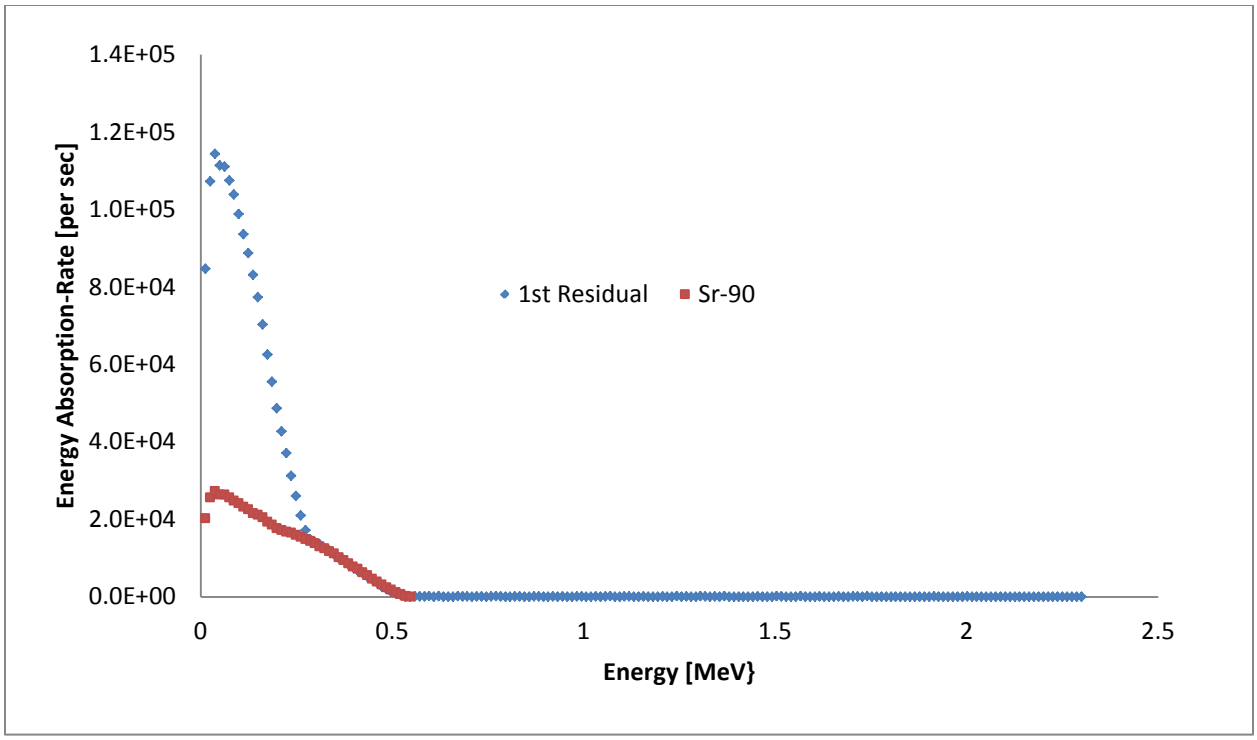


**Figure B-17: 1st residual vs. individual absorption-rate spectrum (Sr-90) in scenario #6**

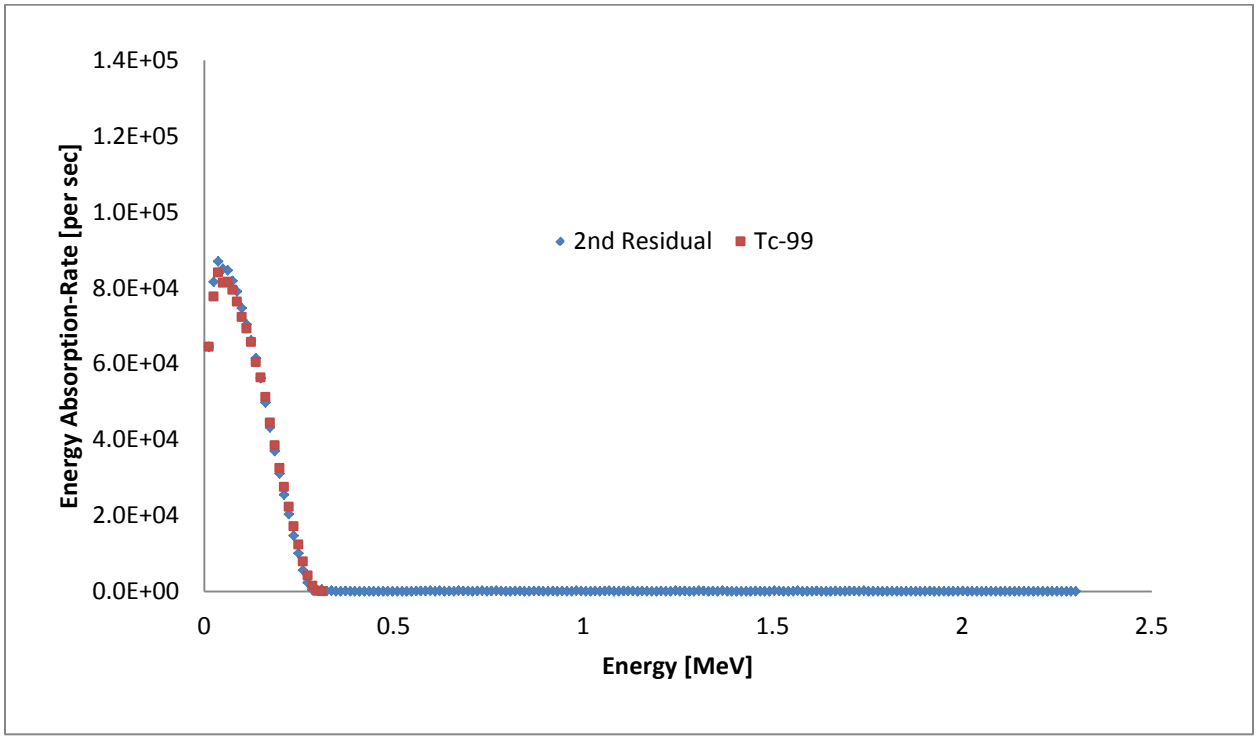


**Figure B-18: 2nd residual vs. individual absorption-rate spectrum (Tc-99) in scenario #6**

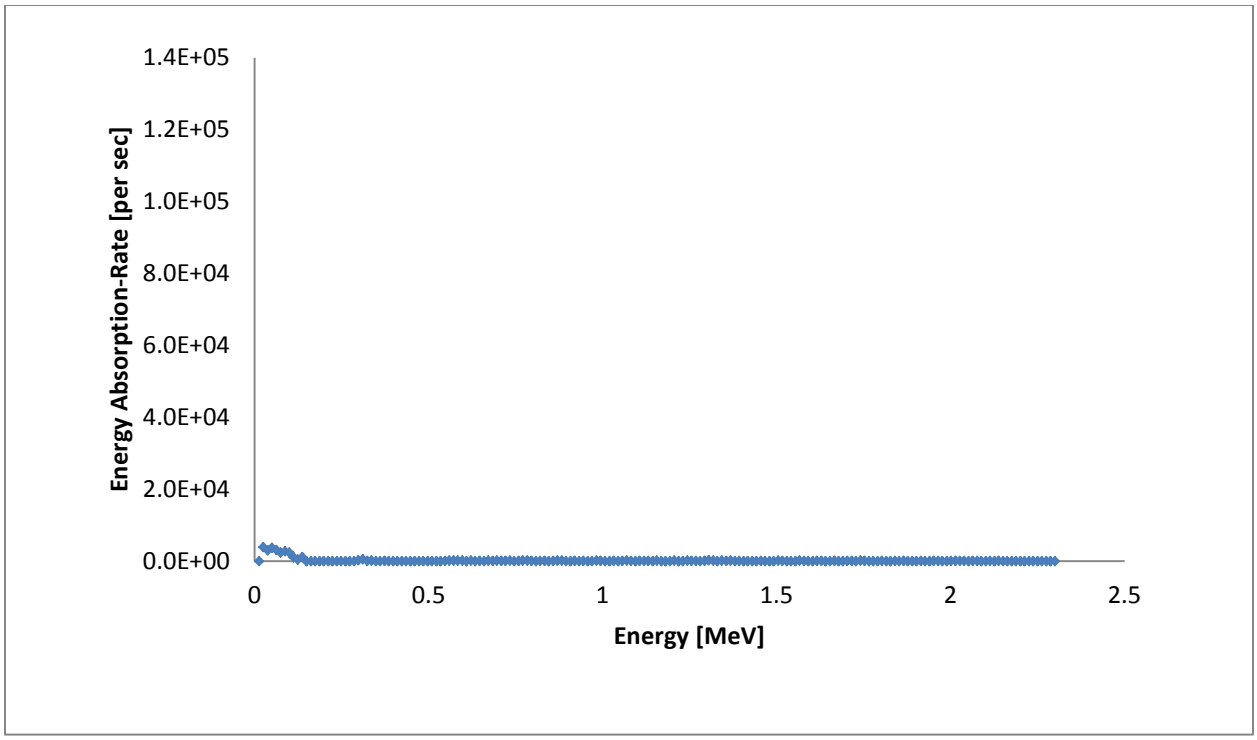


**Figure B-19: 3rd residual in scenario #6**

**Scenario #7:**

**Table B-5: Results for scenario #7**

| Radionuclide | C-14 | Tc-99 | Sr-90 | Y-90 | Total |
|---|---|---|---|---|---|
| MF | 100 | 0 | 0 | 50 | 150 |
| Percentage of MF (%) | 66.7 | 0 | 0 | 33.3 | 100 |
| Activity (beta/sec) | 3100000 | 0 | 0 | 5900000 | 9000000 |
| Percentage of Activity (%) | 65.6 | 0 | 0 | 34.4 | 100 |

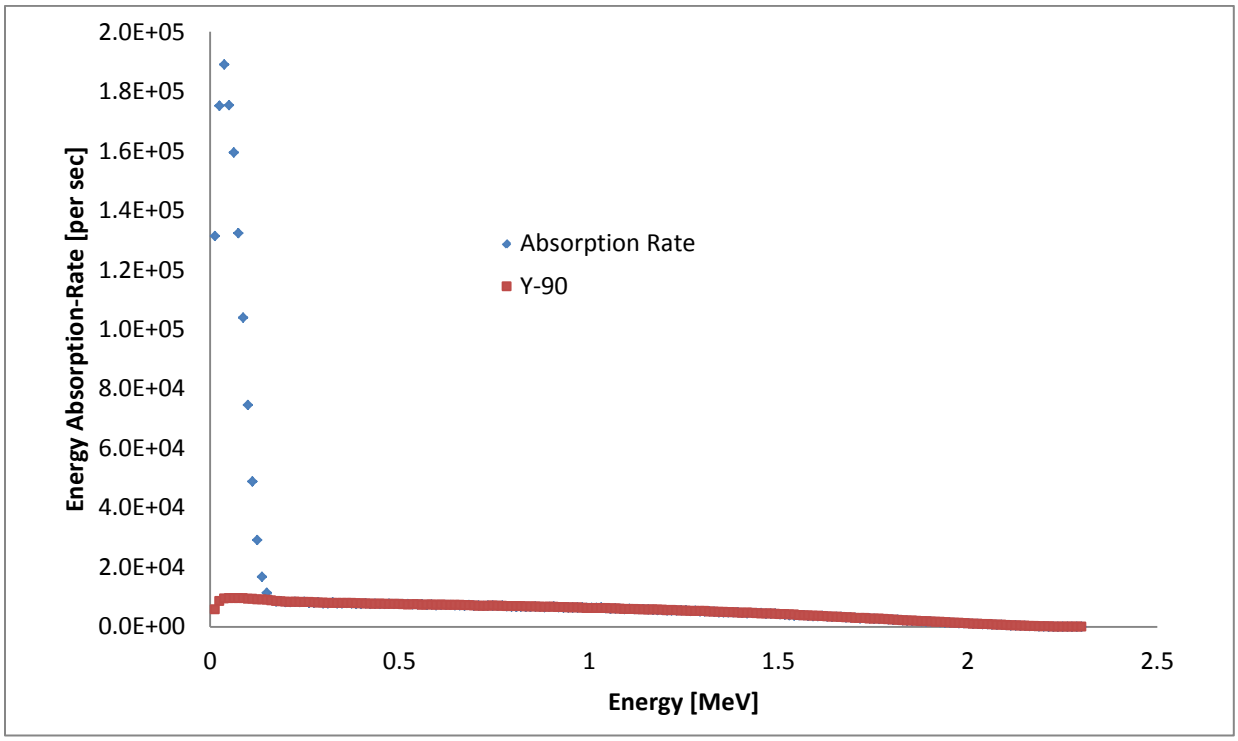


**Figure B-20: Mixed absorption-rate spectrum vs. individual absorption-rate spectrum(Y-90) in scenario #7**

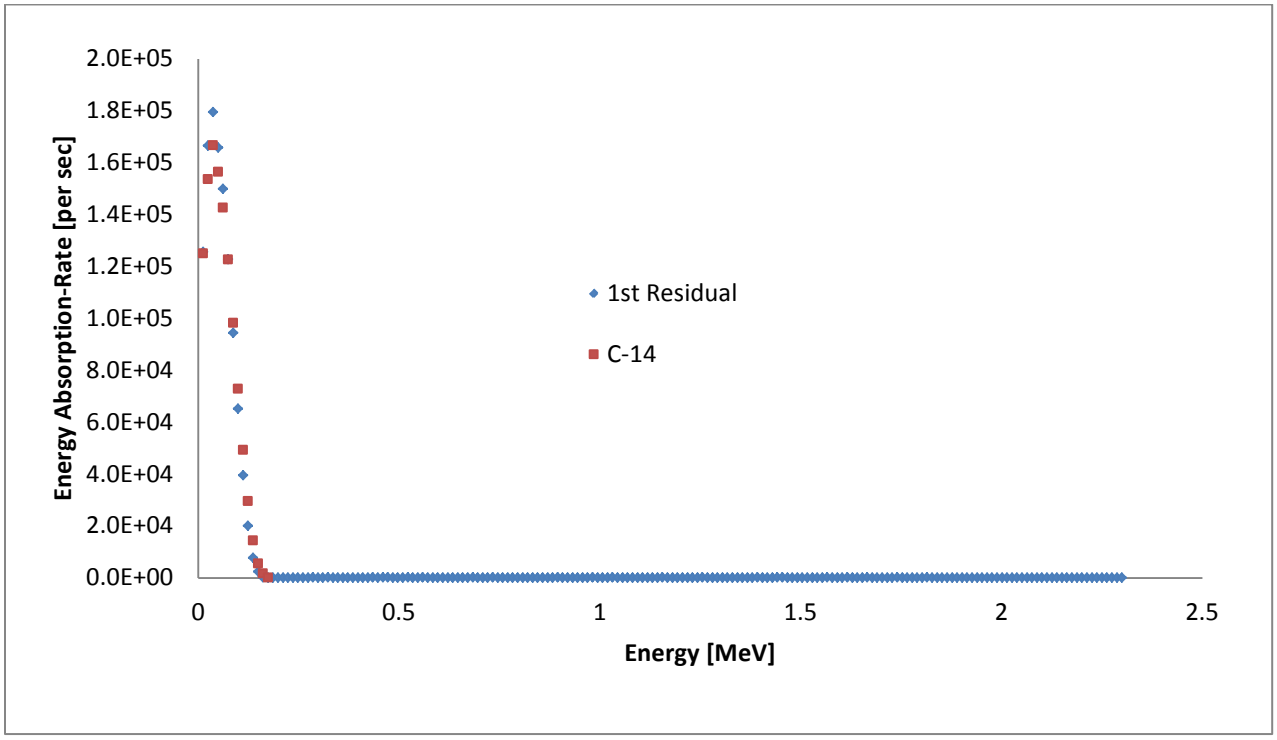


**Figure B-21: 1st residual vs. individual absorption-rate spectrum (C-14) in scenario #7**

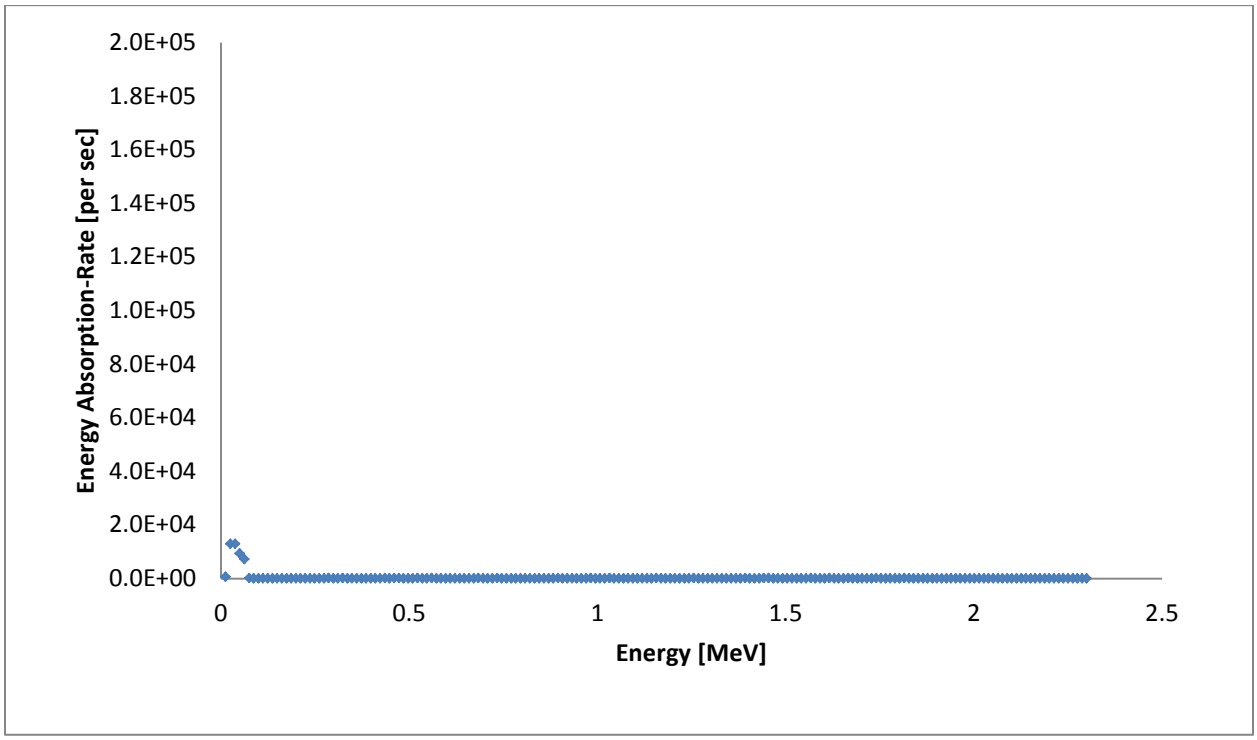


**Figure B-22: 2nd residual scenario #7**

**Scenario #8:**

**Table B-6: Results for scenario #8**

| Radionuclide | C-14 | Tc-99 | Sr-90 | Y-90 | Total |
|---|---|---|---|---|---|
| MF | 100 | 50 | 0 | 0 | 150 |
| Percentage of MF (%) | 66.7 | 33.3 | 0 | 0 | 100 |
| Activity (beta/sec) | 660000 | 340000 | 0 | 0 | 1000000 |
| Percentage of Activity (%) | 66 | 34 | 0 | 0 | 100 |

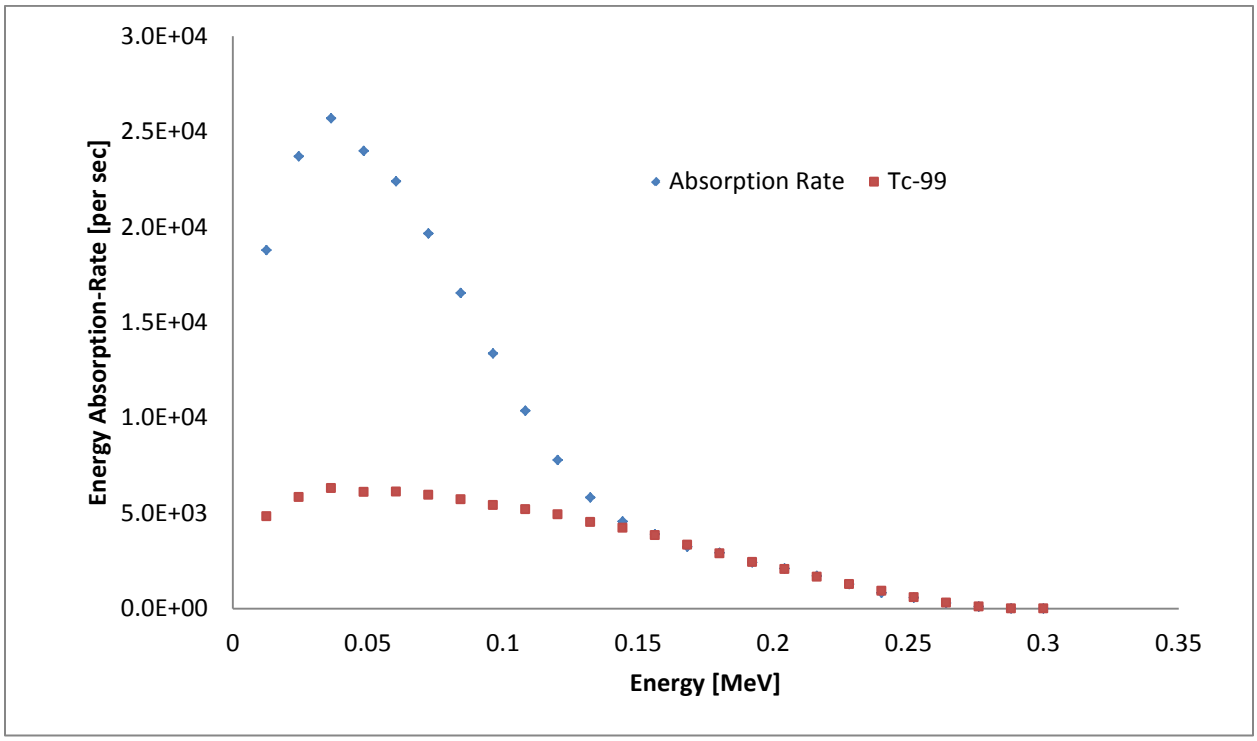


**Figure B-23: Mixed absorption-rate spectrum vs. individual absorption-rate spectrum (Tc-99) in scenario #8**

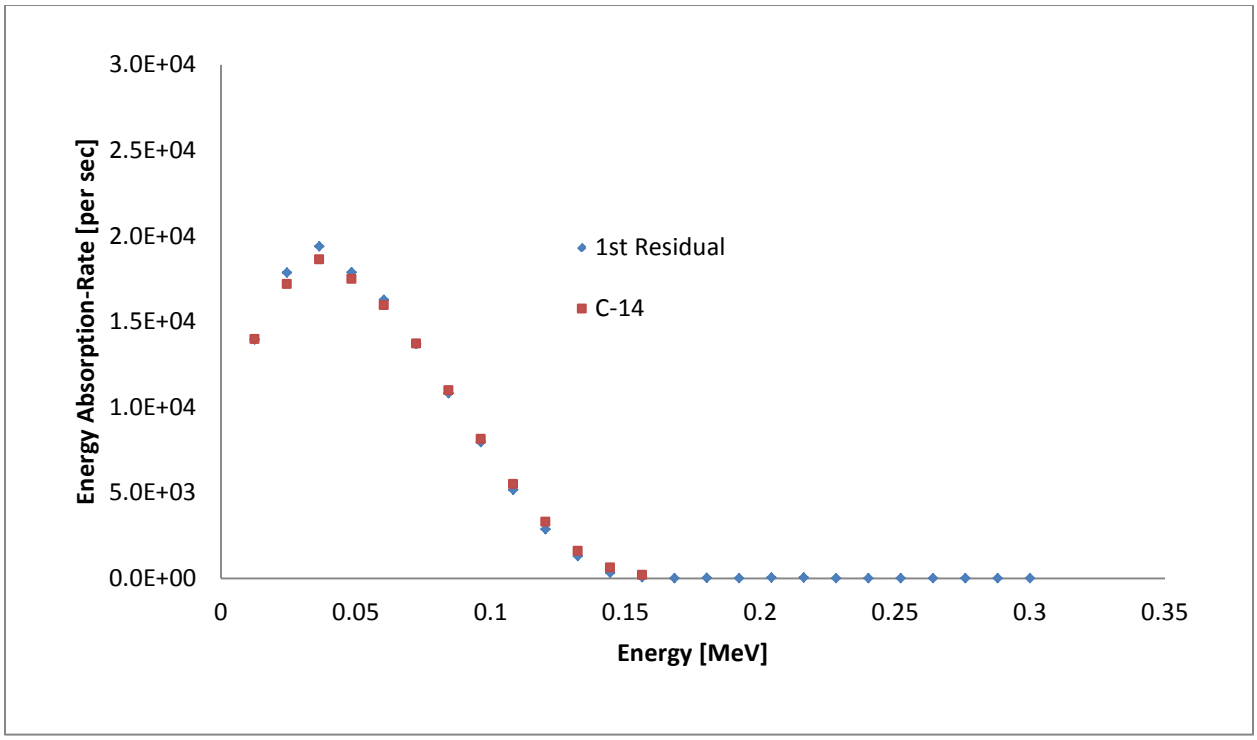


**Figure B-24: 1st residual vs. individual absorption-rate spectrum (C-14) in scenario #8**

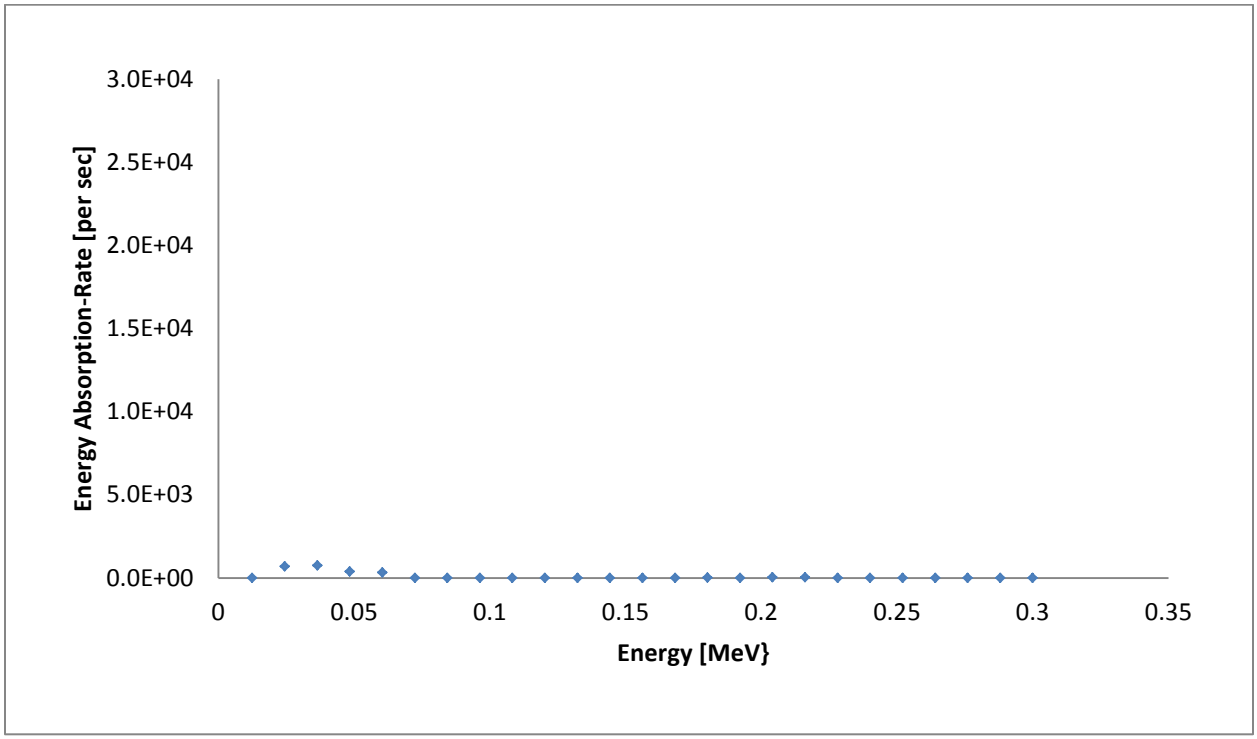


**Figure B-25: 3rd residual in scenario #8**

**Scenario #9:**

**Table B-7: Results for scenario #9**

| Radionuclide | C-14 | Tc-99 | Sr-90 | Y-90 | Total |
|---|---|---|---|---|---|
| MF | 0 | 100 | 50 | 0 | 150 |
| Percentage of MF (%) | 0 | 66.6 | 33.3 | 0 | 100 |
| Activity (beta/sec) | 0 | 1980000 | 1020000 | 0 | 3000000 |
| Percentage of Activity (%) | 0 | 66 | 34 | 0 | 100 |

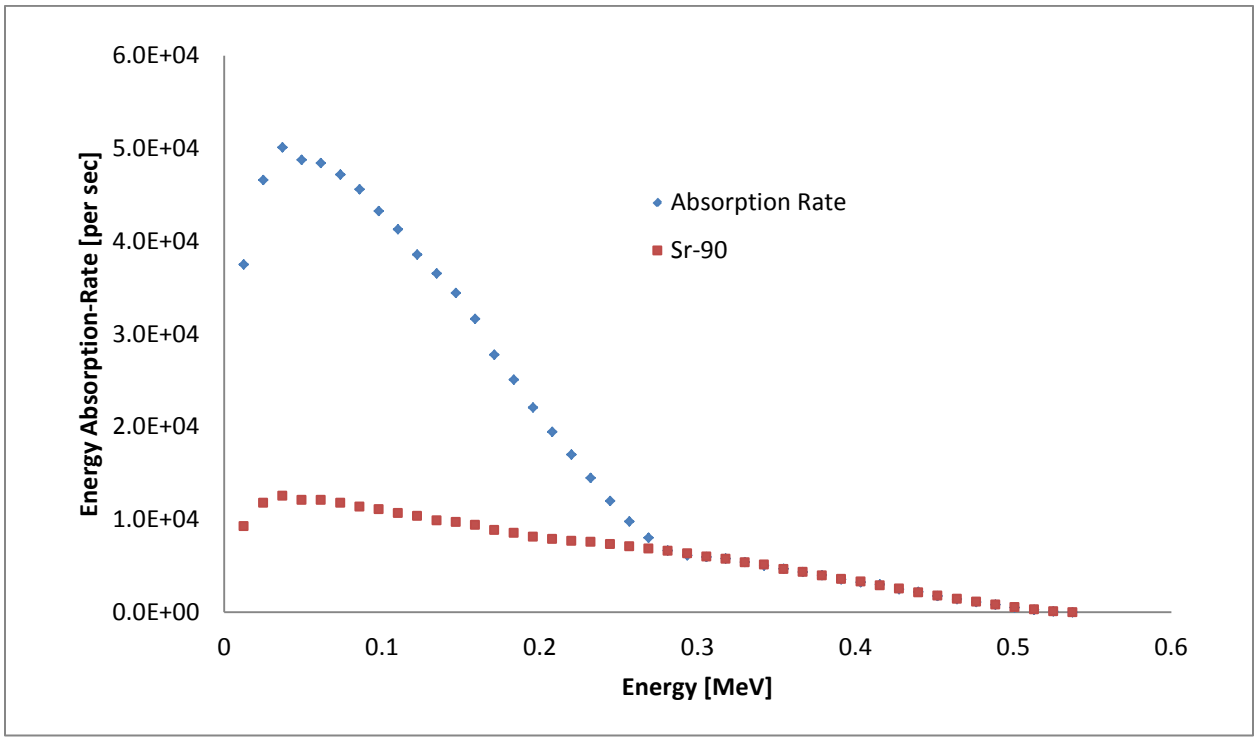


**Figure B-26: Mixed absorption-rate spectrum vs. individual absorption-rate spectrum (Sr-90) in scenario #9**

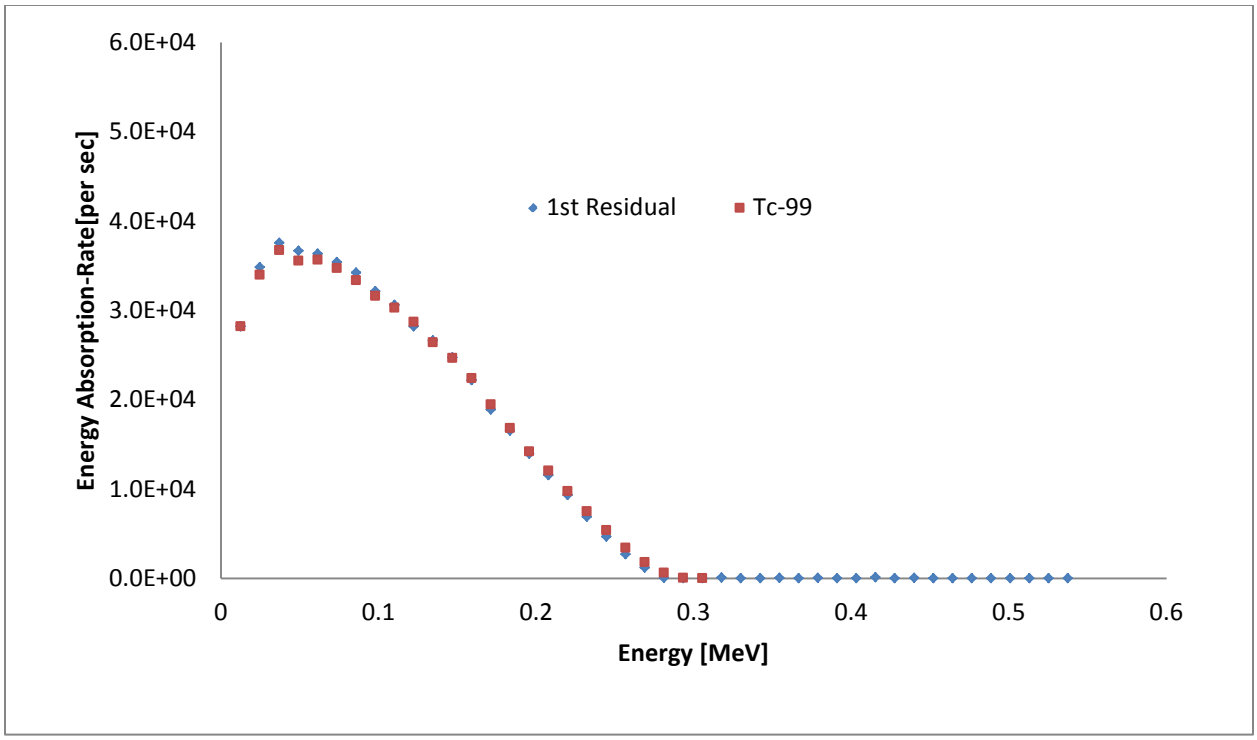


**Figure B-27: 1st residual vs. individual absorption-rate spectrum (Tc-99) in scenario #9**

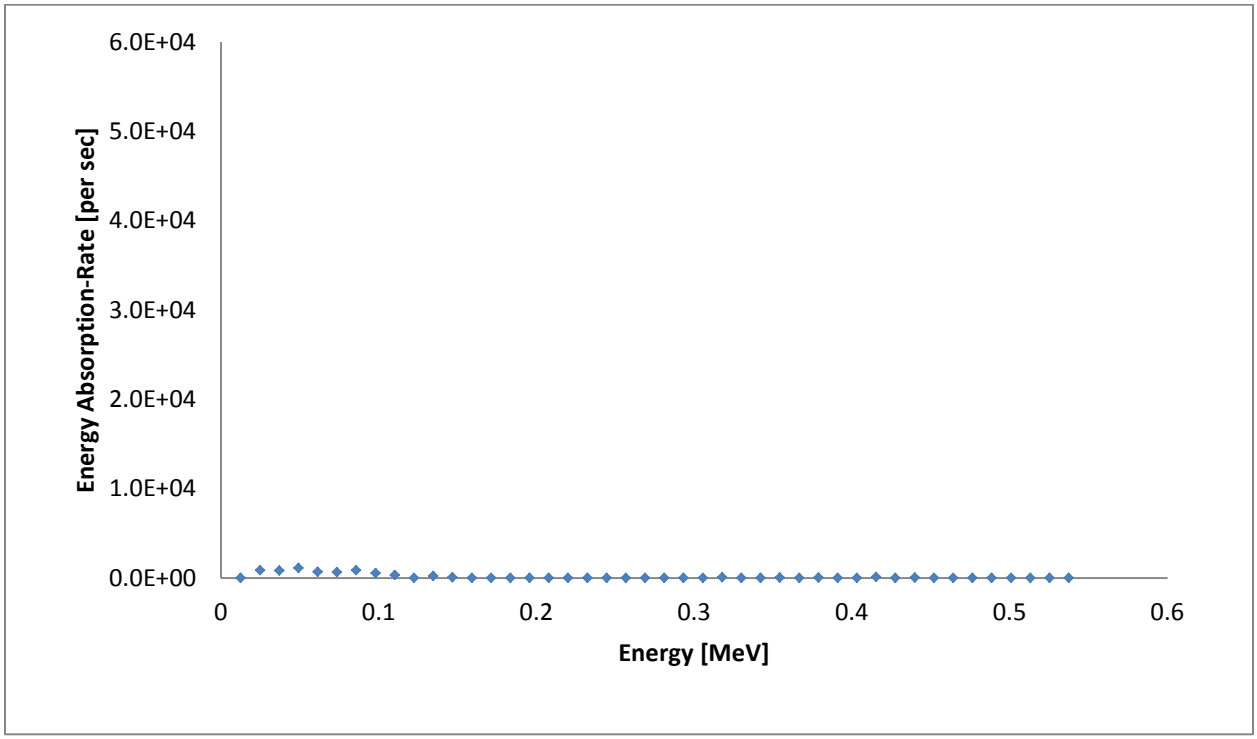


**Figure B-28: 3rd residual in scenario #9**